Tropical climate and vegetation cover during Heinrich event 1: Simulations with coupled climate-vegetation models

Dissertation zur Erlangung des akademischen Grades eines Doktors der Naturwissenschaften

Dr. rer. nat.

im Fachbereich 5 (Geowissenschaften)

der Universität Bremen

vorgelegt von

Dian Noor Handiani

Bremen, Oktober 2012

Erklärung

Name: Dian Noor Handiani
Anschrift: Woltmershauser straße 464, 28197 Bremen, Deutschland

Hiermit versichere ich, dass ich

1. die Arbeit ohne unerlaubte fremde Hilfe angefertigt habe,
2. keine anderen als die von mir angegebenen Quellen und Hilfsmittel benutzt habe und
3. die den benutzten Werken wörtlich oder inhaltlich entnommenen Stellen als solche kenntlich gemacht habe.

Bremen, Oktober 2012

_____

(Unterschrift)

Gutachter

Prof. Dr. Michael Schulz

Prof. Dr. Michal Kucera

Promotionskolloquium: 20.12.2012

Mitglieder der Kommission:

Herr Prof. Dr. Michael Schulz

Herr Prof. Dr. Michal Kucera

Herr Prof. Dr. Gerold Wefer

Frau Prof. Dr. Gesine Mollenhauer

Frau Dr. Lydie Dupont

Frau Annegret Krandick

Table of Content

Acknowledgements i
Summary iii
Zusammenfassung v

1 Introduction 1
1.1 Motivation of study 1
1.2 Tropical climate and vegetation in the Heinrich events 3
1.3 Atlantic Meridional Overturning Circulation (AMOC) 6
1.4 Research objectives 9
1.5 Research approach and chapter outline 10

2 Methodology 11
2.1 The UVic ESCM 11
2.1.1 The atmospheric model 11
2.1.2 The ocean and sea-ice model 13
2.1.3 The land surface and dynamic vegetation models 14
2.2 Plant functional types and biomes 15
2.3 A scheme of biome distribution estimation 16
2.4 Experimental design 17

3 Tropical climate and vegetation changes during Heinrich event 1: a model-data comparison 19
3.1 Abstract 19
3.2 Introduction 20
3.3 Methods and experimental design 22
3.3.1 The UVic ESCM and TRIFFID DGVM 22
3.3.2 Simulation design and boundary conditions 23
3.3.3 Biome analysis from TRIFFID 24
3.4 The equilibrium simulations 26
3.4.1 Pre-industrial simulation (PI_CNTRL) 26
3.4.2 Last Glacial Maximum simulation (LGM) 31
3.5 Heinrich events 1 simulations 34
3.5.1 Changes in climate 34
3.5.2 Changes in vegetation 38
3.5.3 Biome distribution and model-data comparison 39
3.6 Discussion 41
3.7 Summary and conclusions 45
3.8 Acknowledgements 47

4 Climate and vegetation changes around the Atlantic Ocean resulting from changes in the meridional overturning circulation during deglaciation 49
4.1 Abstract 49
4.2 Introduction 50
4.3 Model description and experimental designs 51
4.4 Results 53
4.4.1 The variability of AMOC and physical ocean properties 53
4.4.2 Precipitation and vegetation response 59
4.4.3 Comparison between model and paleovegetation data 62
4.5 Discussion 64
4.6 Conclusion 69
4.7 Acknowledgements 70

5 Tropical vegetation response to Heinrich event 1 as simulated with the UVic ESCM and CCSM3 71
5.1 Abstract 71
5.2 Introduction 72
5.3 Models and experimental design 73
5.4 Results 76
5.4.1 Climate changes 76
5.4.2 The vegetation cover response 79
5.4.3 Biomes distribution comparison 82
5.5 Discussion 84
5.6 Conclusion 87
5.7 Acknowledgements 88

6 Summary of the results 89
6.1 The HE1 climate and vegetation in the tropics 89
6.2 The BA climate and vegetation in the region around the Atlantic Ocean ... 91
6.3 A method for estimating a biome distribution from model outputs 92

7 Conclusion and Outlook 93
7.1 Conclusion 93
7.2 Outlook 94

Appendix 95
Biomes estimation flow chart 95

Bibliography 97

Acknowledgments

The first three years of this PhD were financially supported by the Deutsche Forschungsgemeinschaft (DFG) as part of the German contribution to the Integrated Ocean Drilling Program (SPP 527) "Abrupt Climate Change in the African Tropics (ACCAT)" and the DFG Research Center/Excellence Cluster "The Ocean in the Earth System", and the finishing stage of the study was funded by "The Excellent Scholarship Program by Bureau of Planning and International Cooperation", Secretary-General of Ministry of Education and Culture, Indonesia. The work itself was carried out at the Geosciences Department of the University of Bremen, in Germany. I would like to thank the Center for Marine Environmental Sciences (MARUM) and the University of Bremen for giving me the opportunities to attend several international courses, workshops and conferences.

I would like to express my gratitude to Prof. Michael Schulz and Dr. André Paul for giving me the experience to work in such an inspiring and motivating environment, and my high appreciation to André especially for his daily patient assistance. His guidance in introducing me into the world of paleoclimate modeling enables me to finish this challenging study. I would like to thank to Dr. Lydie Dupont for her guidance through understanding the pollen proxies study and also together with André in helping me to improve my writing skill as well as to direct my research. I would thank to all the co-authors for their inputs and suggestions in writing my research papers. I also thank Xiao Zhang who simulated the HE1 experiment on the CCSM3, which are used and analysed in this study. I would also like to thank Dr. Andreas Manschke for solving quickly all computer problems, as well as Leslie Sütterlin for her great help with all administration-related work. A general thanks to all the Geomod members for their support and valuable suggestions during the group seminars and also for the many entertaining cakes and coffee breaks, especially Vidya, Ute, Heather, Claudia, Takasumi, Gerlinde, Nilima, Huadong and others.

Special thanks to my officemates, Thejna, Xiao and Amanda, who have been supportive in every way. I definitely will miss you guys! A special thank to Rima, her beloved husband (Ayi) and "little" Khansa, who sincerely were willing to share their home, during my time in Bremen. General thanks to all Indonesian friends in Bremen, foremost Family Vidjaja for allowing me being part of their family and they have become my second family during my study. I want to deeply thank my long distance Indonesian friends, "Mba" Annastasia, Ulfah, Vigi, Winda, Al-azhar, Aradea and also my teacher back in Indonesia, Dr. Nining Sari Ningsih for their encouragement, endless support and friendship. Despite the distance, they were always there for me and it means a lot. Finally, I would like to express my entire gratitude to my family, who were always my best supporters through my whole life, especially my mom within these recent years, her tremendous support and faith in me were the driving forces behind everything I did.

Summary

This study focuses on the climate and vegetation responses to abrupt climate change in the Northern Hemisphere during the last glacial period. Two abrupt climate events are explored: the abrupt cooling of the Heinrich event 1 (HE1), followed by the abrupt warming of the Bølling-Allerød interstadial (BA). These two events are simulated by perturbing the freshwater balance of the Atlantic Ocean, with the intention of altering the Atlantic Meridional Overturning Circulation (AMOC) and also of influencing the Intertropical Convergence Zone (ITCZ) and its associated rainbelt. The University of Victoria Earth System-Climate Model (UVic ESCM) is applied in these experiments. The plant-functional types and the temperature from the model output are used for calculating the biome distribution, which is then compared to the available pollen records. In addition, an inter-model comparison for the HE1 is carried out by comparing the UVic ESCM with the Community Climate System Model version 3 (CCSM3).

In the UVic ESCM, the HE1 climate is imitated by adding freshwater to the St. Lawrence River where it runs into the North Atlantic Ocean, which causes a slowdown of the AMOC. The weakening of the AMOC is followed by a cooler climate in the North Atlantic Ocean and a warmer climate in the South Atlantic Ocean. This surface temperature see-saw between the Northern and Southern Hemispheres causes a southward shift of the tropical rainbelt. The simulated drier climate north of the Equator during the HE1 event causes an increase of desertification and the retreat of broadleaf forests in West Africa and northern South America. On one hand, the model results for the HE1 event can be shown to be in agreement with the pollen records from tropical Africa and northern South America. On the other hand, the model fails to predict savannah and grassland in western tropical South America. In addition, the model predicts similar biome distributions for the pre-industrial as well as the last glacial climate, except in tropical northern Africa (the Sahel region), western South America, and central North America. These regions are warmer and wetter during the pre-industrial climate compared to the Last Glacial Maximum climate, which means more tropical forest and savannah cover in the pre-industrial time period and further

extensions of warm temperate forests and grassland during the Last Glacial Maximum. Detailed results of the HE1 experiment are presented in Chapter 3.

We intensify the AMOC in our BA event experiment by applying two mechanisms: the addition of freshwater to the Southern Ocean under present-day climate conditions, and the extraction of freshwater from the North Atlantic Ocean against a glacial climate background. Both mechanisms produce a warmer climate in the North Atlantic Ocean and a cooler climate in the South Atlantic Ocean, which leads to a northward shift of the tropical rainbelt. These experiments suggest that grassland, boreal forest, and warm temperate forest could be found in Europe and North America during the BA event. The predictions of grassland on the west coast of North America conforms with the terrestrial records of Walker Lake, showing mostly xerophytic shrubland caused by a dry climate. Another match can be shown for sites in southwestern Europe and the Mediterranean, where steppe forest is mostly recorded. However, the model fails to simulate temperate forest in southeastern North America and in southern Europe. Detailed explanations of these results can be found in Chapter 4.

The inter-model comparison suggests that the UVic ESCM using a simplified atmospheric component is still capable of demonstrating the effects of a shift of the ITCZ, although a distinct tropical precipitation pattern is only shown in the CCSM3 with a much more realistic representation of the atmospheric processes. Nevertheless, the changes of the tropical vegetation cover during the HE1 experiment are similar in both models. Grass cover increases in tropical North Africa, and tree cover is reduced in tropical northwest Africa and South America. Correlations and discrepancies between model results and pollen records vary between the two models, except that they both agree over equatorial western Africa and South America. The detailed results are presented in Chapter 5.

In summary, the study demonstrates and explains the response of climate and vegetation cover to abrupt climate changes during the last glacial period in the tropics and in the region around the Atlantic Ocean. Furthermore, a direct comparison between model output and pollen records provides new insights in the potential of proxy data-model comparisons.

Zusammenfassung

Diese Studie beschäftigt sich mit der Reaktion von Klima und Vegetation auf die abrupten Klimaveränderungen während der letzten Kaltzeit. Zwei abrupte Klimaereignisse innerhalb dieser Zeit werden erforscht: das Heinrich-Ereignis 1 (HE1) und das Bølling-Allerød (BA)-Interstadial. Diese beiden Ereignisse werden simuliert, indem Süßwasser dem Atlantik zugeführt wird, um die meridionale Umwälzbewegung im Atlantischen Ozean ("Atlantic Meridional Overturning Circulation", AMOC) sowie die intertropische Konvergenzzone ("Intertropical Convergence Zone", ITCZ) zu beeinflussen. Diese Simulationen verwenden das "Earth System-Climate Model" (UVic ESCM) der University of Victoria. Die Pflanzenfunktionstypen ("plant-functional types", PFTs) und die Temperatur aus dem Model fließen in die Berechnung der Biomverteilungen ein, die mit den vorhandenen Pollendaten verglichen werden. Außerdem wird ein Modellvergleich für das HE1 durchgeführt und das UVic ESCM mit dem "Community Climate System Model version 3" (CCSM3) verglichen.

Im UVic ESCM wird das HE1-Klima durch Zufuhr von zusätzlichem Süßwasser aus dem Sankt-Lorenz-Strom in den Nordatlantik simuliert. Sie verursacht eine Verlangsamung der AMOC und damit ein kühleres Klima im Nordatlantik und ein wärmeres Klima im Südatlantik. Diese "Oberflächentemperaturwippe" zwischen der nördlichen Hemisphäre und der südlichen Hemisphäre führt zu einer Südwärtsverschiebung der ITCZ. Das simulierte trockenere Klima während des HE1-Ereignisses verursacht nördlich des Äquators eine verstärkte Wüstenbildung sowie einen Rückgang des Laubwaldes in Westafrika und dem nördlichen Südamerika. Eine Übereinstimmung zwischen dem simulierten HE1 und den Pollendaten besteht zwischen dem tropischen Afrika und dem nördlichen Südamerika. Hingegen zeigt das Modell Schwächen in der Beschreibung der Savannen und Graslandschaften im westlichen tropischen Südamerika. Davon abgesehen sind die simulierten Biomverteilungen für das vorindustrielle Klima und das Klima der letzten Eiszeit ähnlich, mit Ausnahme des tropischen Nordafrikas (der Sahel-Region), des westlichen Südamerikas und des zentralen Nordamerikas. Diese Regionen haben ein wärmeres und feuchteres Klima während der vorindustriellen Periode im Vergleich zum letzten glazialen Maximum. Daher ist der tropische Regenwald und die

Savanne in der vorindustriellen Periode verbreiteter, während der gemäßigte Regenwald und die Grassavanne im letzten glazialen Maximum ausgeprägt vorkommen. Die detaillierten Ergebnisse werden in Kapitel 3 dargestellt. Die AMOC verstärkt sich in unserem BA-Ereignis-Experiment durch die Anwendung von zwei Mechanismen: durch Zufuhr von Süßwasser in den Südlichen Ozean unter den gegenwärtigen Klimabedingungen und durch Entzug von Süßwassers aus dem Nordatlantik vor dem Hintergrund glazialer Klimabedingungen. Beide Mechanismen erzeugen ein wärmeres Klima im Nordatlantik und ein kühleres Klima im Südatlantik und verursachen eine Nordwärtsverschiebung der ITCZ. Diese Simulationen deuten darauf hin, dass während des BA-Ereignisses die Grassavanne, der boreale Wald und der gemäßigte Regenwald in Europa und Nordamerika vorkommen können. Die Grassavanne an der Westküste von Nordamerika stimmt mit den terrestrischen Aufzeichnungen des Walker Lake überein, welche überwiegend xerophytisches Buschland aufgrund des trockenen Klimas zeigen. Eine weitere Übereinstimmung ist im Südwesten Europas und im Mittelmeergebiet zu finden, welche überwiegend einen Steppenwald aufzeigen. Das Model kann jedoch nur unvollständig den gemäßigten Wald im Südwesten von Nordamerika und Südeuropa simulieren. Detaillierte Ergebnisse werden in Kapital 4 dargestellt.

Der Modellvergleich zeigt, dass auch das UVic ESCM mit seiner vereinfachten atmosphärischen Komponente die Auswirkungen einer Verschiebung der ITCZ aufzeigen kann. Ausgeprägte tropische Niederschlagmuster finden sich dagegen nur im CCSM3, das die atmosphärischen Prozesse deutlich besser repräsentiert. Trotzdem sind die Änderungen der tropischen Vegetationsbedeckung während des HE1-Experiments in beiden Modellen ähnlich. Die Grasbedeckung vergrößert sich im tropischen Nordafrika, und die Baumbedeckung wird im tropischen Nordwestafrika und Südamerika reduziert. Die Übereinstimmungen und Abweichungen zwischen den Modellergebnissen und den Pollendaten sind unterschiedlich, aber beide Modelle stimmen bezüglich äquatorialem Westafrika und Südamerika überein. Die detaillierten Ergebnisse sind in Kapitel 5 zu finden.

Zusammenfassend kann diese Untersuchung die Klima- und Vegetationsänderungen in den Tropen und in den Regionen um den Atlantischen Ozean aufgrund abrupter Klimaänderungen während der letzten glazialen Periode darlegen und erklären. Weiterhin liefert der direkte Vergleich zwischen Modellergebnissen und Pollendaten einen neuen Einblick in das Potential von Proxydaten-Model-Vergleichen.

Chapter 1

Introduction

1.1 Motivation of study

Over the past decades the public has seen that modern climate is not as stable as it might have thought. As a result of this, public awareness of the possibility that global warming may lead to abrupt climate change is growing. Abrupt climate change may be defined as large changes in climate taking place within such a short period of time that adaptation is difficult (e.g., thirty years, Clark et al., 2002b) and often developing more rapidly than the initial forcing (e.g., Rahmstorf, 2002; Alley et al., 2003). It is further understood that this kind of climate behaviour can occur when the climate system crosses a critical threshold, defined as the limit between two different climate states (National Research Council, 2003). It has been asserted that abrupt climate change is unlikely to occur in the near future (IPCC, 2007), but understanding the phenomenon might prevent severe future consequences for humans and natural ecosystems.

Heinrich events (HEs) are one of the abrupt climate changes (Bond et al., 1993; Broecker, 1994) that were recorded in high-latitude records from the last glacial (MIS 2-4, MIS = Marine Isotope Stage; 71-14.5 ka BP, ka BP = thousands of years before present), and the most recent of the HEs is the Heinrich event 1 (HE1, ca. 16 – 18 ka BP). The HEs are characterized by large iceberg discharges recorded in North Atlantic Ocean sediments (Heinrich, 1998; Hemming et al., 2004), coinciding with a strong reduction in sea-surface salinity (Bond et al., 1993) and sea-surface temperature (SST) in the North Atlantic Ocean on a centennial time scale (e.g., Sarnthein et al., 2001), and they are ended by abrupt warming, taking place within decades (Cortijo et al., 1997). Although these records are taken from the North Atlantic Ocean, it is possible that changes also occurred in other regions, e.g. in the tropics or even over the entire globe, and that the changes were not confined to climate, but might also have influenced vegetation patterns since vegetation and climate are tightly coupled.

Regarding the tropics, the HE1 period is linked to a southward shift of the Intertropical Convergence Zone (ITCZ) and its associated rainbelt (e.g., Behling et al., 2000). The records from the region around the Atlantic Ocean show, e.g. in northern tropical South America (Cariaco Basin, González et al., 2008), decreased rainfall and humidity, and therefore more open vegetation during HEs. In southern tropical South America (northeast Brazil, Ledru et al., 2001; Jennerjahn et al., 2004; Dupont et al., 2009) on the other hand, the records show increased rainfall associated with an increase in vegetation cover. Furthermore, the climate and vegetation cover during the HE1 period give contrasting signals for tropical Africa as compared to tropical South America. Vegetation records from southwest equatorial Africa (Angola) suggest a different response of the vegetation cover as compared to South America and northwest equatorial Africa (Dupont and Behling, 2006), and these differences in behaviour are not yet understood. Moreover, a new compilation of pollen records from the tropics and subtropics around the Atlantic Ocean during the last glacial period, which has potential to dechiper these differences, has been well documented (Hessler et al., 2010; Jiménez-Moreno et al., 2010; Fletcher et al., 2010).

Recent coupled ocean-atmospheric modelling studies (e.g., Ganopolski and Rahmstorf, 2001; Claussen et al., 2003; Timmermann et al., 2005; Flückiger et al., 2006; Kageyama et al., 2010; Merkel et al., 2010) have replicated abrupt climate change using freshwater hosing experiments in a glacial climate and they have also begun to investigate the impact of abrupt climate change. The understanding of the response of vegetation and climate in the tropics around the Atlantic Ocean during abrupt climate change is very limited, however.

For the above reasons, this modelling study has aimed for a better understanding of: (1) how the abrupt climate change signals in the North Atlantic region can be transmitted and influence the low-latitude ocean-atmosphere system, (2) the physical mechanism of the tropical rainbelt as a potential driver for influencing tropical vegetation and how it is connected to abrupt climate change in the North Atlantic region, and (3) the possibility of comparing model results with available pollen records for the period around the changes of HE1. Indeed, by incorporating past climate modelling of the HEs into climate and vegetation reconstruction, the responses of changing climate and vegetation cover can be assessed, and hence this cooperative study can be valuable for both the modelling and reconstruction communities.

1.2 Tropical climate and vegetation in the Heinrich events

Paleoclimatic records show that HEs are associated with major abrupt cooling events and coincide with a global or at least hemisphere-wide climatic footprint (Bond et al., 1993; Grimm et al., 1993). An abrupt cooling in Greenland during these periods (as well as during the Dansgaard-Oeschger or D-O events, Dansgaard et al., 1993; Bond et al., 1993) is suggested by Greenland ice core ($\delta^{18}O$) records. Apparently, Antarctic ice core records exhibit less abrupt, smaller amplitude millennial climate changes (Clark et al., 2007) as represented by A-events (Fig. 1.1).

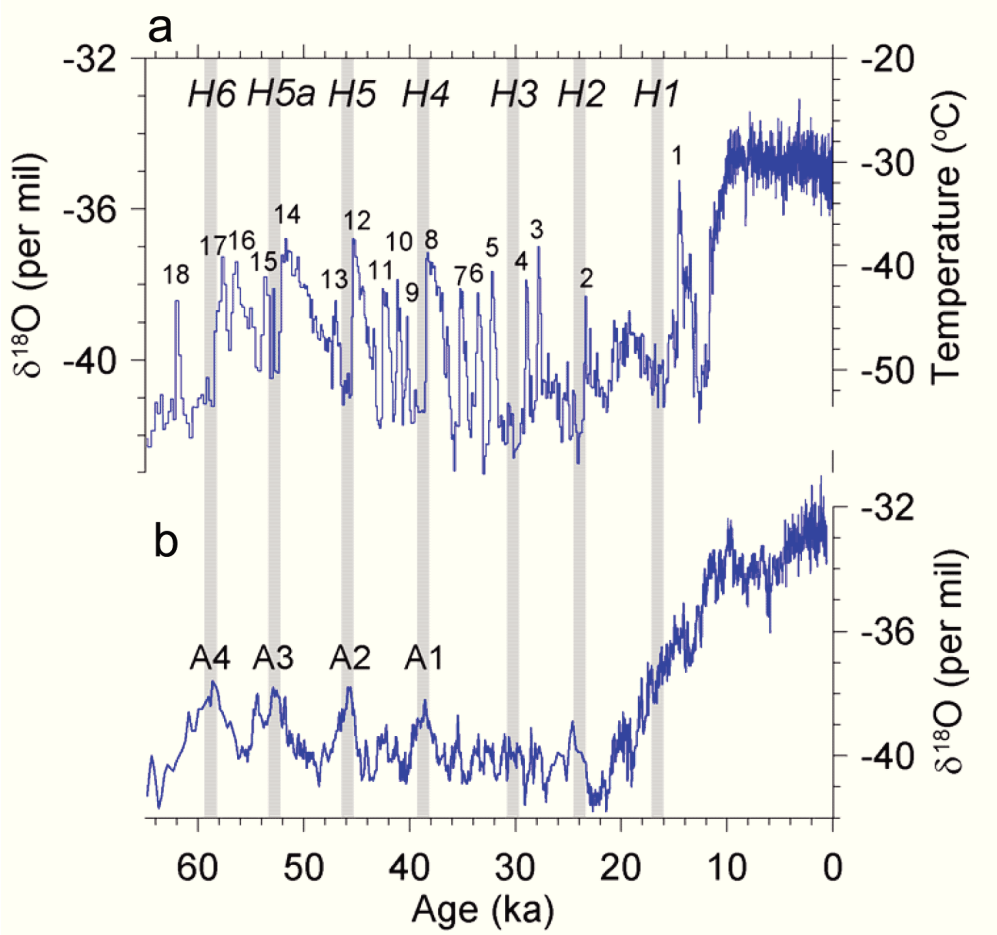

Figure 1.1 Records of $\delta^{18}O$ in glacial ice showing typical climate changes for the interval from 65,000 years ago to the present (a) from a Greenland ice core (GISP2) showing eighteen warm peaks associated with D-O events (Grootes et al., 1993; Stuiver and Grootes, 2000), (b) from Antarctica (Byrd, Johnsen et al., 1972; Hammer et al., 1994) showing four Antarctic warm events identified as A1-A4. The Heinrich events are denoted by gray bars; $\delta^{18}O$ is a proxy for air temperature, with a more positive value corresponding to a warmer temperature (Cuffey and Clow, 1997). *From Delworth et al. (2008).*

Synchronization of Greenland and Antarctic ice core records (e.g., Blunier et al., 1998; Blunier and Brook, 2001; EPICA Community Members, 2006) suggests a see-saw relationship between temperatures of the Northern and Southern Hemispheres, where

the thermal contrast between hemispheres is greatest at the time of the Heinrich events (Fig. 1.1).

The strong cooling of HE is hypothesized to originate from a disturbed ocean circulation, weakened by the meltwater from the armadas of icebergs released during the event (Bond et al., 1993; Broecker, 1994; McMannus et al., 2004; Sakai and Peltier, 1995). According to Alley and MacAyeal (1994) the Laurentide ice sheet could have contained enough detritus to account for all the ice rafted detritus (IRD) of a Heinrich event. However, some of the IRD has an Eurasian origin; according to Hemming (2004), this holds for HE1, HE2, HE4 and HE5.

During the HEs in the North Atlantic Ocean, coeval events in the tropics were recorded, although marine and terrestrial records show climatic responses to the HEs that differed from one place to another, either in signal strength or in spatial distribution. This is especially true of equatorial South America, where wetter and drier climates were recorded asynchronously in its northern and southern parts (Arz et al., 1998; Behling et al., 2000; González et al., 2008), with vegetation cover showing similar response. This correlation links to the ITCZ southward shift hypothesis, which suggests that during a HE, the tropical rainbelt migrated southward, resulting in locations south of the Equator becoming wetter than locations north of the Equator (e.g., Chiang and Koutavas, 2004). This also documented in other records, e.g. datasets from northern tropical Australia suggest a wetter climate during HEs (Turney et al., 2006; Muller et al., 2008), while the Arabian Peninsula had an unusually dry climate (Ansari and Vink, 2007). Moreover, records from around HE1 show an arid and dry climate in equatorial northern Africa (western Sahel – Mulitza et al., 2008; Tjallingii et al., 2008) and a low SST in equatorial southern Africa (Angola), where an increase in mountain forest pollen was also recorded (Dupont et al., 2008).

There are compilations of well-documented pollen records from the tropics and sub-tropics around the Atlantic Ocean covering the time period of the last glacial (Hessler et al., 2010; Fletcher et al., 2010; Jiménez-Moreno et al., 2010). From this vegetation dataset it can be seen that the vegetation response to the abrupt climate change varied from one area to another (Fig. 1.2). As an example, during the first Heinrich event (HE1, 18–16 ka BP) grassland, shrubland, and savannah were predominantly recorded in eastern tropical Africa where a dry climate dominated, warm-temperate forest was recorded in western tropical Africa (present-day Angola), and tropical forest was recorded in sites in Ivory Coast and Cameroon. Records from South America show a

wetter vegetation (e.g., tropical and warm-temperate forest) in northeastern Brazil, while Colombia (northwestern South America) was predominantly covered by savannah and grassland (Hessler et al., 2010). Meanwhile, during the Bølling-Allerød (BA) warm interval following HE1, boreal or warm-temperate forest became dominant in southwestern North America, which indicates a warm and wet climate (Jiménez-Moreno et al., 2010). Records from Europe show that the continent was covered by warm-temperate forest, which also corresponds to a relatively warm and humid climate (Fletcher et al., 2010).

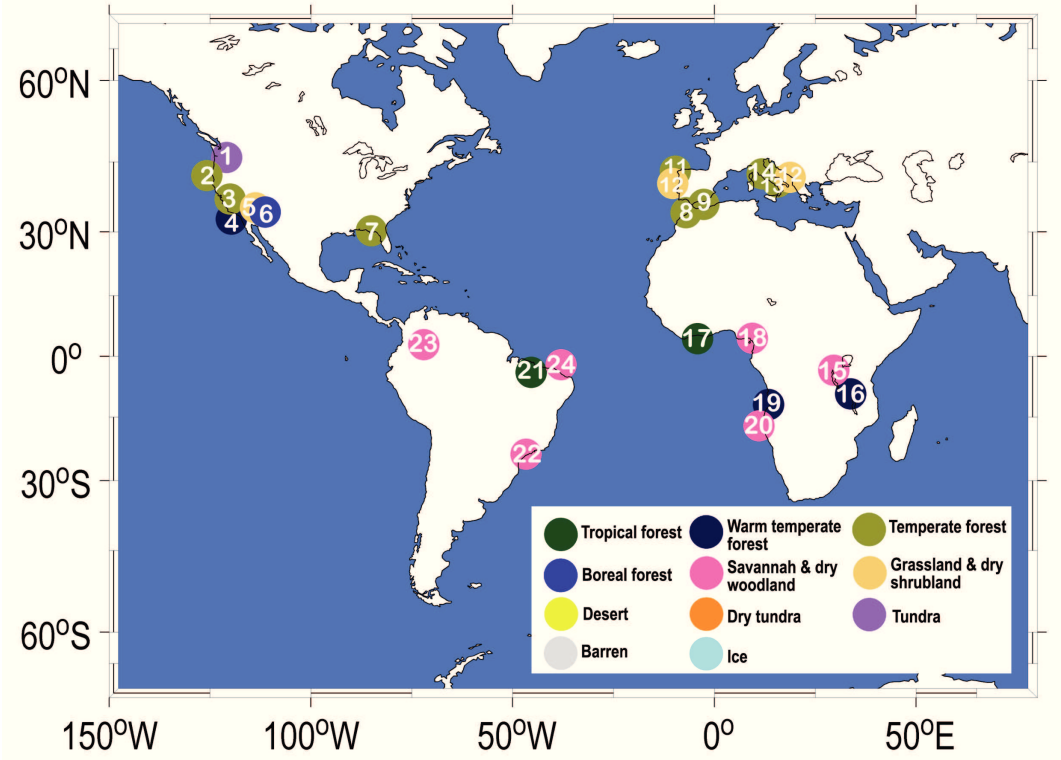

Sites:

1. Carp Lake
2. EW-9504-17PC
3. ODP 893A
4. F2-92-P29
5. Walker Lake
6. Potato Lake
7. Camel Lake
8. ODP site 976
9. MD95-2043
10. MD95-2039
11. MD99-2331
12. Lago Grande di Monticchio
13. Valle de Castiglione
14. Lagaccione
15. Kashiru Bog
16. Lake Masako
17. KS 84-063
18. Barombi Mbo
19. ODP 1078C
20. GeoB 1023
21. Lake Cacó
22. Colônia
23. La laguna
24. GeoB 3910-2

Figure 1.2 Sites of HE1 pollen records in the tropics compiled by Hessler et al. (2010) and BA pollen records in North America and southern Europe compiled by Jiménez-Moreno et al. (2010) and Fletcher et al. (2010). These also include the biome reconstruction of each site as represented by the colour of the circle (see legend for biome distribution).

Attempts of explaining the differences in the climatic responses of the tropics to abrupt climate change have led to some contrasting hypotheses. One of them suggests that the tropics could be a trigger for abrupt climate change. Since the tropical Atlantic SST exerts a strong control on the global atmospheric circulation, shifts in it could lead to changes in the transport of water-vapour from the tropics to extratropics. The net freshwater balance of the Atlantic Ocean would in turn affect the density of the ocean surface waters and the northward penetration of latent heat (e.g. Clement and Cane, 1999; Rahmstorf, 2002). Another possible trigger for abrupt climate change could be a change in the Atlantic Meridional Overturning Circulation (AMOC), which is suggested by rapid variations of the air temperature in Greenland that may reflect sudden changes of the strength of the AMOC (e.g., Broecker et al., 1985, Broecker et al., 1990). A strong AMOC delivers heat to the high latitudes of the North Atlantic Ocean, warming the climate there and also of northwestern Europe; whereas a weak AMOC leads to cooling over the same region. Although it remains to be shown how the AMOC switches from one mode to the other, recent paleoclimate reconstructions have supported this AMOC hypothesis (e.g. McMannus et al., 2004).

1.3 Atlantic Meridional Overturning Circulation (AMOC)

The AMOC is suggested to have large influence on the abrupt climate change during the occurrence of an HE (e.g., Bard et al., 2000). The AMOC is defined as the zonally-integrated, north-south volume flux in the Atlantic Ocean, which in numerical ocean model is typically quantified by a meridional transport stream function. The term AMOC itself does not give us any information on what drives this circulation, even though the related term thermohaline circulation implies a specific driving mechanism related to density (e.g., Wunsch, 2002). The reason it is also called the thermohaline circulation is that it involves warm, saline surface water that flows northward, is cooled and sinks at high latitudes and forms cold, dense North Atlantic Deep Water (NADW) that flows southward, mainly as a deep western boundary current, until it reaches the Southern Ocean, where it mixes with the rest of the World Ocean's water masses (Fig. 1.3). The total AMOC at any specific location may include contributions from the thermohaline circulation, as well as contributions from wind-driven overturning cells, and it is difficult to separate both of these contributions completely from each other. Here we recognize that changes in the thermohaline forcing of the AMOC, and particularly those taking place in the higher latitudes of the North Atlantic Ocean, are ultimately most relevant to the issue of abrupt climate change.

Present-day deep-water formation occurs in the high northern and southern latitudes, which creates the NADW and the Antarctic Bottom Water (AABW), respectively. The AABW is denser than the NADW, which makes the AABW flow under the NADW, and penetrate all the way north to ~30°–50°N. The AABW gets diluted by mixing processes, upwells and then flows southward together with the NADW as a deep western boundary current. In the Atlantic subarctic, Arctic Intermediate Water is formed, and in the Antartic Convergence Zone, Antarctic Intermediate Water (AAIW) is formed (Gordon, 1986).

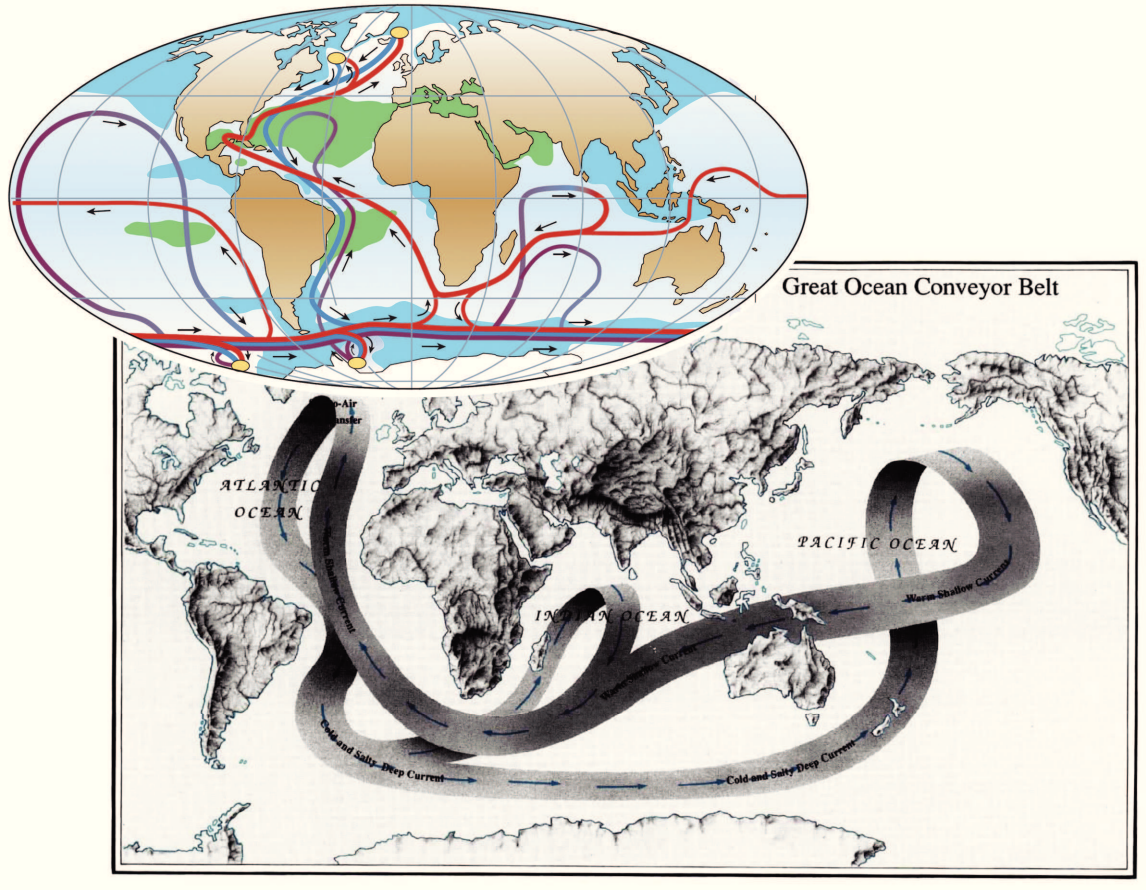

Figure 1.3 The "Great Ocean Conveyor Belt" (Broecker, 1987), a cartoon of the global circulation of ocean waters (illustration by Joe Le Monnier, Natural History Magazine). Superimposed: a highly simplified sketch of the thermohaline circulation. Red denotes near-surface waters that flow towards the main deep-water formation regions (yellow ovals; in the North Atlantic Ocean, the Ross Sea and the Weddell Sea) and recirculate at depth (deep currents denoted in blue, bottom currents in purple). The green shading indicates salinity above 36‰, blue shading denotes salinity below 34‰. *From Rahmstorf (2002)*.

The AMOC of the past is understood by reconstructing ocean temperature and salinity levels from ocean sediment cores using various proxies (e.g. Elliot, et al., 2002). These multiple proxies indicate that the AMOC underwent several large and abrupt changes

between 11.5 – 19 ka BP. Proxies of temperature and precipitation suggest that corresponding changes in climate can be associated with these changes in the AMOC and its attendant feedbacks (Broecker et al., 1985; Clark et al., 2002; Alley, 2007). Many of the AMOC proxy records from marine sediments show that the changes in deep water properties and flow were quite abrupt, but due to slow sedimentation rates and mixing of the sediments at the sea floor these records can only provide an upper bound on the transition time between one circulation state and another. Radiocarbon data from fossil deep-sea corals, however, show that deep water properties can change substantially in a matter of decades (Adkins et al., 1998). Several possible freshwater forcing mechanisms that may explain this variability have been identified, although there are still large uncertainties in understanding the relationship between these mechanisms and changes in the AMOC (e.g., Kuhlbrodt et al., 2007).

The "dynamic proxies" for the AMOC (grain size and Pa/Th ratios of deep-sea sediments) can also be used to reconstruct past AMOC behaviour. Starting at ~19 ka BP and onwards, these proxies show shifts that indicate a reduction in the rate of the AMOC (Manighetti and McCave, 1995; McManus et al., 2004). By ~17.5 ka, the Pa/Th ratios almost reach the ratio at which they are produced in the water column, requiring a slowdown or shutdown of deep water renewal in the deep Atlantic (Siddall et al., 2007). The cause of this extreme slowdown of the AMOC is often attributed to the first Heinrich event, which is connected to a massive release of icebergs from the Laurentide Ice Sheet into the North Atlantic Ocean (Broecker, 1994; McManus et al., 2004; Timmermann et al., 2005). This interval of a collapsed AMOC continued until ~14.6 ka, when the dynamic proxies indicate a rapid resumption of the AMOC to near-interglacial rates. This rapid change in the AMOC was accompanied by an abrupt warming throughout much of the Northern Hemisphere associated with the onset of the Bølling-Allerød warm interval (Clark et al., 2002b). The renewed overturning filled the North Atlantic basin with NADW, as shown by Cd/Ca ratios (Boyle and Keigwin, 1987) and Nd isotopes (Piotrowski et al., 2004) from the North and South Atlantic, respectively.

The possibility of AMOC changes in the coming decades or centuries has been investigated using modelling studies. As stated before, some of the past abrupt climate changes are considered to have resulted from rapid reorganizations of the thermohaline circulation (e.g., Broecker 1997; Clark et al., 2002) that are related to changes in surface buoyancy fluxes, which could also be induced by anthropogenic climate change (Dixon et al., 1999; Gregory et al., 2005). A so-called hosing experiment studies the sensitivity of

the AMOC, and it considers freshwater to be one possible external forcing source. Numerous coupled atmosphere-ocean model experiments have shown that freshwater hosing can trigger a (partial) "shut down" of the meridional overturning circulation (e.g., Sakai and Peltier, 1997; Kageyama et al., 2010; Roche et al., 2010). In these studies, the effect of the freshwater discharge is typically simplified to a homogenous and instantaneous dumping of freshwater on a designated ocean area, broadly corresponding to a region where icebergs melted, e.g., the "Ruddiman-Belt" (between 40°–55°N and 10°–60°W; Ruddiman, 1977), or the Hudson Strait. However, while this working hypothesis is quite simple, it does not explain the cause of the iceberg discharge in the first place. Solving this problem would require precise chronologies of oceanic, atmospheric and ice-sheet events before, during and after the Heinrich events.

1.4 Research objectives

The main objective of this dissertation is to improve the understanding of how the abrupt climate change around HE1 could propagate and influence the climate and vegetation in the tropics. The abrupt climate change itself is tightly connected with the AMOC, which transports a substantial amount of heat from the tropics and the Southern Hemisphere towards the North Atlantic, where it is transferred to the atmosphere. Many paleorecords from different tropical regions indicate abrupt climate changes that are remarkably coherent with the millennial scale of abrupt climate changes recorded in the Greenland ice cores, indicating that changes in the AMOC might have significant global-scale impacts on the tropics.

To cover the main objective, the following research questions are posed:

1. What are the mechanisms in the ocean-atmosphere system that can transmit signals of North Atlantic abrupt climate change to the tropics and influence its vegetation?
2. To what extent can changes in the AMOC through a southward shift of the tropical rainbelt affect tropical vegetation?
3. Can the comparison between model results and pollen reconstructions contribute to identify the limitations of the models ability to simulate the climate system?

In order to answer these scientific questions, several freshwater hosing experiments were conducted using two different climate system models under glacial as well as interglacial climate background conditions. Since both climate system models included a vegetation component, the model results could be compared to pollen data.

1.5 Research approach and chapter outline

This study employs two numerical climate system models to solve the objectives stated in the previous section:

1. It mainly applies the University of Victoria Earth System-Climate Model (UVic ESCM, Weaver et al., 2001), an Earth System Model of Intermediate Complexity (EMIC, Claussen et al., 2002).
2. To enable a model inter-comparison, it also includes results from the Community Climate System Model version 3 (CCSM3, Collins et al., 2006), a comprehensive coupled atmosphere-ocean general circulation model (the low-resolution version of CCSM3, Yeager et al., 2006).

Both models include a Dynamic Global Vegetation Model (DGVM).

This dissertation is divided in seven chapters. The first chapter provides the introduction to this study. The model is described and discussed in Chapter 2, together with a method of comparison between model results and paleovegetation data. Chapters 3, 4, and 5 show the results of this study, divided into three manuscripts. Chapter 3 refer to the manuscript published in Climate of the Past in 2012, entitled *Tropical climate and vegetation changes during Heinrich Event 1: a model-data comparison*. This manuscript presents the results of the water hosing experiments of the HE1 under glacial and interglacial climate background conditions. The responses of climate and vegetation in the tropical region around the Atlantic Ocean were analysed, and furthermore, the simulated vegetation was compared with available pollen records. The results of the simulation of the abrupt warming of the BA event, following the HE1 are presented in the second manuscript (Chapter 4) with the title *Climate and vegetation changes around the Atlantic Ocean resulting from changes in the meridional overturning circulation during deglaciation*. They include the response of climate and vegetation to various water hosing experiments where the source of freshwater not only come from the North Atlantic Ocean, but also from the Southern Ocean. The third manuscript (Chapter 5), *Tropical vegetation response to Heinrich Event 1 as simulated with the UVic ESCM and CCSM3*, addresses the comparison of tropical climate and vegetation responses during HE1 between two models, the UVic ESCM and the CCSM3. Chapter 6 is a summary of this study, while conclusions and suggestions for future research are provided in Chapter 7. Appendix contains a flow chart for estimating the biome distribution from the output of the UVic ESCM and the CCSM3, respectively.

Chapter 2

Methodology

2.1. The UVic ESCM

The UVic ESCM is an EMIC (Claussen et al., 2002), and most of the results discussed in this study are from UVic ESCM simulations. The model core is described in detail by Weaver et al. (2001), however, this study uses the more recent UVic ESCM version 2.8, which includes a three-dimensional general ocean circulation model, a two-dimensional atmospheric model, a thermodynamic and dynamic sea ice model, and also a simple land surface model coupled with a DGVM. The model has a global domain, and all of the components share a similar horizontal grid resolution, 3.6^{o} in longitude and 1.8^{o} in latitude. The model has been calibrated and validated under present-day (Weaver et al., 2001) and various past climate conditions (e.g., Meissner et al., 2003). The model has also been used in freshwater perturbation experiments (e.g., Schmittner et al., 2002b; Weaver et al., 2003; Trevena et al., 2008) and to investigate vegetation responses during glacial inception (Meissner et al., 2003). The following sub-sections provide a brief description of the atmospheric, ocean, and land-vegetation components of the UVic ESCM.

2.1.1. The atmospheric model

The atmospheric model in the UVic ESCM is based on a two-dimensional energy-moisture balance model by Fanning and Weaver (1996). The model is based on the vertically integrated energy and moisture balance equations, and hence compressed into a single atmospheric layer. There are two main simplifications in the atmospheric component. Firstly, the prognostic equations for the conservation of momentum are replaced by specified winds derived from the NCEP reanalysis data (Kalnay et al., 1996). Secondly, the atmospheric heat and moisture transports are modelled on diffusion,

although moisture can also be advected by prescribed wind fields. Cloud radiative feedback is not included in the model. Sea-level, air temperature and specific humidity are the two prognostic variables.

The vertically integrated thermodynamic energy equation can be expressed as

$$\rho_a h_t c_{pa} \frac{\partial T_a}{\partial t} = Q_{HT} + Q_{SW} C_A + Q_{LH} + Q_{LW} + Q_{SH} - Q_{PLW}, \quad (1)$$

where T_a is the sea level air temperature, ρ_a is the air density, h_t = 8.4 km is a constant scale height for thermal energy, and c_{pa} = 1004 $Jkg^{-1}K^{-1}$ is the specific heat capacity of air at constant pressure. Q_{HT} is the heat transport parameterized by Fickian diffusion; Q_{SW} is the incoming shortwave radiation at the top of the atmosphere, with C_A = 0.3, which is a coefficient to parameterized atmospheric absorption; Q_{LH} is the latent heat flux into the atmosphere; Q_{LW} is the net upward longwave radiation flux into the atmosphere; Q_{SH} is the sensible heat flux calculated from a bulk formula; Q_{PLW} is the outgoing planetary longwave radiation that parameterizes the water vapour feedback and the radiative forcing associated with changes in atmospheric CO_2. All these terms are sources and sinks of atmospheric heat, which are expressed in the right-hand side of Eq. 1.

Meanwhile, the vertically integrated moisture balance equation can be expressed as

$$\rho_a h_q \left\{ \frac{\partial q_a}{\partial t} - \nabla \cdot (\kappa \nabla q_a) \right\} = \rho_o (E - P), \quad (2)$$

where h_q = 1.8 km is a constant scale height for specific humidity; q_a is the surface specific humidity; κ is an eddy diffusivity; E is evaporation or sublimation which is calculated from a bulk formula, and P is precipitation that occurs in the form of rain or snow when the relative humidity exceeds 90%.

Furthermore, a dynamic wind feedback parameterization allows for a wind perturbation to be applied when simulating past climates. With respect to orbital forcing and the atmospheric CO_2 concentration, the model resolves the annual cycle, the incoming solar radiation at the top of the atmosphere depends on orbital parameters, and the atmospheric CO_2 forcing is applied to the model as a decrease in outgoing longwave radiation.

2.1.2. The ocean model

The ocean component is the Modular Ocean Model (MOM, version 2.2, Pacanowski, 1995), which solves the three-dimensional primitive equations for an ocean general circulation model (GCM). It calculates the velocity in the zonal, meridional and vertical directions as well as the three-dimensional tracer field of temperature and salinity. Density is defined as a nonlinear function of temperature, salinity and pressure.

The momentum and tracer equations are:

$$\frac{\partial u}{\partial t} = \frac{-1}{\rho_o r_e \cos\phi}\frac{\partial p}{\partial \lambda} + \frac{\partial}{\partial z}\left(A_v \frac{\partial u}{\partial z}\right) + \Im\left(A_h, u, v\right) + \frac{uv\tan\phi}{r_e} + fv - L(u), \tag{3}$$

$$\frac{\partial v}{\partial t} = \frac{-1}{\rho_o r_e}\frac{\partial p}{\partial \phi} + \frac{\partial}{\partial z}\left(A_v \frac{\partial v}{\partial z}\right) + \Im\left(A_h, v, -u\right) - \frac{u^2\tan\phi}{r_e} - fu - L(v), \tag{4}$$

$$\frac{\partial T}{\partial t} + L(T) = \frac{\partial}{\partial z}\left(k_v \frac{\partial T}{\partial z}\right) + \nabla\left(k_h \nabla T\right), \tag{5}$$

$$\frac{\partial S}{\partial t} + L(S) = \frac{\partial}{\partial z}\left(k_v \frac{\partial S}{\partial z}\right) + \nabla\left(k_h \nabla S\right), \tag{6}$$

$$\frac{\partial w}{\partial z} + \frac{1}{r_e \cos\phi}\left(\frac{\partial u}{\partial \lambda} + \frac{\partial\left(v\cos\phi\right)}{\partial \phi}\right) = 0, \tag{7}$$

$$\frac{\partial p}{\partial z} = -g\rho, \tag{8}$$

where u, v and w are the velocity components in the zonal, meridional and vertical directions, respectively; f is the Coriolis parameter; r_e is the radius of the earth; p is the pressure; ρ_o or ρ is the representative density of sea water; t is time; g is acceleration due to gravity; A_v = 1 x 10^{-3} m^2 s^{-1} is the vertical eddy viscosity; $\Im$ is the horizontal Laplacian operator; A_h = 2.5 x 10^5 m^2 s^{-1} is the horizontal eddy viscosity; L is the advection operator; T is potential temperature and S is salinity.

The ocean model has nineteen vertical levels that increase parabolically in thickness from 50 m at the surface to 518 m at the deepest level. A parameterization of sub-grid scale mixing is used to capture the effect of mesoscale eddies, in which diffusion occurs along and across isopycnals (Gent and McWilliams, 1990). A brine rejection parameterization during sea-ice formation (Duffy and Calderia, 1997) is included, and

improves intermediate water properties (Duffy et al., 1999, 2001). Deep sills in ocean bathymetry are modified, which deepens the Denmark Strait to 700 m and removes Iceland. This influences the flow over deep sills, which is important for the process of the NADW formation. Hence the northward heat transport in the North Atlantic Ocean improves (Weaver et al., 2001).

2.1.3. The land surface and dynamic vegetation models

The land model of the UVic ESCM is a single soil-layer version of the Met Office Surface Exchange Scheme (MOSES, Cox et al., 1999), and it supports the dynamic vegetation model Top-down Representation of Interactive Foliage and Flora Including Dynamics (TRIFFID). There are nine surface types identified in the MOSES model, five of them are vegetation types simulated in TRIFFID, i.e. broadleaf trees, needleleaf trees, C3 grasses, C4 grasses and shrubs, in addition to urban, inland water, bare soil and ice (Essery et al., 2001).

Diffusion of soil moisture in the land model is calculated within four layers of soil, and soil water phase change effects were ignored. The thicknesses of the soil layers are 0.1, 0.25, 0.65, and 2.0 m, from the surface downwards. Total moisture flux in the land surface depends on evaporation from the canopy store, vegetation transpiration, bare soil evaporation and sublimation from the snow surface. The key components of MOSES have been validated independently, e.g. the soil thermodynamic and phase change modules (Christensen and Cox, 1995), and the canopy conductance and photosynthesis modules (Cox et al., 1998). Moreover, this version of MOSES, as well as its coupling to the UVic ESCM, is described extensively in Meissner et al. (2003).

The Hadley Centre's TRIFFID model (Cox, 2001) is coupled interactively with the UVic ESCM (as described in Meissner et al., 2003). It simulates the plant distribution and soil carbon based on CO_2 fluxes, which induces changes of the land-atmosphere interaction. The surface CO_2 fluxes depend on photosynthesis and plant respiration, which are calculated in the MOSES model. The plant distribution is explicitly updated in the TRIFFID model. The PFT coverage updates are based on the availability of net carbon and the competition among other plant types using a Lotka-Voltera approach (Hughes et al., 2004). Furthermore, soil carbon increases by litter falls such as a leaf drop, and large scale disturbances which reduce the vegetated area. The soil carbon is returned to the atmosphere through microbial respiration, which depends on soil moisture and

temperature. A carbon cycle module has been included in the TRIFFID model, although this study did not activate the ocean carbon component.

2.2. Plant functional types and biomes

The vegetation module is included in paleoclimatic simulations, in order to capture biophysical and biogeochemical feedback mechanisms affecting climate change. It also allows for the validation of models against palaeo-ecological proxy data (e.g., pollen). The vegetation patterns in the model are represented as the distribution of either plant functional types (PFT) of biomes.

Campbell (1996) defines biomes as the world's major (plant and animal) communities, which are classified according to the predominant vegetation, and characterized by adaptations of organisms to that particular environment. Common biomes that can be found in the present include: tropical rainforest, temperate forest, conifer forest (taiga), shrubland, grassland, desert, savannah, and wetlands. For example, land biomes are characterized by the dominant vegetation expressed in wide categories, such as tropical rain forest, grassland, or tundra. The definition of biomes usually does not take into account the kind of human land use that takes place within their boundaries. Biomes may, however, be considered as indicators of what agricultural or forest practice can potentially be carried out in a given region (Cramer, 2002).

PFTs are groups of plant species, where each functional group comprises plant types which display similar behaviour in a given process (Prentice et al., 1992). They were developed to parameterize the interaction between land and vegetation in coupled earth-climate models. Moreover, a classification based on the biome distribution can be difficult when photosynthesis and carbon cycle mechanisms are included in the land model. Savannah, for example, is a mixed biome which contains both grasses and trees. This leads to difficulties when a separation has to be created based on physiological differences between grasses and trees, which have different rooting depths and different ways to carry out photosynthesis. It is also difficult to classify grassland biomes, because photosynthesis and stomatal conductance differ between C3 and C4 plants. Therefore, a combination of PFTs can be found in any one biome. Defining vegetation cover as PFTs is also necessary for reducing complexity and undefined characteristics of vegetation diversity in functions and structures. Consequently, long-term simulations of coupled paleoclimate-vegetation models mostly use PFTs to represent vegetation cover, although

each model is formulated differently with respect to the number and definition of the PFTs.

2.3. A scheme of biome distribution estimation

For this study, a comparison of vegetation distribution between model results and paleovegetation data was unavoidable. Recent available paleovegetation data is distributed into biomes, which is different from the distribution of vegetation in the models. A comparison between model and data becomes possible if vegetation covers in both model and data are ordered into similar types, either as biomes or as PFTs. This study generates the biome distribution from model outputs, either by combining the PFT fraction and environmental constraints (e.g., Roche et al., 2007), or by limiting the PFT fraction (e.g., Crucifix et al., 2005) combined with the air surface temperature (e.g., Schrugers et al., 2006). However, each model defines the PFTs differently, which influences the estimation of biome distribution.

The biome distribution estimation scheme for our TRIFFID output is inspired by the BIOME 4 model (Kaplan et al., 2003). The BIOME 4 model is developed from the biome model approach by Prentice et al. (1992). It is a coupled biogeography and biogeochemistry model, which predicts twenty-eight major global biomes. This model generates the PFTs based on long term averages of monthly mean temperature, sunshine, and precipitation that are used to calculate distinctive bioclimatic parameters, e.g., the temperature of the coldest month (Tc), the temperature of the warmest month (Tw), annual moisture availability, and the number of growing degree-days above 0ºC and 5ºC (GDD0 and GDD5, respectively). In addition, the model also requires soil texture and depth information to determine water holding capacity and percolation rates, while the CO_2 rates are specified. Moreover, each PFT in the model is assigned bioclimatic limitations, which determine whether it can be present in a given cell or not. To identify the biome distribution for a given grid cell, the model ranks the tree and non-tree PFTs of the calculated grid cell. The ranking also defines the computed biogeochemical variables, which includes the Net Primary Productivity (NPP), the Leaf Area Index (LAI) and the annual mean soil moisture. A combination of PFT ranking and biogeochemical variables leads the cell to be assigned to one of the twenty eight biomes defined in the model.

The biome distribution estimation scheme is built by combining the information from the BIOME4 model and other studies (e.g., Crucifix et al., 2005; Roche et al., 2007). Our

scheme combines the potential PFTs with environmental limitations. The potential PFTs are classified based on Crucifix et al. (2005), and the environmental limitations are chosen based on the BIOME4 model. A detailed application of this scheme with a comparison between model and paleovegatation data is given in Chapter 3. In Chapter 5, a different earth climate model is used (the CCSM3, Collins et al., 2006), and its output is also converted into a biome distribution. The biome estimation scheme for the CCSM3 output is based on a study by Schrugers et al. (2006), which is limiting the PFT fraction by combining them with the surface temperature.

2.4. Experimental design

In Chapter 3, a detailed freshwater experiment which replicates the HE1 is discussed. The experiment was done by adding freshwater to the mouth of the St. Lawrence River, at a constant rate of 0.1 Sv, for 500 years. The experiment used two different climate background conditions: the last glacial maximum (LGM) and the pre-industrial. The climate background conditions include orbital parameters and atmospheric CO_2 concentrations for each time period.

The experiment concerned with the onset of the BA after the HE1 is reviewed in Chapter 4. It is an extension of a study by Weaver et al. (2003). There are three sets of experiments, with different climate background conditions: the pre-industrial, the LGM and the 16 ka BP period. Each set is calculated in two stages. Firstly, the HE1 climate is simulated by adding freshwater to region in the North Atlantic Ocean, increasingly from 0 to 0.2 Sv. Secondly, the climate after the HE1, with a recovered AMOC, is replicated by adding freshwater linearly from 0 to 1 Sv for 500 years in a region west of West Antarctica. Afterwards, the simulation is continued for 1000 years without freshwater perturbation.

Two climate systems models with atmospheric complexity modules of different complexity are compared in Chapter 5. The purpose of the comparison is to understand the role of atmospheric processes in the tropics during the HE1 including the vegetation response. Each model is applied in a similar manner. The HE1 is replicated by adding freshwater to the Atlantic Ocean at a constant rate of 0.2 Sv for 500 years of simulation, and the LGM climate is used as its background. The model-data comparison does not only cover the tropical region around the Atlantic Ocean, but also extends to tropical Asia.

CHAPTER 2. METHODOLOGY

Chapter 3

Tropical climate and vegetation changes during Heinrich Event 1: a model-data comparison

D. Handiani, A. Paul and L. Dupont
(Published in *Climate of the Past*, doi:10.5194/cp-8-37-2012)

3.1 Abstract

Abrupt climate changes from 18 to 15 thousand years before present (kyr BP) associated with Heinrich Event 1 (HE1) had a strong impact on vegetation patterns not only at high latitudes of the Northern Hemisphere, but also in the tropical regions around the Atlantic Ocean. To gain a better understanding of the linkage between high and low latitudes, we used the University of Victoria (UVic) Earth System-Climate Model (ESCM) with dynamical vegetation and land surface components to simulate four scenarios of climate-vegetation interaction: the pre-industrial era, the Last Glacial Maximum (LGM), and a Heinrich-like event with two different climate backgrounds (interglacial and glacial). We calculated mega-biomes from the plant functional types (PFTs) generated by the model to allow for a direct comparison between model results and palynological vegetation reconstructions.

Our calculated mega-biomes for the pre-industrial period and the LGM corresponded well with biome reconstructions of the modern and LGM time slices, respectively, except that our pre-industrial simulation predicted the dominance of grassland in southern Europe and our LGM simulation resulted in more forest cover in tropical and sub-tropical South America.

The HE1-like simulation with a glacial climate background produced sea-surface temperature patterns and enhanced inter-hemispheric thermal gradients in accordance with the "bipolar seesaw" hypothesis. We found that the cooling of the Northern Hemisphere caused a southward shift of those PFTs that are indicative of an increased desertification and a retreat of broadleaf forests in West Africa and northern South America. The mega-biomes from our HE1 simulation agreed well with paleovegetation data from tropical Africa and northern South America. Thus, according to our model-data comparison, the reconstructed vegetation changes for the tropical regions around the Atlantic Ocean were physically consistent with the remote effects of a Heinrich event under a glacial climate background.

3.2 Introduction

Heinrich events (HE) are associated with abrupt climate changes (Bond et al., 1993; Broecker, 1994) and correlated with a slowdown or collapse of the Atlantic Meridional Overturning Circulation (AMOC) and a reduced formation of North Atlantic Deep Water (NADW) (e.g. Vidal et al., 1997; Cortijo et al., 1997; McManus et al., 2004). They are characterized by distinct layers of ice-rafted debris in ocean sediments, which stem from the melting of large icebergs in the North Atlantic Ocean that originated from the disintegrating Laurentide and Fennoscandian ice sheets (Bond et al., 1992, 1993; Broecker et al., 1992; Grousset et al., 2000; Hemming, 2004). Consequently, these events resulted in ice-sheet thinning and rising sea level (Yokoyama et al., 2001; Chappell, 2002; Flückiger et al., 2006). Currently, it is debated whether the iceberg discharges were the consequence or the cause of a weakened AMOC (Flückiger et al., 2006; Clark et al., 2007), although it is widely accepted that these events impacted the climate of mid- and high latitudes in the Northern Hemisphere (e.g. Schmitter et al., 2002).

The AMOC links climate change in the Northern Hemisphere with that of the Southern Hemisphere. This is expressed in the bipolar seesaw hypothesis, whereby a cooling in the Northern Hemisphere is associated with a warming in the Southern Hemisphere (Broecker et al., 1985). Records from the Southern Hemisphere indicate a higher SST during HE1 (Lamy et al., 2007; Barker et al., 2009), while several modeling studies confirm the importance of this mechanism for regional climate changes during the glacial period (Meissner et al., 2003; Crucifix et al., 2005; Roche et al., 2007). Nevertheless, how cooling in the North Atlantic Ocean and warming in the South Atlantic Ocean during HE1 are linked to changes in the vegetation around the tropical Atlantic has not been sufficiently clarified.

Past studies focusing on processes in the mid- to high latitudes of the Northern Hemisphere successfully attributed abrupt climate change to changes in the AMOC (e.g. Mc-Manus et al., 2004). Other studies suggest that tropical regions are also affected by climate change related to HEs (Arz et al., 1998; Peterson et al., 2000; Altabet et al., 2002). Although it is probably not a driver of abrupt climate change, the tropical climate may react very sensitively to changes in the AMOC and act as an amplifier (Chiang, 2009). The climatic shifts around the tropical North Atlantic Ocean are associated with large changes in the vegetation distribution, which is likely the result of a southward shift of the tropical rainbelt, as indicated by records from the Cariaco Basin (Hughen et al., 2004; Gonzalez et al., 2008), Northeast Brazil (Behling et al., 2000; Ledru et al.,

2006; Dupont et al., 2009), and North West Africa (Mulitza et al., 2008; Hessler et al., 2010). These data emphasize the importance of the tropics and the changes in tropical vegetation during periods of abrupt climate change.

By better understanding the connection between the variability of tropical vegetation and climate changes at high northern latitudes, we may enhance our ability to predict and explain the response patterns of global vegetation to abrupt climate change. Therefore, we want to examine how vegetation around the tropical Atlantic may have responded to changes in AMOC intensity during the HE1 period. Earlier model studies simulated changes during HE1 by perturbing the freshwater budget of the northern North Atlantic Ocean starting from an interglacial or glacial background climate. These studies have addressed several aspects of AMOC changes during the HE1 period such as the response time of the terrestrial biosphere (Scholze et al., 2003), the comparison between numerical model results and a pollen record from the Alboran Sea (Kageyama et al., 2005), the effect on global terrestrial carbon storage (Köhler et al., 2005), and the contribution of the terrestrial and marine carbon cycle (Menviel et al., 2008). Additionally, model studies of the HE1 period by Kageyama et al. (2005) suggest the dominance of grassland in southern Europe (the Mediterranean) due to a lower coldest-month temperature in that area; Menviel et al. (2008) found a change towards drier climate conditions in equatorial and northern South America. However, our understanding is limited of how the vegetation patterns around the tropical Atlantic were affected during the HE1 period.

Tropical vegetation is mostly sensitive to changes in regional precipitation, which are mainly related to shifts of the Intertropical Convergence Zone (ITCZ). The position of the ITCZ over the tropical Atlantic Ocean is, in turn, linked to North Atlantic sea surface temperatures (SSTs) over the last glacial period, as suggested by several proxy studies (e.g. Peterson et al., 2000; Mulitza et al., 2008). During HE1, the northernmost position of the ITCZ likely shifted southward leading to a drier climate in West Africa and northern South America (e.g. Hughen et al., 2004; Menviel et al., 2008). However, Collins et al. (2011) suggest that the tropical rainbelt, which is associated with the yearly migration of the ITCZ, contracted rather than shifted southwards during the HE1 period.

To model the dynamic tropical vegetation response, we used an EMIC containing a Dynamic Global Vegetation Model (DGVM), i.e. the University of Victoria Earth System-Climate Model (UVic ESCM, version 2.8, cf. Weaver et al., 2001). We considered the

effect of a slow-down of the AMOC for two different background climate states, corresponding to the pre-industrial and the Last Glacial Maximum (LGM, about 23 to 19 kyr BP) time periods. To simplify the comparison between the model results and paleovegetation reconstructions, we computed the biome distribution from the simulated plant-functional type (PFT) coverage and climate. Up until now, only a few studies have attempted to calculate the biome distribution (Crucifix et al., 2005; Roche et al., 2007) and none as yet has compared the model results with data from the Atlantic tropical region during HE1.

The paper is arranged accordingly. The model and biome analysis method is described in Sect. 3.3 together with the experimental setup. In Sects. 3.4 and 3.5, we present the results of the simulations for the pre-industrial, LGM and HE1 time periods in terms of the change in climate and biome distribution in the tropical Atlantic region, and we then compare them to paleoclimate proxies and paleovegetation records. Section 3.6 discusses the results, also in comparison to other Atlantic regions and in relation to the climate state background. Summary and conclusions appear in Sect. 3.7.

3.3 Methods and experimental design

3.3.1. The UVic ESCM and TRIFFID DGVM

The UVic ESCM incorporates an energy-moisture balance atmospheric model (Fanning and Weaver, 1996), a dynamic global vegetation model (Cox, 2001), a three dimensional ocean general circulation model (Pacanowski, 1995), and a dynamic-thermodynamic sea ice model (Hibler, 1979; Hunke and Dukowicz, 1997; Bitz et al., 2001). The model has a grid cell resolution of $3.6^{o} \times 1.8^{o}$ (longitude×latitude) with one vertically-averaged layer in the atmospheric model, and 19 vertical levels in the ocean model. The annual cycle of incoming solar radiation (insolation) for present and past orbital configurations is included as an external forcing factor (Berger, 1978). In addition, we use a mean-monthly wind stress climatology created from daily reanalysis data from 1958–1998 (Kalnay et al., 1996) to force the ocean and sea-ice components of the model.

The UVic ESCM also contains a land surface scheme MOSES 2 (Cox et al., 1999) and a DGVM called TRIFFID (Top-down Representation of Interactive Foliage and Flora Including Dynamics – Cox, 2001) as described by Meissner et al. (2003). The TRIFFID model calculates the plant distribution based on the CO_2 fluxes between land and atmosphere and as represented by the structure and coverage of five Plant Functional Types (PFTs) and soil carbon storage. The CO_2 flux depends on climate and the CO_2

concentration gradient between the land and atmosphere, which is calculated in MOSES 2. Any change in the CO_2 flux causes corresponding changes in PFT coverage and structure. In TRIFFID, carbon fluxes in each PFT are derived from the photosynthesisstomatal conductance model developed by Cox et al. (1999), which utilizes an existing model of leaf-level photosynthesis in C_3 and C_4 plants (Collatz et al., 1991). In TRIFFID and MOSES 2, five PFTs (broadleaf trees, needleleaf trees, C_3 grasses, C_4 grasses, and shrubs) serve as vegetated land cover types. Non-vegetated land cover types consist of bare soil, inland water, and continental ice (Cox, 2001). To simplify the comparison of the TRIFFID output with available paleovegetation reconstructions, we developed an algorithm to compute biomes from a combination of PFTs and climate model output. For a full description, see the biome analysis Sect. 2.3.

3.3.2. Simulation design and boundary conditions

The control simulation (PI_CNTRL) was forced by boundary conditions characteristic of the pre-industrial period with an atmospheric CO_2 concentration of 280 ppm, a solar constant of 1365 Wm^2, a present-day wind field, orbital parameters from 1950 AD, and ice sheet topography and vegetation distribution from modern observations (Meissner et al., 2003), and it was integrated over a period of 2000 years to reach an (quasi-) equilibrium state. The equilibrium LGM run used the orbital parameters for 21 kyr BP, an atmospheric CO_2 concentration of 200 ppm and the ICE-5G ice-sheet reconstructions for the last glacial maximum (Peltier, 2004); it was integrated over the same period of time.

To investigate Heinrich like-climate (HE1) conditions and analyze the vegetation distribution in the tropics, we forced the UVic ESCM by adding freshwater in the North Atlantic Ocean using last glacial maximum (or glacial, HE1 GL) and pre-industrial (or interglacial, HE1 IGL) boundary conditions. The two HE1 experiments started from an equilibrium state (i.e., the HE1 GL from the LGM equilibrium simulation, and HE1 IGL from the PI_CNTRL simulation). In each HE1 simulation, we added freshwater to the North Atlantic region at the St. Lawrence River mouth (Fig. 3.1 region A) during a 500 year period at a constant rate of 0.1 Sv (1 Sv = 10^6 m^3 s^{-1}) (cf. Hemming, 2004). These two HE1 simulations with two different climate backgrounds were used to reveal differences in vegetation response with respect to a reduced and a collapsed AMOC. An overview of all simulations in this paper is given in Table 3.1. For all analyses, we used the mean-annual results for analyzing the climate conditions and the vegetation distribution.

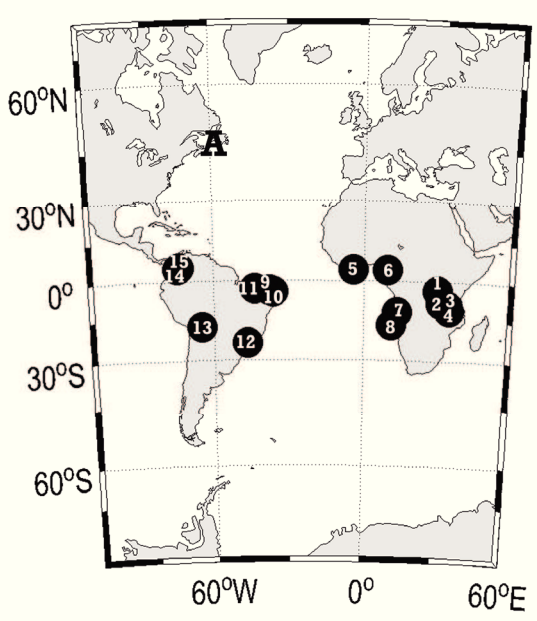

Figure 3.1 Freshwater discharge location for our Heinrich Event 1 climate-like simulations (St. Lawrence River, location A) and paleovegetation proxy locations (black circles, numbers refer to the sites listed in Table 3.4) covering the Heinrich Event 1 period from Hessler et al. (2010) in tropical Africa and South America.

Table 3.1 Boundary conditions (including atmospheric CO_2 in atmosphere, amount and location for freshwater perturbation) and simulation design for all simulations analysed in the present paper.

Simulation	Orbital parameter	CO_2 concentration	Freshwater anomaly amount (Sv)	Freshwater anomaly Location	Years simulation
Equilibrium					
PI_CNTRL	Pre-industrial	280			2000
LGM	21 kyr BP	200			2000
Heinrich event					
HE1_IGL	Pre-industrial	280	0.1	A	500
HE1_GL	21 kyr BP	200	0.1	A	500

3.3.3. Biome analysis from TRIFFID

In order to compare the model output with paleovegetation reconstructions, we generated vegetation distributions in terms of biomes using the PFT coverage and temperatures from the UVic ESCM output. The simulated atmospheric temperature was used to calculate the parameters constraining biomes, such as temperature of the coldest month (Tc), temperature of the warmest month (Tw), and the number of growing degree-

days above 0ºC and 5ºC (GDD0 and GDD5, respectively). These constraints were chosen based on the definition of biomes in the BIOME 4 model (Kaplan et al., 2003).

Table 3.2 Distribution of dominant PFTs which is based on the percentage of PFT coverage.

Dominant PFTs or PFTs mixture	PFT coverage
	BL, NL, SH, C_3, C_4 over 50 %
Broadleaved trees (BL)	BL $\geq$ 50 %
Needleleaved trees (NL)	NL $\geq$ 50 %
Shrubs (SH)	SH $\geq$ 50 %
C_3 grass (C_3)	$C_3 \geq$ 50 %
C_4 grass (C_4)	$C_4 \geq$ 50 %
	BL, NL, SH, C_3, C_4 less than 50 %
Mixed trees	BL + NL $\geq$ 50 %
Mixed vegetation (without trees)	SH + C_3 + $C_4 \geq$ 50 %
Open vegetation	20 % $\leq$ BL + NL + SH + C_3 + $C_4 \geq$ 50 %
Barren soil	BL + NL + SH + C_3 + C_4 < 20 %

The dominant PFT in each grid cell is evaluated based on the percentage of PFT coverage. If the percentage of PFT coverage is over 50%, the PFT potential is set equal to the dominant PFT (broadleaved trees, needleleaved trees, shrubs, C_3 grass, or C_4 grass). If it is less than 50%, the grid cell is designated as mixed trees if it is dominated by tree PFTs, mixed vegetation if non-trees PFTs are dominant, open vegetation if all PFTs are between 20% and 50%, and desert if all PFTs together is less than 20% (Crucifix, 2005).

To attain the biome distribution, we calculated the potential PFT coverage for each grid cell based on the fractional PFT coverage (Table 3.2; Crucifix et al., 2005), and then combined both the environmental limitation and the potential PFTs (Table 3.3; Prentice et al., 1992; Harrison and Prentice, 2003; Roche et al., 2007). By a "potential PFT", we mean either the dominant PFT or a mixture of PFTs in each grid cell, which we calculated based on the percentage of PFT coverage. We finally compared the biome distribution based on the model output with biome distributions derived from paleovegetation reconstructions. To simplify the comparison, we used nine biomes which are classified as the "mega-biomes" in BIOME 6000 (Harrison and Prentice, 2003), and the global data sets from Prentice et al. (2000), Harrison et al. (2001), Bigelow et al. (2003), and Pickett et al. (2004) (see also http://www.bridge.bris.ac.uk/resources/Databases/BIOMES_data). The nine biomes included are tropical forest, warm-

temperate or mixed forest, temperate montane forest, boreal forest, savannah and dry woodland, grassland and dry shrub land, desert, dry tundra, and tundra.

Table 3.3 The combination of environmental constrains and potential PFTs are used to compute the biome distribution from UVic ESCM results.

Biome	Dominant PFTs or PFTs mixture	Environmental Constrain				
		T_c	GDD5	GDD0	T_w	
		min	min	min	min	max
Tropical forest	BL trees	15.5				
Warm-temperate forest	BL trees or mixed trees	5				
Temperate forest	BL trees or NL trees or mixed trees	−2				
Boreal forest	BL trees or NL trees or mixed trees	−32.5				
Savanna and dry woodland	Grass or mixed vegetation or open vegetation	17				
Grassland and dry shrubland	Grass or mixed vegetation or open vegetation		500		10	
Desert	Barren soil				22	
Dry tundra	SH or mixed vegetation					15
Tundra	SH or mixed vegetation			800		15

The land temperatures from the UVic ESCM are used to calculate the temperature of the coldest month (Tc), growing degree-days relative to 0ºC and 5ºC (GDD5 and GDD0), and temperature of the warmest month (Tw) following BIOME4 (Kaplan et al., 2003). The assignment of a particular biome to a grid cell is based on the BIOME 6000 project version 4.2 after Prentice et al. (1992), Harrison and Prentice (2003), and Roche et al. (2007).

3.4 The equilibrium simulations

Our equilibrium simulations PI_CNTRL and LGM represent two background climate states of the Earth system corresponding to pre-industrial and LGM boundary conditions, respectively. Generally the UVic ESCM reaches a nearequilibrium state after about 2000 years of integration; by that time the annually-averaged surface fluxes are close to zero (Weaver et al., 2001).

3.4.1. Pre-industrial simulation (PI_CNTRL)

The equilibrium climate conditions resulting from the preindustrial control simulation (PI_CNTRL) are summarized in Fig. 3.2. The simulated SSTs (Fig. 3.2b) are in general agreement with the World Ocean Atlas (Conkright et al., 1998). However, there is a cold bias in the tropical Atlantic Ocean, a warm bias along the mid-latitude Atlantic coasts (e.g. the west coast of southern Africa and east coast of North America), and a cold bias in the Gulf of Alaska and the Greenland, Iceland and Norwegian seas (cf. Weaver et al., 2001). Tropical (between 30ºN to 30ºS) annual mean precipitation simulated in PI_CNTRL ranged from 0.1 m yr^{-1} to 2.5 m yr^{-1} (Fig. 3.2c). Low precipitation values (below 0.5 m yr^{-1}) occurred in southern Africa and southern South America, in the high latitudes in both hemispheres, and in northern subtropical Africa. High terrestrial precipitation (above 1.5 m yr^{-1}) occurred in northern South America, central North

America and central Africa, while oceanic precipitation was highest (above 2.0 m yr^{-1}) over the equatorial East Pacific and Indian Oceans. Although the simulated precipitation patterns are similar to the NCEP/NCAR reanalysis data (Kalnay et al., 1996; Weaver et al., 2001) (e.g. both data and model have high precipitation in northern South America and central Africa), there are differences in position or intensity. For example, the simulated precipitation in northern South America is less intense than observed. The maximum of precipitation was simulated over the western Pacific Ocean, while the data shows it in north western South America.

The evaporative loss over the oceans simulated in PI_CNTRL reached approximately 1.5 to 2.0 m yr^{-1}, and in some cases more than 2.0 m yr^{-1} (Fig. 3.2d). Evaporation in northern and southern high latitudes, as well as in subtropical regions such as northern Africa, the Middle East, and Australia, was relatively low (below 0.4 m yr^{-1}). In northern South America and central Africa, the evaporative loss from land was estimated at about 1.0 m yr^{-1}, which was less than over the adjacent North or South Atlantic Oceans. These patterns in the PI_CNTRL simulation correspond well to the NCEP/NCAR data, which show low evaporation rates in northern Africa and Australia and high evaporation rates in northern South America and central Africa. Our simulation compares better to observations than the present-day simulation by Weaver et al. (2001), possibly because our version of the UVic ESCM includes a DGVM that leads to a more realistic representation of the hydrological cycle.

The PI_CNTRL simulation also indicated a net gain of freshwater in northeast and southern South America as well as in central Africa (Fig. 3.2e). A net gain of freshwater corresponds to more precipitation than evaporation, leading to better conditions for a more robust tree cover (e.g. tropical forest). The zonally integrated meridional overturning circulation in the Atlantic Ocean (AMOC) for the PI_CNTRL simulation indicates a North Atlantic Deep Water (NADW) cell and an Antarctic Bottom Water (AABW) cell (Fig. 3.2f). This pattern is typical of an active mode of the Atlantic thermohaline circulation under conditions similar to the present day. The maximum of the streamfunction was 21 Sv and found between 35° and 40°N at 1000m depth. The export of NADW across the equator into the South Atlantic Ocean was about 14 Sv, which is comparable to observations (for example, Lumpkin and Speer, 2007, give a value of 17.9 ± 3.1 Sv). The AABW that originated from the Southern Ocean flowed across the equator into North Atlantic Ocean at a rate of 2 Sv and penetrated as far north as about 20° N.

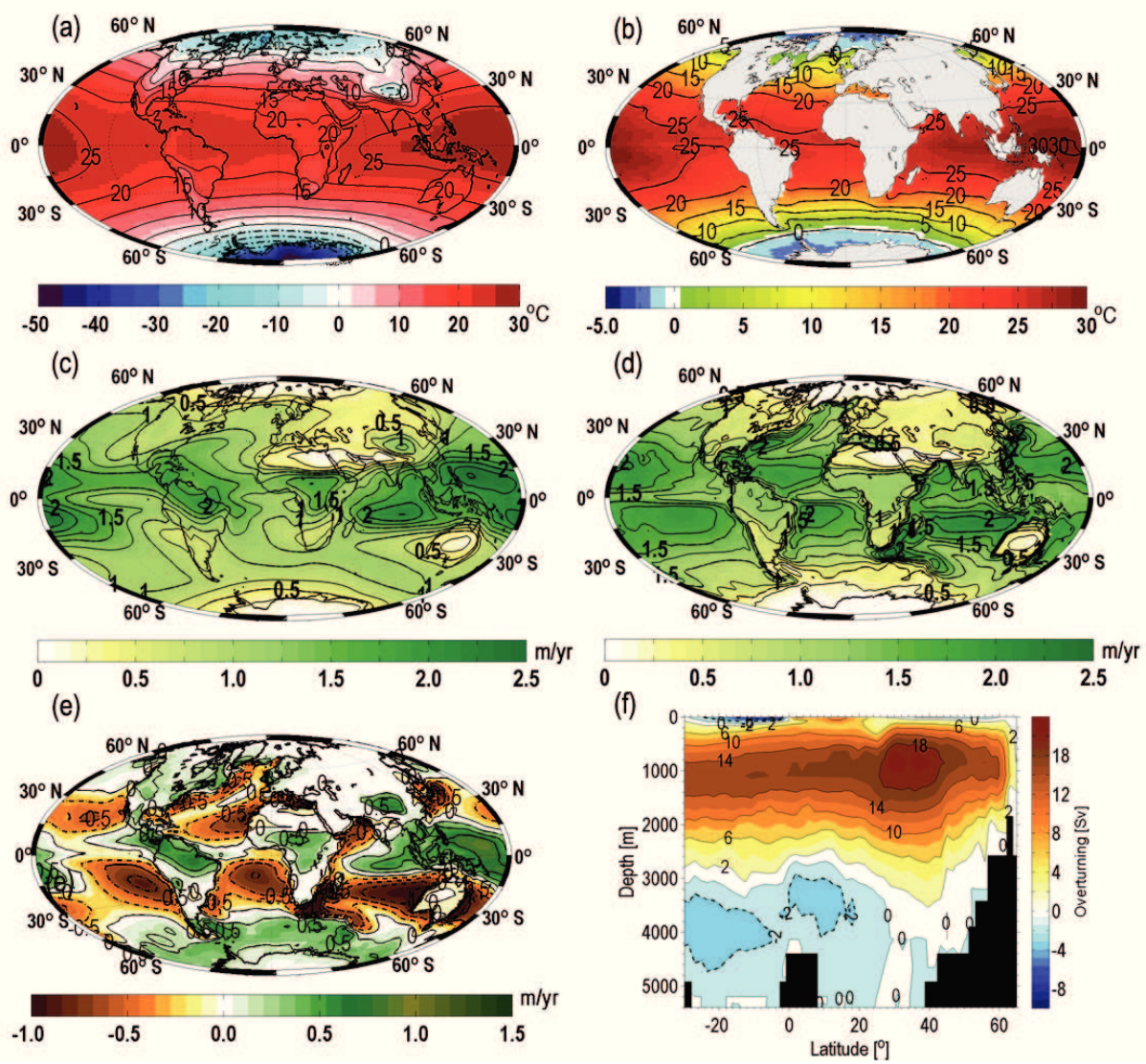

Figure 3.2 Annual-mean of (a) surface air temperature (SAT), (b) sea surface temperature (SST), (c) precipitation, (d) evaporation, (e) precipitation minus evaporation (P−E), and (f) zonally integrated meridional overturning streamfunction in the North Atlantic for the pre-industrial simulation (PI_CNTRL). Contour intervals in SAT and SST are 5ºC. Contour intervals of the streamfuction of AMOC formation is 4 Sv (1 Sv = 10^6 m^3 s^{-1}). Solid line contours indicate a clockwise circulation while dotted lines denote a counterclock-wise circulation.

The vegetation cover in the UVic ESCM is represented by PFTs, which in our study were used to calculate the biome distribution. Fig. 3.3 shows the annual-mean PFT distribution for the PI_CNTRL simulation as a fraction of the area covered in each grid cell of the model. Broadleaf trees were dominant in the tropics (e.g. in South America, Africa, and the Indo-Pacific region between 15ºN to 15ºS). Needleleaf trees were dominant in northern high latitudes such as northern Siberia and North America, but also at high elevation in northern India (Himalayan Mountains), where the fractional cover is between 40 to 90%. The C_3 grasses covered a large area of the globe and reached high percentages in northern Eurasia and North America. The C_4 grasses were

simulated in Southeast Africa with low percentages (around 10%), while a coverage of more than 80% was reached in North Africa, northern India, and Australia.

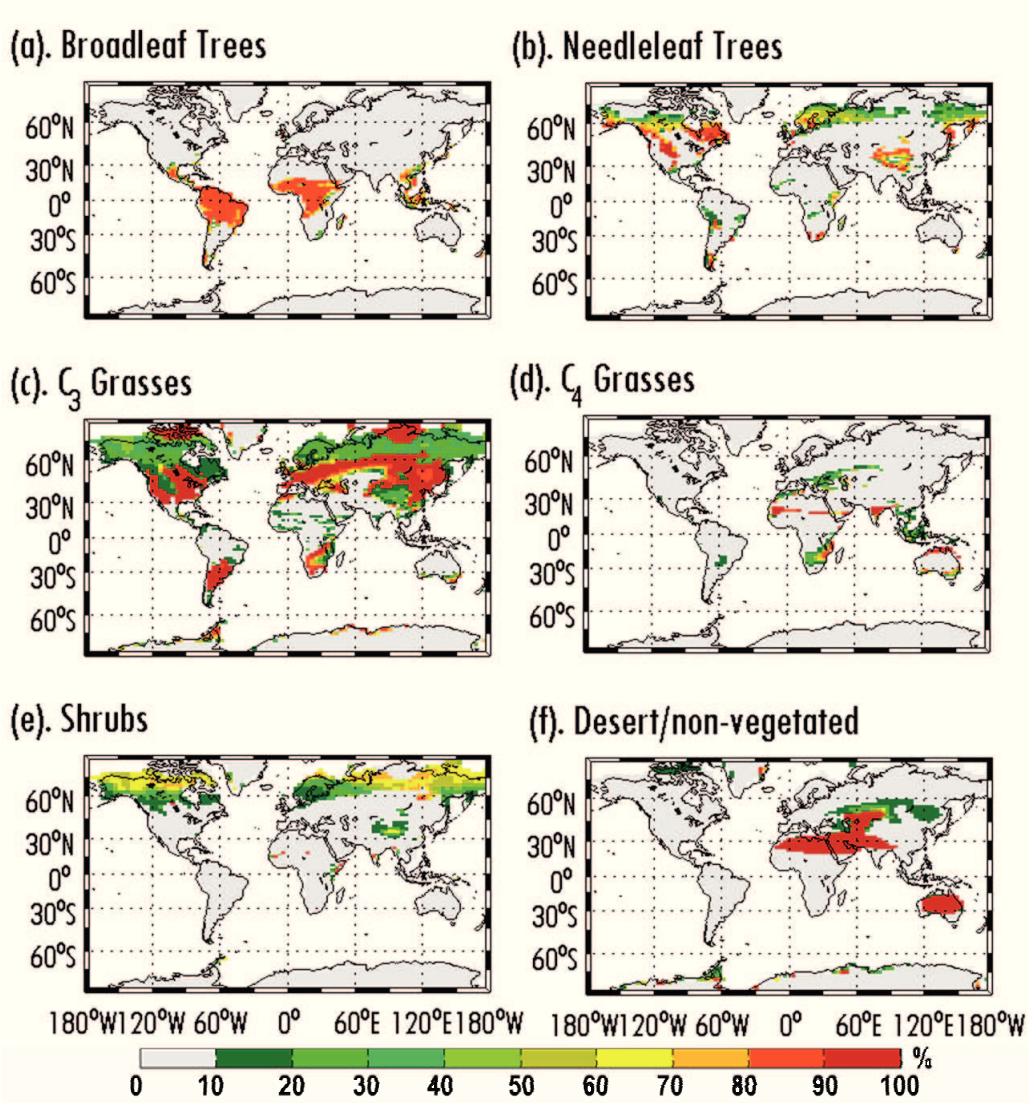

Figure 3.3 Annual-mean of plant functional type (PFT) covers for; (a) broadleaf trees, (b) needleleaf trees, (d) C_3 grass, (d) C_4 grass, (e) shrubs, and bare soil coverage (f) desert/not vegetated for the PI_CNTRL simulation

This type of grasses is better adapted to a dry and hot climate, while the C_3 grasses grow preferentially in a cooler and wetter climate. Shrubs are also representative of a cooler climate and occur together with needleleaf trees in northern Siberia and North America. Our results mostly agree with the PFT distribution simulated by Meissner et al. (2003), except that they obtain more broadleaf trees in Central America and a higher percentage (mostly above 60%) of needleleaf trees at the northern high latitudes.

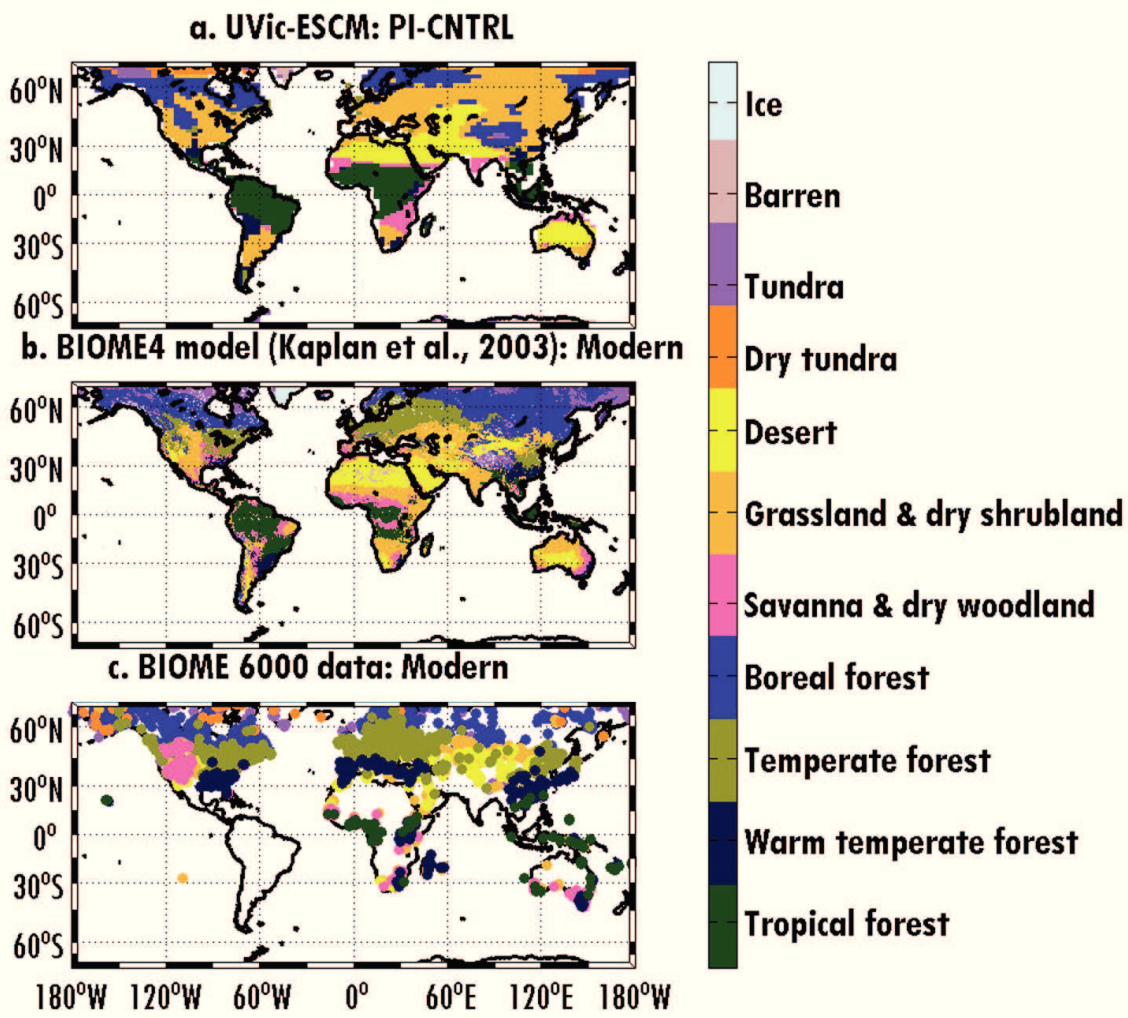

Figure 3.4 Mega-biome distribution for (a) PI_CNTRL biomes simulated in UVic ESCM, (b) modern biomes by the BIOME 4 (Kaplan et al., 2003), and mapping of modern pollen samples by BIOME 6000 (Prentice and Webb, 1998). The UVic ESCM biomes are computed as a combination of environmental constrains and potential PFTs, and the mega-biomes are defined after Harrison and Prentice (2003).

The biome distribution is plotted in Fig. 3.4. A high fractional coverage of tropical forest is shown in northern South America in areas such as the Amazon rain forest, northern Brazil, Venezuela, Colombia, and Peru. The tropical forest cover, represented by the broadleaf trees PFT in the model, was similar to results by Meissner et al. (2003) and Crucifix et al. (2005). However, our model simulated tropical forest in northern Venezuela and Northeast Brazil, whereas today these regions are covered by savannah, grassland, and shrubland as shown by the BIOME 4 model (Kaplan et al., 2003; Fig. 3.4b).

In our control simulation, tropical North America was dominated by tropical forest, although we find small areas of savannah in Central America. This biome pattern agrees with Kaplan et al. (2003), who obtain tropical forest, savannah, and temperate forest in

this region, and it is also similar to the findings by Crucifix et al. (2005) and Meissner et al. (2003), who predict a dominance of tropical forest biomes over broadleaf forest cover. Sub-tropical North America was estimated to be dominated mostly by grassland while small areas of boreal and temperate forests were found in central North America. However, a different distribution is reported by Crucifix et al. (2005), Meissner et al. (2003) and Kaplan et al. (2003) who estimate a dominance of temperate and boreal forest, and also regionally of desert and grassland.

Observations made by Loveland et al. (2000) and the BIOME 6000 project (Fig. 3.4c) conclude that the area is dominated by open shrubland or savannah in western North America, grasslands in the central region, and mixed boreal and temperate forest in eastern North America. Thus our model did not reproduce the observed vegetation distribution in North America, neither regarding location nor in terms of the general pattern. The discrepancy is likely due to an overestimation of C_3 grasses precluding the simulation of dominant tree cover and hence, the formation of mixed boreal and temperate forest mega-biomes.

In experiment PI_CNTRL, we simulated tropical forests in western and central Africa between 20ºN and 20ºS. In the Sahel region and along the east coast of Africa, the biome distribution was mostly savannah, while to the south mixed grassland and warm temperate forest prevailed. These patterns generally agree with both the BIOME 4 model and BIOME 6000 data (Fig. 3.4b and 3.4c). The BIOME 4 model estimates grassland and savannah in the Sahel, tropical forest along the west coast and extending into central Africa (Angola, Congo, and Zambia), and grasslands in eastern Africa. The BIOME 6000 data shows mostly tropical forest in western equatorial Africa, and grassland and savannah in the Sahel. Our model failed to simulate desert and savannah at the southern tip of Africa, where the BIOME 4 model and BIOME 6000 data show a mix of savannah, desert, warmtemperate forest, and grassland. Another discrepancy occurs in southern Europe, where the biomes estimated in the PI_CNTRL simulation did not reveal a warm-temperate forest as evidenced by data from the BIOME 6000 project. It seems that our model overestimated the growth of C_3 grasses in those areas, and hence Europe and Eurasia were covered by the grassland biome in our simulation.

3.4.2. Last Glacial Maximum simulation (LGM)

The LGM experiment simulated cooler surface air temperatures (SATs) and SSTs than the PI_CNTRL (Fig. 3.5a and 3.5b). The largest SAT cooling occurred near the ice sheets

(up to −20ºC and −40ºC different from PI_CNTRL in North America and Antarctica, respectively). However, there was also a moderate cooling of SAT in the tropics (Fig. 3.5a) where differences between LGM and PI_CNTRL were around 3ºC. The largest SST anomaly occurred in the western North Atlantic Ocean where the differences between LGM and PI_CNTRL reached more than 9ºC, while the cooling in the tropics amounted to 3º and 2ºC (Fig. 3.5b). The LGM precipitation patterns were overall similar to PI_CNTRL, except that the intensity was reduced by 0.3 to 0.5 m yr^{-1} (Fig. 3.5c). As in the PI_CNTRL simulation, the AMOC in the LGM simulation (Fig. 3.5d) was also in the active mode. The maximum of the meridional overturning streamfunction was 7 Sv less than in the PI_CNTRL simulation (13.5 Sv as compared to 21 Sv), located further south and at a slightly shallower depth (~100m less). NADW was transported across the equator and exported to the South Atlantic Ocean at a rate reduced by about 40% (from 14 Sv to 8 Sv), while the inflow of AABW from the South Atlantic Ocean was similar (2 Sv) but reached further northward (up to 25ºN) to replace part of the NADW.

Differences between the LGM and the PI_CNTRL biomes were most pronounced in northern and eastern Africa and western South America (Fig. 3.6a), where drier biomes were predicted for the LGM. Otherwise, our LGM results were similar to those of our PI_CNTRL simulation (Figs. 3.4a and 3.6a), especially in northern South America (tropical forest) and southern South America (grassland and dry shrubland), although we found a few locations in South America where the biome distribution was different. In western South America, warm-temperate forest changed to boreal forest, and warm-temperate forest extended from middle and eastern Brazil to western Brazil, indicating reduced temperature and precipitation that affected the PFT coverage in the LGM simulation. The LGM simulation also indicated drier conditions in southeast South America by the presence of grasslands and shrublands. Our results generally agree with the LGM simulations by Crucifix et al. (2005) and Henrot et al. (2009), which show a dominance of open vegetation and C_3 grasses. Paleovegetation reconstructions from plant fossil and proxy data sources such as in Ray and Adams (2001) also suggest drier conditions in these areas which are dominated by desert and semi-desert.

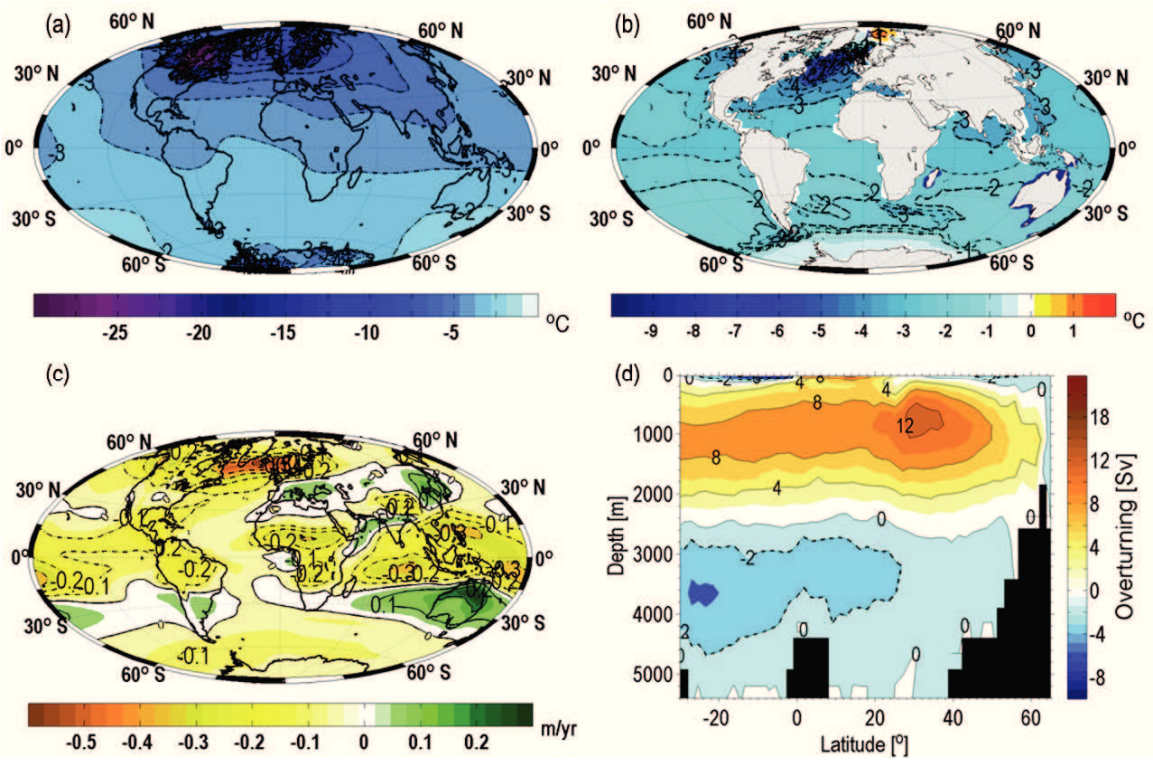

Figure 3.5 Annual-mean anomaly showing differences between the LGM and the PI_CNTRL simulations for: (a) surface air temperature (SAT), (b) sea surface temperature (SST), (c) precipitation, and (d) the zonally integrated meridional overturning streamfunction (Sv) in the North Atlantic for the LGM simulation with a fixed volume contour interval of 4 Sv similar as Fig. 3.2f. Contour intervals for SAT and SST are 1° C.

In central North America temperate forest was partly replaced by boreal forest. The vegetation in our LGM simulation showed a similar bias in North America as the PI_CNTRL simulation. The C_3 grass cover was overestimated in comparison to other simulations (e.g. Crucifix et al., 2005; Roche et al., 2007), which predict a dominance of cool forest biomes such as needleleaf, mixed and temperate broadleaf forests, even though they also simulate warm grasses and savannah in eastern regions and tropical forest in western regions. Similarly, the BIOME 6000 project reconstructions predict boreal and temperate forest in eastern North America and a dominance of savannah in western North America. All models seem to be consistent with the proxy data that indicate the presence of vegetation adapted to cooler conditions during the LGM compared to the present day, although the location and biome types do not exactly match those of the vegetation reconstructions.

Our LGM simulation yielded warm-temperate forest and grassland in the Sahel region in contrast to tropical forest and savannah in the PI_CNTRL simulation. The LGM tropical forest cover showed a similar pattern but with lower percentages than in the PI_CNTRL simulation. A decrease of tropical forest in central Africa is consistent with a

lower temperature and reduced precipitation during the LGM (Figs. 3.2 and 3.5). This pattern agrees with reconstructions by Ray and Adams (2001) and Dupont et al. (2000), who found a reduction in tropical forest in western and central Africa during the LGM period. Our model also agrees with pollen data from BIOME 6000 which show tropical forest on the west coast of Africa and grasslands in southern and northern Africa. Both equilibrium climate simulations PI_CNTRL and LGM predicted similar dominant biomes in the Indonesian Archipelago (tropical forest) and in Australia (savannah, grassland, and desert). The difference in biomes between the pre-industrial and LGM simulations is only through a reduction in vegetation cover, where savannah in northern Australia and grasslands in southern Australia were replaced by desert. Our results for southern Australia were consistent with the LGM simulation by Roche et al. (2007) and are supported by proxy data (Harrison and Prentice, 2003).

3.5 Heinrich Events 1 simulations

3.5.1. Changes in climate

Our HE1 simulations corresponded to a 1.6×10^{6} km^{3} release of freshwater and an associated global sea level rise of 4.5 m after 500 years. This amount of water was enough to cause cessation of NADW formation in the HE1_GL simulation, while in the HE1_IGL simulation it was only reduced from 21 Sv to 16 Sv (Fig. 3.7). Correspondingly, the surface salinity in the North Atlantic Ocean was strongly reduced by up to 5 psu in the HE1_GL simulation (in particular near the St. Lawrence River mouth and off western Europe and northwest Africa), while the surface salinity in the HE1_IGL simulation was only reduced by 0.5 psu. In the South Atlantic Ocean, the strongest sea surface salinity (SSS) anomaly of up to 1 psu occurred off Southwest Africa (Fig. 3.8, left panels). These findings are consistent with other studies examining changes in AMOC strength after adding freshwater to the Northern Hemisphere to imitate the HE1 period and showing either a decrease in the AMOC strength (Weaver et al., 2003) or a complete collapse (Menviel et al., 2008; Köhler et al., 2005) followed by a cooling of the North Atlantic Ocean during HE1.

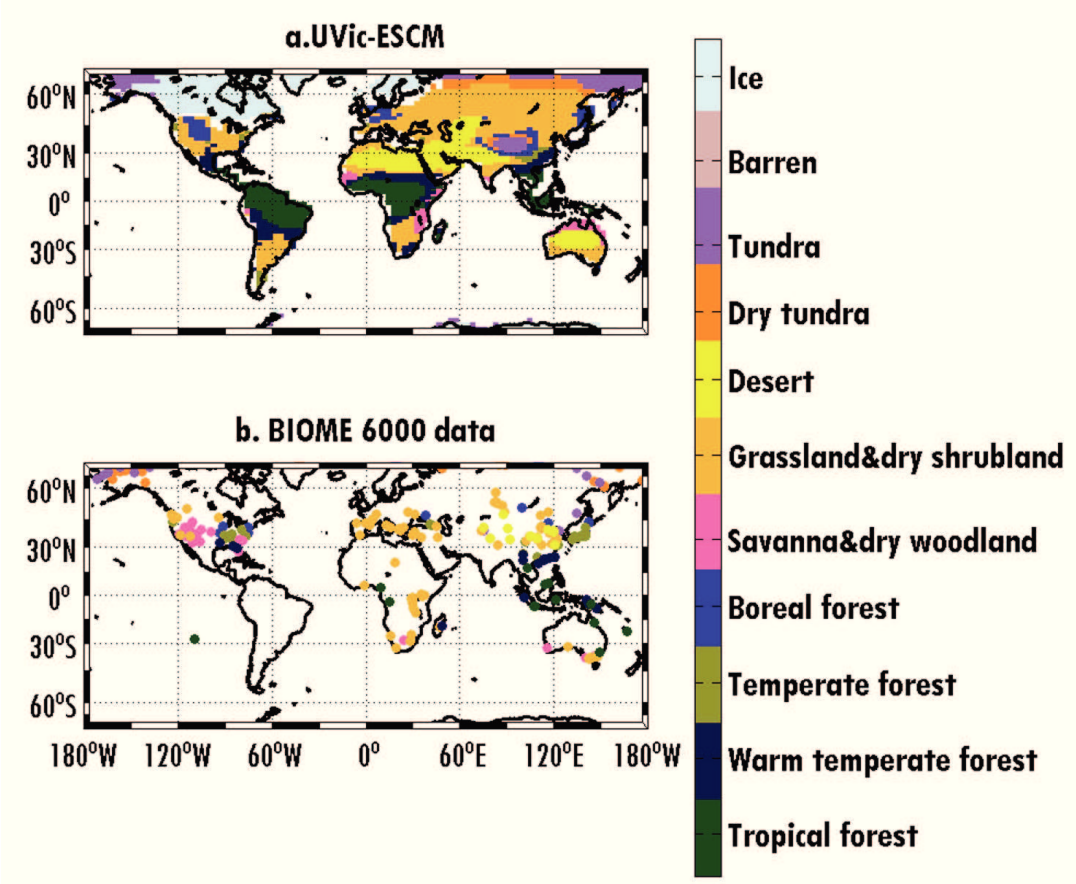

Figure 3.6 Mega-biome distribution for the last glacial maximum (LGM, 21 kyr BP): (a) LGM biomes simulated by the UVic ESCM, (b) paleovegetation mapping by BIOME 6000 (Prentice and Webb, 1998).

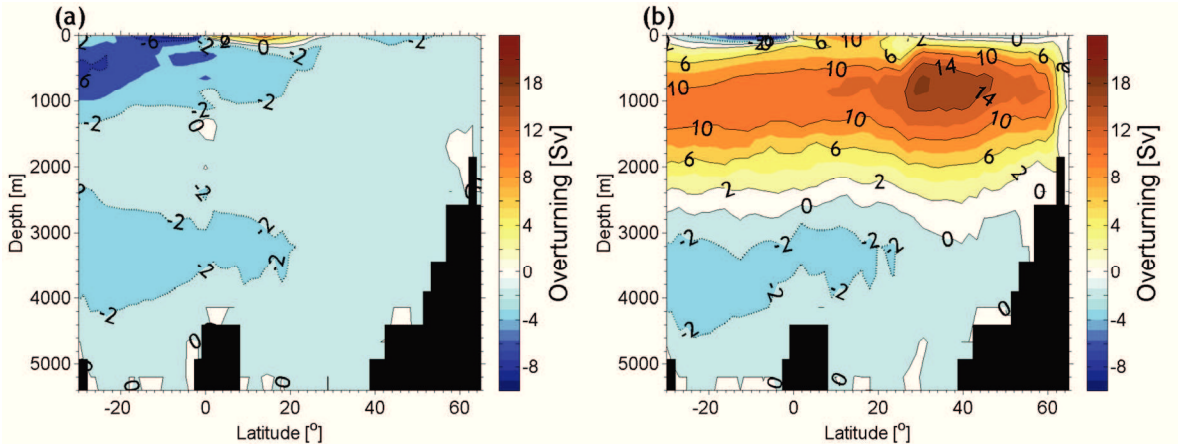

Figure 3.7 Zonally integrated meridional overturning streamfunction (Sv) in the North Atlantic after 500 yr of (a) HE1_GL and (b) HE1_IGL simulations. Contour interval is a fixed volume of 4 Sv (1 Sv = 10^6 m^3 s^{-1}). Solid line contours indicate a clockwise circulation and dotted line contours denote a counterclock-wise circulation.

The HE1 simulations were characterized by cooling over the northern North Atlantic Ocean (Fig. 3.8, middle panel). This cooling was most pronounced in the HE1_GL simulation with SAT anomalies below −2.7°C, (Fig. 3.8, top middle panel) while in the

HE1 IGL simulation the largest negative anomaly was only around −0.5º C (Fig. 3.8, bottom middle panel). Our HE1_GL anomaly is consistent with Menviel et al. (2008) and Kageyama et al. (2010), who also found a stronger North Atlantic cooling in their HE1 simulation using a glacial climate background state instead of an interglacial one. Furthermore, slightly warmer SATs were found in the Southern Hemisphere and the North Pacific region, with maximum positive anomalies in the HE1_GL simulation exceeding 0.6ºC. The largest positive anomalies in the HE1_IGL simulation were only around 0.3ºC, and occurred over the tropical Indo-Pacific Ocean (southern India, northern Australia, and Southeast Asia).

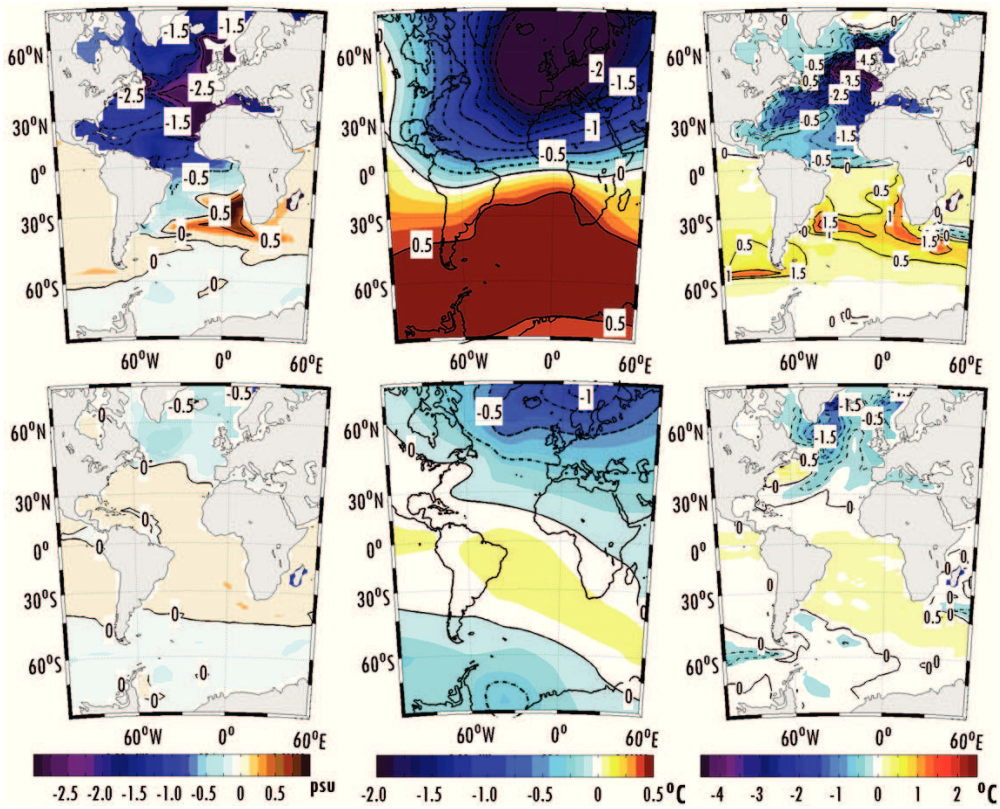

Figure 3.8 Annual-mean anomaly showing differences between the HE1_GL and the LGM simulations (top panel) and the HE1_IGL and the PI_CNTRL simulations (bottom panel) for sea surface salinity (SSS, left panel), surface air temperature (SAT, middle panel), sea surface temperature (SST, right panel).

The SST anomalies of the HE1 simulations reflect the bipolar seesaw effect in the North and South Atlantic Oceans (Fig. 3.8, right panels), which in turn is connected to precipitation changes in the tropics. The largest negative SST anomaly occurred in the eastern North Atlantic Ocean and reached around −4º C in the HE1_GL simulation (Fig. 3.8, top right panel). The largest positive SST anomaly (above 1.8ºC) appeared along the west coast of southern Africa and at the high latitudes of the South Atlantic Ocean.

The precipitation response was strong in the HE1_GL simulation (Fig. 3.9, top left panel), while it was negligible in the HE1_IGL simulation (Fig. 3.9, bottom left panel). Precipitation decreased in the Sahel region, the Middle East, Europe and around the Gulf of Mexico, with maximum negative precipitation anomalies of −0.2 m yr^{-1}. Precipitation increased in Southwest Africa (Angola and Namibia) and southeast Argentina, with maximum positive anomalies exceeding 0.16 m yr^{-1}. In contrast, in the HE1 IGL simulation estimated anomalies were between −0.02 m yr^{-1} and +0.02 m yr^{-1}, only. A similar anomaly pattern is also found in other studies (e.g. Köhler et al., 2005; Menviel et al., 2008; Kageyama et al., 2010), in which it is attributed to a southward shift of the ITCZ. Due to the simplicity of the wind scheme in our atmospheric model the precipitation anomaly in our HE1 GL did not show a southward shift of ITCZ.

The net surface freshwater flux (precipitation minus evaporation minus runoff) anomaly between the HE1_GL and the LGM simulations over the Atlantic Ocean suggests that most of the North Atlantic Ocean gained more freshwater than it received. The opposite pattern is found in the northern and southern subtropical Atlantic Ocean, while the net surface freshwater flux remained nearly the same in the tropical Atlantic Ocean (Fig. 3.9, top right panel). The net surface freshwater flux anomaly under pre-industrial boundary conditions (Fig. 3.9, bottom right panel) had a pattern similar to the one under LGM boundary conditions, except that the intensity was reduced due to different responses to the freshwater perturbation in the two climate states.

The slowdown of the AMOC and reduced deepwater formation in the HE1 simulations (Fig. 3.7) were associated with a seesaw pattern in temperature and precipitation at the sea surface (Figs. 3.8 and 3.9). The freshwater discharges to the North Atlantic Ocean changed the density of surface water, prevented the NADW from sinking, and resulted in a reduction or shutdown of deepwater formation. The meridional overturning streamfunction shows that the formation of NADW collapsed in the HE1_GL simulation (Fig. 3.7a) and that AAIW (Antarctic Intermediate Water) became the dominant water mass, spreading further north until 20°N. The streamfunction in the HE1_IGL simulation (Fig. 3.7b) is similar to that of the PI_CNTRL simulation (Fig. 3.2f), except that the maximum strength was reduced from 21 Sv to 16 Sv. The weak AMOC response in HE1_IGL corresponds to weak changes in SST and precipitation.

3.5.2. Changes in vegetation

The HE1_GL simulation showed a much more pronounced vegetation change than the HE1_IGL simulation (Fig. 3.10). This is most evident in northern Africa (Sahel region) and western Asia (near present-day East Kazakhstan). These changes corresponded to changes in climate, as for example in the Sahel region, where precipitation was reduced by 0.2 m yr^{-1} in the HE1_GL simulation as compared to the LGM equilibrium simulation (Fig. 3.9, top left panel). This resulted in a change in PFT coverage from robust broadleaf and needleleaf forest to grassland and shrubland cover (tree cover was reduced by more than 60%). In other parts of the Sahel, grass and shrub covers decreased by more than 60% and were replaced by desert. These vegetation changes, from forest to grass and shrubs, and from grass and shrubs to desert, indicate a drier climate in the HE1 simulation than in the LGM equilibrium simulation.

South of the equator, the vegetation response in the HE1_GL simulation corresponding to a slight warming was not as robust as north of the equator. For example, in southwestern Africa precipitation increased regionally, consequently broadleaf trees cover increased by 49%, while at the same time grass and shrub cover decreased by 51% (Fig. 3.10). In the HE1_IGL simulation, changes were much smaller or even insignificant (increase or decrease are less than 10 %). Grass and shrub cover in northern tropical and sub-tropical regions (0º to 30ºN) in the HE1_GL simulation went almost unchanged, except for a small region in West Africa, where grasses increased by around 20% and consequently trees decreased by a similar amount. Both HE1 simulations indicated cooler and drier climatic conditions around the North Atlantic Ocean and a succession in vegetation cover in northern Africa from forest to grassland and from shrub to desert. Over the South Atlantic region, the HE1 simulations resulted in warmer and wetter climatic conditions in parallel with a regional increase of tropical forest cover in Southwest Africa. However, the increase in precipitation in South America in the HE1 simulations did not cause any change in vegetation cover compared to the equilibrium simulations. The vegetation response in Southwest Africa generally agrees with Menviel et al. (2008) who found that a wetter climate in the Southern Hemisphere did not lead to large changes in land carbon storage, and resulted in less forest cover in the Southern Hemisphere except for Southwest Africa and western South America.

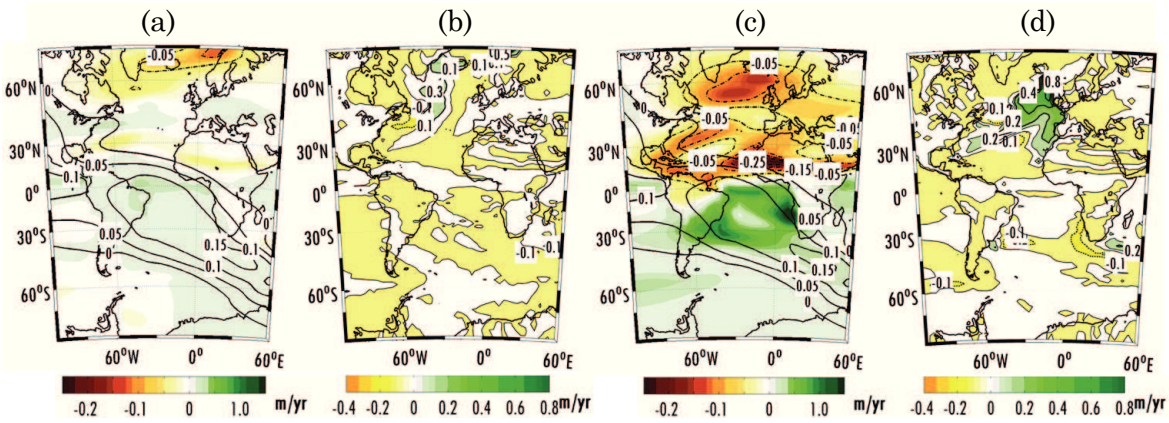

Figure 3.9 Annual-mean anomaly showing differences between the HE1_GL and the LGM simulations (top panel) and the HE1_IGL and the PI_CNTRL simulations (bottom panel) for precipitation (left panel), and net flux freshwater (precipitation−evaporation−runoff, P −E −R, right panel).

3.5.3. Biome distribution and model-data comparison

To compare the HE1 simulations with vegetation proxies, we focus on the discussion of vegetation changes in the HE1_GL simulation. The biome distribution diagnosed from our HE1_GL simulation is compared with pollen records from tropical Africa and South America (Fig. 3.11 and Table 3.4, Hessler et al., 2010). Both the climate and the biome distribution exhibited a shift towards drier conditions in tropical Africa, while wetter conditions existed in South America and southern tropical Africa. The tropical African biomes (not including the Sahel) were dominated by tropical forest from western to central Africa (e.g. Gabon, Congo, Cameroon, Nigeria, Zaire, and Burundi), while in the East (e.g. Tanzania and Kenya) a mix of warm temperate, boreal forest, and savannah was simulated (Fig. 3.11), in accordance with a wetter climate. Even when the differences in climate were not pronounced, e.g. between West and East Africa, distinctly different biomes were established.

The simulated tropical African vegetation generally agrees with several palynological vegetation reconstructions for West and East Africa (Hessler et al., 2010; Kageyama et al., 2005). However, in Burundi (central Africa), proxy records indicate a cool and dry climate dominated by grassland and savannah, while our model predicted tropical forest (Table 4). Furthermore, these records indicate that northern tropical Africa (i.e. the Sahel region) experienced drier conditions suggesting that the biomes changed from grasslands to desert in the eastern Sahel, warm-temperate forest to grasslands in the western Sahel, and tropical forest to warm-temperate forest in the central Sahel. This

supports our model result in that due to changes in climate the PFT cover in the Sahel region changed from forests to grasses or from shrubs to desert.

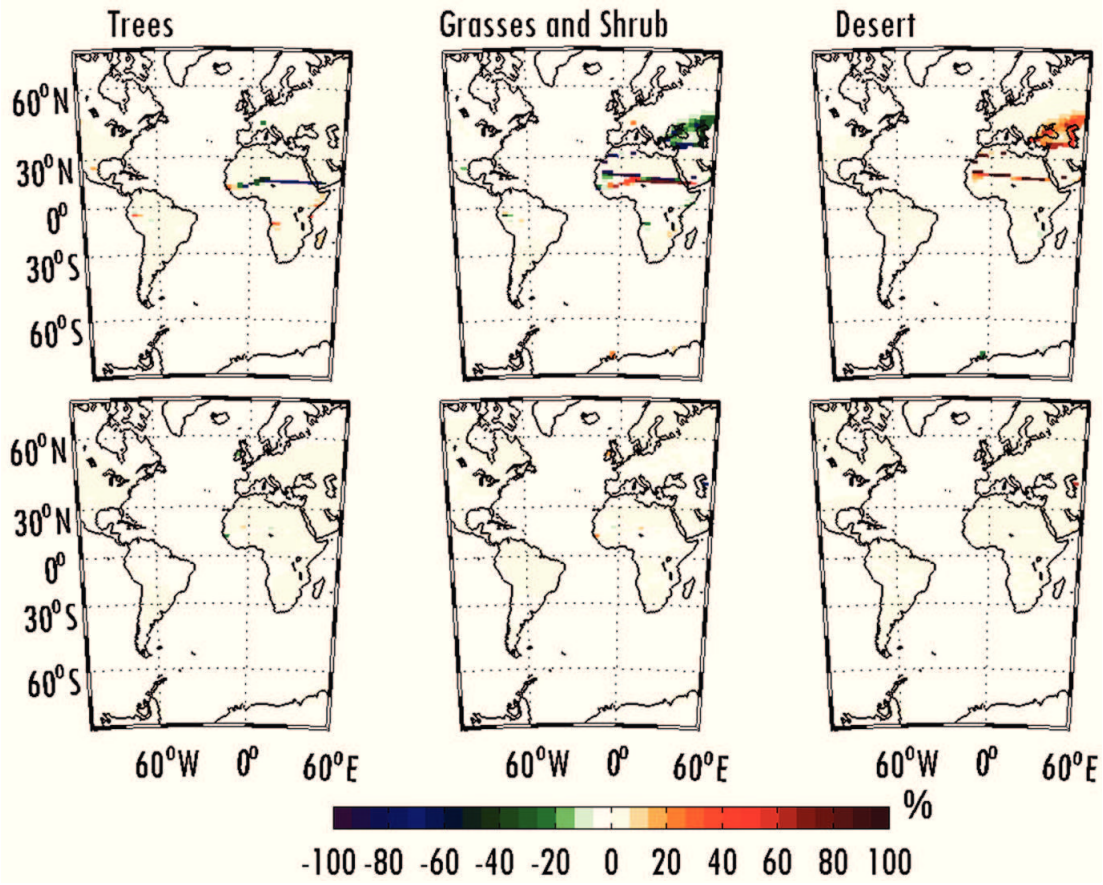

Figure 3.10 Annual-mean PFT differences in percent coverage between HE1_GL and LGM (top panel) and HE_IGL and PI_CNTRL (below) for trees (left panel), grasses and shrubs (middle panel), and desert, non-vegetated coverage (right panel).

The changes in biome distribution of the HE1_GL simulation in northern and southern subtropical Africa show opposing trends towards drier biomes in the north and wetter biomes in the south, but the change south of the equator is far smaller than north of it. In northern subtropical and equatorial Africa our model suggested a drier climate and, accordingly, desert cover expanded in these regions. Furthermore, our model suggested the dominance of grassland in southern Europe, which agrees with pollen reconstructions from the Mediterranean (Kageyama et al., 2005) suggesting an increase in grasslands due to a lower coldest-month temperature.

The HE1_GL simulation did not indicate major biome changes in tropical South America as compared to the LGM simulation (Fig. 3.11). In Northeast Brazil, the model simulated tropical forest instead of steppe and semi-desert as suggested by pollen reconstructions (Hessler et al., 2010), although the precipitation and surface air temperature decreased

from LGM to HE1 (Fig. 3.9, top left panel and Fig. 3.8, top middle panel). The simulated climate of northern tropical South America (e.g. Venezuela) was drier with a maximum precipitation anomaly of around −0.08 m yr^{-1} (Fig. 3.9, top left panel). However, in our simulation the tropical forest remained (Fig. 3.11), although biogeochemical data from this region suggest an increase in savannah cover (Jennerjahn et al., 2004), and palynological data of older Heinrich events (HE3, HE4, HE5, HE5a and HE6) also indicate an increase in savannah (Behling et al., 2000). Northwest South America received less precipitation in the HE1_GL simulation. Again, the biome distribution remained similar to the LGM simulations, while reconstructions from La Laguna de Bogotá in Colombia indicate savannah and grassland (Helmens et al., 1996). Discrepancies in northern South America indicate that climate changes of the HE1_GL simulation were not strong enough to influence the biome coverage, or that our vegetation model was not sensitive enough. On the other hand, our biome distribution in northwest Brazil of the HE1_GL simulation is in good agreement with reconstructions from Lake Caçó (Ledru et al. 2006), where tropical forests were dominant and indicate a wetter climate during the HE1 period. Furthermore, the HE1_GL simulation predicted a dominance of desert in the Middle East and western Asia and Arabia, while tundra expanded in northern Eurasia, in Siberia, and over the Tibetan Plateau.

3.6 Discussion

Our two equilibrium simulations represent warm and cold conditions during interglacial and glacial climates and provide two different backgrounds for the HE1 simulations. The largest cooling in air and sea-surface temperature between the PI_CNTRL and LGM simulations in the North Atlantic Ocean was due to the presence of ice-sheets in North America. However, the most recent SST reconstruction by the MARGO project (2009) shows a more pronounced cooling in the eastern than in the western North Atlantic Ocean. The disagreement with our model results is most likely due to misplaced deepwater formation sites in the pre-industrial control experiment. Comparable mismatches have also been observed in other coupled atmospheric-ocean models simulating LGM climate (Kageyama et al., 2006).

In the tropics, the SAT difference between the PI_CNTRL and LGM simulation is ~1°C overland and ~2°C over the Atlantic Ocean, while the SST difference is 2–3°C, in agreement with the MARGO reconstruction (MARGO, 2009) and other modeling studies (e.g. Crucifix et al., 2005; Otto-Bliesner et al., 2006; Kageyama et al., 2006; Roche et al.,

2007). The general agreement with reconstructions from proxy data supports that the LGM simulation delivered a suitable background climate for the Heinrich Event 1 simulations.

The warm (PI_CNTRL) and cold (LGM) background climate states also differed in the AMOC, with a reduced formation of NADW and a stronger AABW inflow into the Atlantic Ocean under LGM conditions. This is in agreement with some other model simulations (e.g. Weaver et al., 2001; Weber and Drijfhout, 2007; Kageyama et al., 2010), but at odds with others (e.g. Roche et al., 2007; cf. Otto-Bliesner et al., 2007). Proxy data (Pa/Th ratios) from ocean sediment cores suggest a weaker AMOC strength during the LGM period (Yu et al., 1996; Marchal et al., 2000; McManus et al., 2004; Gherardi et al., 2005), although they are difficult to interpret (e.g. Roche et al., 2007). McManus et al. (2004) analyze a high accumulation core from the deep western Subtropical Atlantic at a depth of 4.5 km, and according to their results, the AMOC during the LGM was reduced by 30% as compared to the present day, which is in broad agreement with our LGM simulation (Figs. 3.2f and 3.5d).

The two different climatic background conditions corresponding to two different states of the AMOC did not change the predicted vegetation distribution (Figs. 3.4, 3.5a, and 3.6a) except in a few locations: in northern tropical Africa (the Sahel region), western South America, and central North America. For example, in central Africa, a warmer and wetter climate was predicted in the PI_CNTRL simulation as compared to the LGM simulation. This resulted in more tropical forest and savannah in the PI_CNTRL simulation, while warm-temperate forest and grassland cover were extended in the LGM simulation. In general, most changes in the vegetation encompassed rather small areas. We may suspect that the initial vegetation conditions for the vegetation model or the relative simplicity of the land-atmosphere model caused the similar vegetation cover estimates of the PI_CNTRL and LGM simulations. However, Hughes et al. (2004) showed that the TRIFFID DGVM is insensitive to the choice of the initial vegetation cover, and Meissner et al. (2003) showed that coupling the TRIFFID model to the UVic ESCM results in predicted vegetation patterns that compare reasonably well to observations.

Tabel 3.4 Comparison of tropical mega-biomes during HE1 period between pollen reconstructions (compiled by Hessler et al. 2010) and model results (computed from HE1_GL using UVic ESCM). The site locations for pollen reconstruction are in equatorial Africa and South America from terrestrial and marine sites (shown in Fig. 3.1). Blue plus sign denotes if data and model results are similar and the red plus sign denotes if data and model results are different.

No.	Latitude and Longitude	Site location name	Potential biome distribution		Comparison between data and model
			Pollen data	Model result	
	equatorial Africa				
	Terrestrial site				
1	3.47° S–29.57° E	Kashiru Bog, Burundi	– Grassland and dry shurbland – Savannah and xerophytic scrubland	Tropical forest	+
2	8.50° S–30.85° E	Lake Tanganyika	– Warm temperate mixed forest – Savannah and xerophytic scrubland	– Boreal forest – Savannah and dry-woodland	+
3	9.33° S–33.75° E	Lake Masoko, Tanzania	– Warm temperate mixed forest – Savannah and xerophytic scrubland	Savannah and dry-woodland	+
4	11.29° S–34.44° E	Lake Malawi	– Savannah and xerophytic scrubland – Tropical forest	Savannah and dry-woodland	+
6	4.51° N–9.40° E	Barombi Mbo, Cameroon	– Savannah and xerophytic scrubland Tropical forest	Tropical forest	+
	Marine site				
5	4.40° N–4.18° W	off Ivory Coast, KS 84-063	– Tropical forest – Warm temperate mixed forest	Tropical forest	+
7	11.92° S–13.40° E	ODP 1078C – Angola	– Warm temperate mixed forest – Temperate-montane forest	– Tropical forest Temperate forest	+
8	17.15° S–11.02° E	GeoB 1023 – Cunene River Mouth	– Savannah and xerophytic scrubland – Grassland and dry shurbland	Grassland and shrubland	+
	South America				
	Terrestrial site				
11	2.97° S–43.42° W	Lake Caçó – NE Brazil	– Warm temperate mixed forest – Tropical forest	Tropical forest	+
12	23.87° S–46.71° W	Colônia, Brazil	– Savannah and xerophytic scrubland – Grassland and dry shurbland	– Temperate forest – Grassland and dry shrubland	+
13	17.83° S–64.72° W	Siberia, Bolivia	– Temperate-montane forest – Grassland and dry shurbland	Temperate forest	+

Table 3.4 continued.

No.	Latitude and Longitude	Site location name	Potential biome distribution		Comparison between data and model
			Pollen data	Model result	
14	4.92° N–74.03° W	La Laguna, Bogotà, Colombia	– Savannah and xerophytic scrubland – Grassland and dry shurbland	Tropical forest	+
15	4.92°N–74.03° W	Fúquene, Colombia	– Savannah and xerophytic scrubland – Temperate-montane forest	Tropical forest	+
	Marine site				
9	3.67° S–37.72° W	GeoB 3104 – off NE Brazil	– Temperate-montane forest – Warm temperate mixed forest	Tropical forest	+
10	4.15° S–36.21° W	GeoB 3910-2 – off NE Brazil	– Savannah and xerophytic scrubland – Warm temperate mixed forest	Tropical forest	+

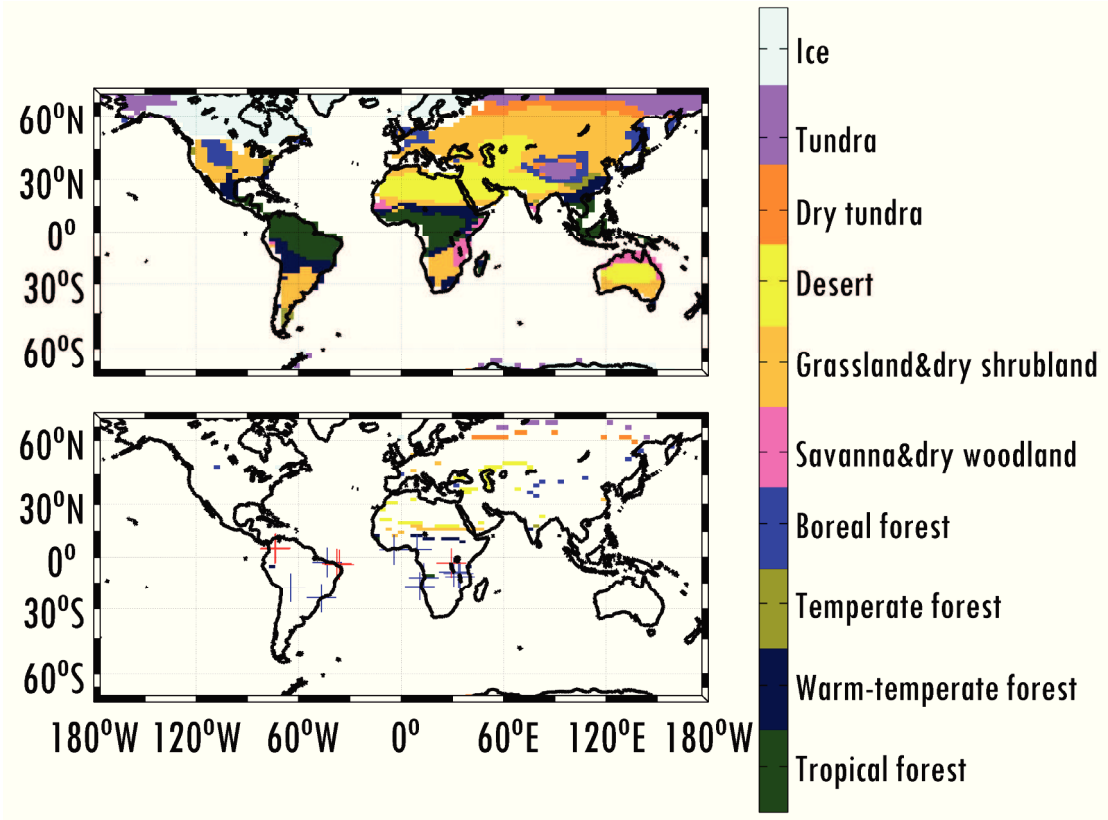

Figure 3.11 Mega-biome distribution computed from UVic ESCM results; (top panel) HE1 GL simulation and (bottom panel) anomaly between HE1 GL and LGM simulations. The anomaly map shows the HE1 GL biome only in those grid cells that differ from the LGM simulation. Blue crosses indicate locations where biomes are similar in the model and the data reconstruction (Hessler et al., 2010); red crosses denote where modeled and reconstructed biomes differ.

The key climate parameters which influence vegetation cover are temperature and precipitation. Our model results from the Heinrich event 1 simulations showed that these climate factors respond to changes in NADW formation. The AMOC reduction or collapse following the freshwater perturbation caused temperature and precipitation changes (Figs. 3.8 and 3.9), and those changes drove a subsequent response in the vegetation distribution, especially around the tropical North Atlantic, in tropical western South America, and in southwestern Asia (Fig. 3.10). In the HE1_GL simulation, the AMOC collapsed (Fig. 3.7a) and the associated heat transfer from low to high latitudes in the Atlantic Ocean was strongly reduced (in accordance with the bipolar seesaw hypothesis, Fig. 3.8). The inter-hemispheric thermal gradient was strengthened due to the cooling in the North Atlantic. This would be expected to shift the ITCZ in the direction of the warmer Southern Hemisphere. The precipitation in our HE1_GL simulation did not indicate a southward shift of ITCZ (Fig. 3.9) due to the lack of a wind feedback in our simulation. The effect of including a geostrophic wind feedback scheme is a matter of further investigation. Nevertheless, our HE1_GL simulation indicated high rainfall south of the equator, which most likely was due to the enhanced evaporation over the ocean and changes in atmospheric moisture transport. On the other hand, the HE1_IGL simulation indicated only a slight reduction of the AMOC strength (Fig. 3.7b), resulting in less pronounced climate changes (Figs. 3.8 and 3.9) and consequently less vegetation response (Fig. 3.10). Another problem in simulating precipitation over tropical land regions is the lack of land surface processes in the coupled land atmospheric model (Weaver et al., 2001) and is most strongly observed in the precipitation pattern over South America. This is probably the main reason why the modeled vegetation deviates so strongly from the biome reconstructions, particularly in eastern and northeastern South America (Fig. 3.11).

3.7 Summary and conclusions

This study investigated the effects of climate change in the region of and around the tropical Atlantic during Heinrich event 1. We presented the distribution of vegetation simulated by the UVic Earth system climate model including a dynamic vegetation module for four scenarios: pre-industrial (PI_CNTRL), freshwater perturbation of the PI_CNTRL equilibrium (HE1_IGL), last glacial maximum (LGM), and freshwater perturbation of the LGM equilibrium simulating Heinrich event 1 (HE1_GL). Adding freshwater to the North Atlantic resulted in a collapse of the Atlantic Meridional Overturning Circulation (AMOC), followed by a cooling of the Northern Hemisphere and

a warming of the Southern Hemisphere (the bipolar seesaw hypothesis), causing a strengthening of the inter-hemispheric thermal gradient. This inter-hemispheric thermal gradient resulted in changes in rainfall patterns driving a southward shift of tropical and subtropical biomes.

The two equilibrium simulations (PI_CNTRL and LGM) allowed analyzing the response of the vegetation cover around the tropical Atlantic to a freshwater perturbation in the North Atlantic Ocean under different climatic background conditions. Our PI_CNTRL biomes were in general agreement with modern biome reconstructions. Discrepancies occurred with respect to the simulation of the dominance of grasslands in southern Europe and the failure to simulate a mixture of savannah and warm-temperate forests along the east coast of South America for the preindustrial period. The climate and biome patterns of tropical and sub-tropical South America of our LGM simulation differ from other model results (Roche et al., 2007) and a data compilation (Ray and Adams, 2001) by suggesting wetter conditions and more forest cover.

The HE1 simulations exhibited a southward shift of the southern desert boundary in northern Africa, but failed to mimic expected changes in eastern South America. The vegetation responded similarly during the HE1 simulations under interglacial (pre-industrial) and glacial (LGM) climatic background conditions, except for northern tropical Africa, western Eurasia, and western South America. The magnitude of the changes in the tree and grass PFTs is larger for glacial than for interglacial climatic background conditions.

The HE1 simulations produced a cooler climate in the Northern Hemisphere, a drier climate in northern tropical Africa and a local warming in the Southern Hemisphere, (cf. Menviel et al., 2008; Kageyama et al., 2009; Swingedouw et al., 2009). In addition, the vegetation responded to a changing climate through an increase in non-forested and desert PFT coverage in northern tropical Africa and a change from warm-temperate to tropical forests in Southwest Africa.

The biome comparison between the HE1 simulations and several data compilations for tropical Africa and South America showed reasonable agreement in vegetation patterns reconstructed from marine and terrestrial records. Limitations in the number of PFTs and modeled biomes on the one hand and the lack of precision of the palynologically reconstructed biomes on the other hand, lead to differences that are difficult to assess. Improvements in the dynamic vegetation modeling can be achieved by the addition of

more PFTs and specific climatic limitations to the defined plant functional types (e.g. instead of one two broadleaved forest PFTs, a tropical and deciduous one). Nevertheless, the simulations showed that a collapse of the AMOC and the associate changes in North Atlantic climate are physically consistent with the reconstructed changes in vegetation in the tropical regions around the Atlantic Ocean during the HE1 period.

3.8 Acknowledgment

This work was funded by the Deutsche Forschungsgemeinschaft (DFG) as part of the German contribution to the Integrated Ocean Drilling Program (SPP 527) "Abrupt Climate Change in the African Tropics (ACCAT)" and DFG Research Center/Excellence Cluster "The Ocean in the Earth System". We thank Maria Fernanda Sanchez-Goñi and an anonymous reviewer for their helpful comments.

Chapter 4

Climate and vegetation changes around the Atlantic Ocean resulting from changes in the meridional overturning circulation during deglaciation

D. Handiani, A. Paul and L. Dupont
(Under review for publication in *Climate of the Past*, doi:10.5194/cpd-8-2819-2012)

4.1 Abstract

The Bølling-Allerød (BA, starting ~14.5 ka BP) is one of the most pronounced abrupt warming periods recorded in ice and pollen proxies. The leading explanation of the cause of this warming is a sudden increase in the rate of deepwater formation in the North Atlantic Ocean and the resulting effect on the heat transport by the Atlantic Meridional Overturning Circulation (AMOC). In this study, we used the University of Victoria (UVic) Earth System-Climate Model (ESCM) to run simulations, in which a freshwater perturbation initiated a BA-like warming period. We found that under present climate conditions, the AMOC intensified when freshwater was added to the Southern Ocean. However, under Heinrich event 1 (HE1, ~16 ka BP) climate conditions, the AMOC only intensified when freshwater was extracted from the North Atlantic Ocean, possibly corresponding to an increase in evaporation or a decrease in precipitation in this region. The intensified AMOC led to a warming in the North Atlantic Ocean and a cooling in the South Atlantic Ocean, resembling the bipolar seesaw pattern typical of the last glacial period.

In addition to the physical response, we also studied the simulated vegetation response around the Atlantic Ocean region. Corresponding with the bipolar seesaw hypothesis, the rainbelt associated with the Intertropical Convergence Zone (ITCZ) shifted northward and affected the vegetation pattern in the tropics. The most sensitive vegetation area was found in tropical Africa, where grass cover increased and tree cover decreased under dry climate conditions. An equal but opposite response to the collapse and recovery of the AMOC implied that the change in vegetation cover was transient and robust to an abrupt climate change such as during the BA period, which is also supported by paleovegetation data. The results are in agreement with paleovegetation records from western tropical Africa, which also show a reduction in forest cover during this time period. Further agreement between data and model results was found for the uplands of North America and southern Europe, where grassland along with warm and dry climates were simulated. However, our model simulated vegetation changes in South

and North America that were much smaller than reconstructed. Along the west and east coast of North America we simulated drier vegetation than the pollen records suggest.

4.2 Introduction

After the cooling associated with Heinrich event 1 (HE1), an abrupt warming of the surface climate at the onset of the Bølling-Allerød period (BA) has been recorded in the North Atlantic Ocean (e.g. Bard et al., 2000; McManus et al., 2004), concurrent with climate changes in the South Atlantic Ocean (e.g. EPICA members, 2006; Barker et al., 2009; Stenni et al., 2011). The climate changes in the two hemispheres follow the pattern of a bipolar seesaw typical of the last glacial period (Stocker and Johnsen, 2003). They are connected to the strengthening of the Atlantic Meridional Overturning Circulation (AMOC) through heat transport driven by two deepwater sources: the North Atlantic Deep Water (NADW) in the Northern Hemisphere, and the Antarctic Bottom Water (AABW) in the Southern Hemisphere (e.g. Broecker, 1998; Stocker, 1998; Stocker et al., 2001). Sea-level reconstructions suggest that the AMOC recovery mechanism is associated with meltwater flux causing the sea-level to rise by several meters within a century (Fairbanks, 1989; Bard et al., 1990; Clark et al., 2002a; Siddall et al., 2004; Bard et al., 2010), although the exact timing and meltwater sources are a matter of current debate (e.g. Peltier et al., 2006; Driesschaert et al., 2007; Stanford et al., 2006).

Model studies have been performed that simulate the recovery of the AMOC after its collapse invoking different mechanisms. The most successful of these are (1) a reduction of the meltwater flux into the North Atlantic Ocean (Ganopolski and Rahmstorf, 2001), (2) negative freshwater forcing of the North Atlantic Ocean (Schmittner et al., 2002b), (3) an additional meltwater flux into the Southern Ocean (Weaver et al., 2003), and (4) warming and sea-ice retreat in the Southern Ocean (Knorr and Lohmann, 2007). Recently, transient model simulations suggest that the large abrupt warming at the onset of the BA period is the result of several overlapping climate responses such as an increase of atmospheric CO_2, the AMOC recovery after HE1, and an overshoot of the AMOC after gradual forcing of the meltwater flux (Liu et al., 2009). In our study, we focus on the effect of the abrupt warming on the vegetation cover during the Late Glacial, with an emphasis on vegetation changes between the HE1 stadial and the BA interstadial as well as the glacial state before HE1.

The pollen assemblage studies in the Atlantic Ocean region indeed show profound changes in the vegetation cover during the BA period. As an example, in west and southwest North America a boreal or warm temperate forest became dominant about 15

ka BP (ka BP = thousands years before present), indicating a warm and wet climate concurrent with the abrupt warming event in Greenland during the final stages of the last glacial period (Jiménez-Moreno et al., 2010). During the same time, much of Europe was covered by warm temperate forest, also corresponding to a relatively warm and humid climate (Fletcher et al., 2010). The pattern of vegetation change in tropical Africa and tropical South America was more complex (Hessler et al., 2010), e.g., the northeastern Brazilian record indicates the occurrence of Atlantic forest and a humid climate during the last phase of HE1, followed by a decline in forest and increase in aridity. In contrast, pollen records from West Africa (Angola and southern Congo) show no clear trend during the BA period, while in east equatorial Africa temperate-montane forest and tropical forest developed when the climate got warmer after HE1.

With these records as a reference, we carried out experiments with a numerical model in an attempt to initiate the recovery of the AMOC after its collapse and simulate the BA warming following HE1. Our experiments were inspired by the simulations of Weaver et al. (2003), who trigger the onset of the BA period by adding freshwater to the South Atlantic Ocean. We used the same Earth System Model of Intermediate Complexity (EMIC) – the University of Victoria Earth System-Climate Model (UVic ESCM) – complemented with a dynamic global vegetation model (Meissner et al., 2003), which enabled us to study the interaction between climate and vegetation during the recovery of the AMOC.

In addition, we also present a preliminary comparison between the model results and pollen records during the onset of the BA warm period using a biome distribution generated from our model output in order to simplify the data-model comparison (Handiani et al., 2012). Thus our study aims to understand the vegetation development at the onset of the BA period and tries to elucidate the interactions between climate and land-cover during periods of abrupt climate change.

4.3 Model description and experimental designs

The UVic ESCM version 2.8 (Weaver et al., 2001) consists of a three-dimensional ocean model (MOM – Modular Ocean Model version 2) (Pacanowski, 1995), a vertically integrated two-dimensional energy-moisture balance model of the atmosphere (Fanning and Weaver, 1996), and a dynamic-thermodynamic sea-ice model (Hibler, 1979; Hunke and Dukowicz, 1997; Bitz et al., 2001). This version further includes an adaptation of the land surface model MOSES2 (Met Office Surface Exchange System version 2) (Cox et al.,

1999) and the dynamic global vegetation model (DGVM) TRIFFID (Top-down Representation of Interactive Foliage and Flora Including Dynamics) (Cox, 2001; Meissner et al., 2003). It also includes a fully coupled carbon cycle, which takes into account the terrestrial carbon fluxes and pools (Meissner et al., 2003; Matthews et al., 2005), as well as the inorganic and organic carbon in the ocean (Ewen et al., 2004; Schmittner et al., 2007). However, our simulations did not include the ocean carbon cycle component.

The coupled climate model is forced by seasonal variations of insolation, wind stress at the ocean surface and land-ice cover. Here we used the global ice sheet reconstruction ICE–5G (Peltier, 2004) for the present day as well as the Last Glacial Maximum (LGM). The TRIFFID model simulates the plant distribution based on carbon fluxes between land and atmosphere. This carbon flux is represented by the structure and coverage of five Plant Functional Types (PFTs) and soil carbon storage. The PFTs are broadleaf and needleleaf trees, C_3 and C_4 grasses, and shrubs. All models used the same horizontal grid resolution of 1.8º latitude by 3.6º longitude.

We carried out three sequences of experiments, each with a similar design except for different forcing and boundary conditions (Table 4.1). The boundary conditions were taken to represent the climate conditions of the present day (PI), LGM (21 ka BP) and HE1 (16 ka BP). Each sequence covered 4500 simulated years. First, the model was spun up for 2000 years. After reaching the equilibrium state, Heinrich climate-like conditions were simulated by increasing the freshwater discharge into the North Atlantic Ocean (region A, Fig. 4.1a) linearly from 0 to 0.2 Sv (1 Sv = 10^6 m^3/sec) over a period of 1000 simulated years. As shown by Weaver et al. (2003), this amount of freshwater perturbation is enough to slow down or terminate the deep-water formation in the UVic ESCM. We tried to re-establish the AMOC after its collapse by adding freshwater to a region west of West Antarctica (region B, Fig. 4.1a) at a rate increasing from 0 to 1 Sv over a period of 500 years. This site was chosen because it is a potential location for freshwater discharge from the melting continental ice sheet and might have played a role in the recovery of the AMOC (Clark et al., 1996; Kanfoush et al., 2000; Weaver et al., 2003) as well as a place of the Antarctic Intermediate Water (AAIW) formation. The final 1000 years of simulation was run without any freshwater perturbation (Fig. 4.2).

Furthermore, we ran an additional simulation with HE1 boundary conditions, called H1_EXT (Table 4.1), in which we applied a strong negative freshwater flux anomaly at a constant rate of -0.3 Sv over a period of 500 years to the North Atlantic Ocean (region C),

which is another possible way of triggering the recovery of the AMOC after its collapse (e.g. Schmittner et al., 2002b). The conditions for the remainder of this simulation were the same as for the final 1000 years of all sequences. Finally, we compared the model result of the H1_EXT experiment with pollen records from the region around the Atlantic Ocean compiled in terms of biomes (Fig. 4.1, Table 4.2). To facilitate this data-model comparison, the results from the DGVM were translated into biomes using the algorithm described by Handiani et al. (2012). This algorithm combines the potential PFTs calculated by the DGVM and environmental constrains such as temperature and the number of growing degree days.

Table 4.1 Experimental design and boundary conditions as well as hosing locations (denoted in Fig. 4.1a).

Experiment	Boundary conditions		The HE1 freshwater hosing experiment			The BA freshwater hosing experiment		
	Insolation	CO_2 (ppm)	Rates (Sv)	Hosing location	Years simulation	Rates (Sv)	Hosing location	Years simulation
PI	1950	310	0-0.2	A	1000	0 -1.0	B	500
GL	21 ka	200	0-0.2	A	1000	0 -1.0	B	500
H1	16 ka	220	0-0.2	A	1000	0 -1.0	B	500
H1_EXT	16 ka	220	0-0.2	A	1000	-0.3	C	500

4.4 Results

4.4.1 The variability of AMOC and physical ocean properties

The model produced different deep-water formation histories for the three different sequences of simulations, initialized from three different climate states (present day, last glacial maximum, and pre-Heinrich event 1; denoted hereafter PI, GL, H1, respectively; cf. Table 4.1). The strongest and deepest AMOC was established in the PI simulation, while the lowest and shallowest developed in the GL simulation. The maximum of the AMOC streamfunction reached 21 Sv, 10 Sv, and 16 Sv in the PI, LGM, and H1 sequences, respectively (Fig. 4.2). In all simulation sequences, the AMOC collapsed after perturbing the freshwater balance in region A, while they performed differently when the freshwater was added to region B.

In the PI sequence, the maximum of the AMOC streamfunction increased from 1 Sv at the end of the freshwater perturbation in region A to 13 Sv at the end of the perturbation in region B (T1 in Fig. 4.2), and it continued to increase up to 21 Sv. In the H1 sequence, the maximum of the streamfunction increased from 1 Sv to only 2 Sv at the end of the

freshwater perturbation in region B and then returned to collapsed conditions until the end of the sequence (Fig. 4.2). However, in the H1_EXT sequence, the AMOC recovered, and the maximum of the streamfunction experienced an overshoot occurring a few decades after the negative freshwater input to region C ceased.

Table 4.2 The pollen records used in the biome reconstruction for the BA period compiled for the terrestrial regions around the Atlantic Ocean (Europe, North America, tropical South America and Africa (see also Fig. 4.1a, 4.1b).

ID No.	Latitude and Longitude	Sites	Biomes reconstruction
North America sites (reference: Jiménez-Moreno et al., 2010)			
1.	45.91°N; 120.88°W	Carp Lake	Tundra
2.	42.23°N; 125.81°W	EW-9504-17PC	Temperate forest
3.	34.28°N; 120.03°W	ODP 893A	Temperate forest
4.	32.90°N; 119.73°W	F2-92-P29	Warm-temperate forest
5.	35.38°N; 111.71°W	Walker Lake	Grassland and dry shrubland
6.	34.45°N; 111.33°W	Potato Lake	Boreal forest
7.	30.26°N; 85.01°W	Camel Lake	Temperate forest
Europe sites (reference: Fletcher et al., 2010)			
8.	36.20°N; 4.30°E	ODP site 976	Temperate forest
9.	36.13°N; 2.62°E	MD95-2043	Temperate forest
10.	40.58°N; 10.35°E	MD95-2039	Grassland and dry shrubland
11.	41.15°N; 9.68°E	MD99-2331 (MD03-2697)	Temperate forest
12.	40.93°N; 15.62°W	Lago Grande di Monticchio	Temperate forest
13.	41.88°N; 12.77°W	Valle di Castiglione	Grassland and dry shrubland
14.	42.57°N; 11.80°W	Lagaccione	Temperate forest
Equatorial Africa (reference: Hessler et al., 2010)			
15.	3.47°S; 29.57°E	Kashiru Bog, Burundi	Savannah and xerophytic scrubland
16.	9.33°S; 33.75°E	Lake Masoko, Tanzania	Warm temperate mixed forest
Equatorial South America (reference: Hessler et al., 2010)			
17.	23.87°S; 46.71°W	Colônia, Brazil	Savannah and xerophytic scrubland
18.	5.45°N; 73.46°W	Fúquene, Colombia	Warm temperate mixed forest
19.	3.67°S; 37.72°W	GeoB 3104 - off NE Brazil	Warm temperate mixed forest

The maximum of the AMOC streamfuction increased quite sharply to 30 Sv, then decreased to 16 Sv after a few hundred years, where it remained until the end of the

simulation (T2 in Fig. 4.2). In contrast, in the GL sequence the maximum of the streamfunction remained unchanged for 500 years after adding freshwater to region B, and the AMOC stayed in a collapsed state until the end (Fig. 4.2).

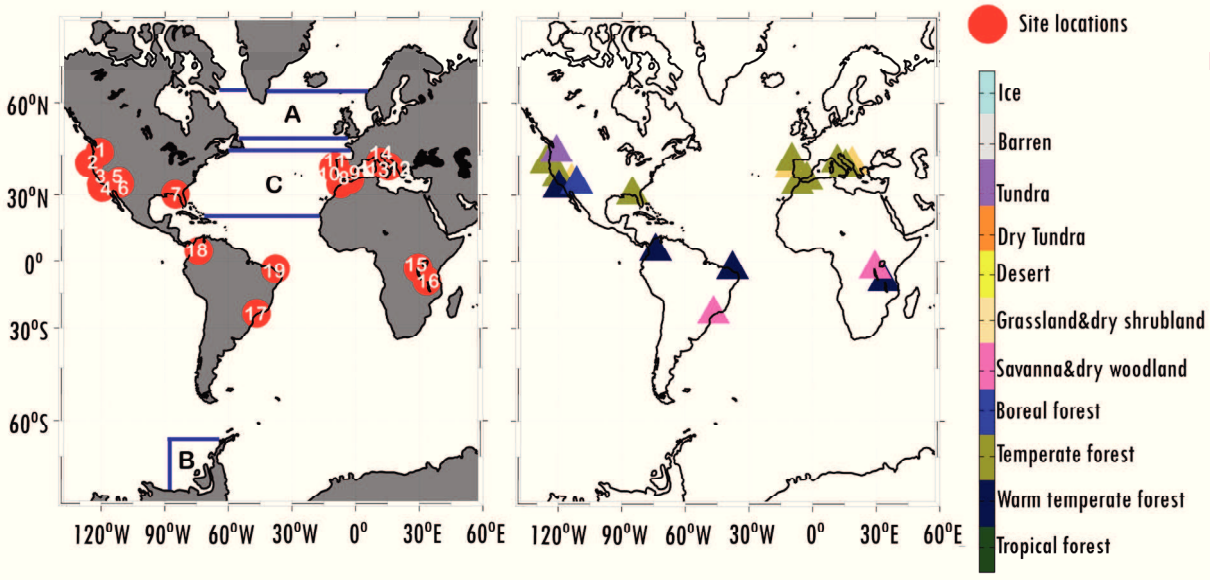

Figure 4.1 (a) Location sites of pollen records mentioned in Table 4.2 and the freshwater discharge locations: east of the St. Lawrence River (region A), west of West Antarctica (region B), the North Atlantic Ocean between latitude of 20°N-50°N (negative discharge in region C). (b) The biomes reconstruction during the onset of BA (see Table 4.2).

The relative abundance of the two major water masses involved in the AMOC, NADW and AABW, is determined by their density. When the density of one water mass increases relatively to the other, it will occupy a larger fraction of the volume of the Atlantic Ocean (Stocker et al., 1992; Schmittner et al., 2002a). Zonally averaged density anomalies in the Atlantic Ocean (Fig. 4.3) show the differences between simulated conditions 500 years after adding freshwater to region B (T1 in Fig. 4.2) and the collapse triggered by perturbing region A (T0 in Fig. 4.2). Furthermore, the individual contributions of temperature and salinity to the density anomalies are indicated. In all sequences, salinity is the dominant component in the total density anomaly after 500 years of adding freshwater to region B. The AAIW freshened significantly in the PI and H1 sequences at time T1 (Figs. 4.3c and 4.3i). In contrast, the AAIW did not show any change in the GL sequence after the freshwater perturbation in region B (Fig. 4.3f). Furthermore, the fate of NADW was different in the three different simulation sequences: it became denser in PI, lighter in H1, and even disappeared in GL. The density anomaly in the H1_EXT simulation (Figs. 4.3j-4.3l) is somewhat similar to that in the PI sequence with freshwater perturbation in region B (Figs. 4.3a-4.3c), but the

AAIW became fresher and the NADW denser after 500 years of extracting freshwater from the North Atlantic Ocean.

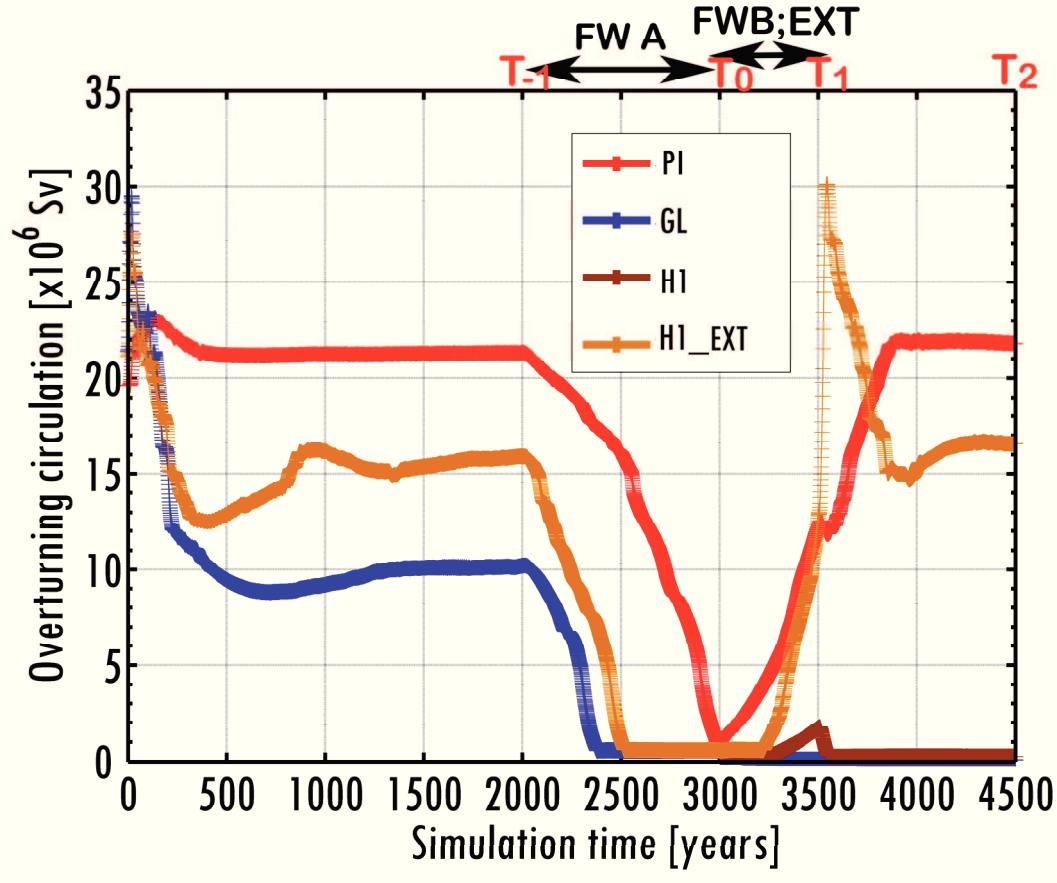

Figure 4.2 The AMOC streamfunction maximum for all sequences (see for experimental setup Table 1). Anomaly plots in the following figures have been calculated between simulation times T1 and T0.

The changes in AMOC strength are better understood in terms of the zonally averaged depth-integrated steric height. We calculated the steric height following Schmittner et al. (2002a), and compared the results at times T1 and T0 (Fig. 4.2). The total steric height gradient ($\Delta\phi$) is shown together with contributions due to temperature ($\Delta\phi_T$) and salinity ($\Delta\phi_S$) changes for each simulation (Fig. 4.4). As suggested by earlier studies (Hughes and Weaver, 1994; Wiebe and Weaver, 1999; Schmittner et al., 2002a), the steric height gradient between the southern tip of Africa (35°S), where the eastern zonal boundary of the Atlantic Ocean ends, and the regions of deep water formation around 60°N is proportional to the strength of the AMOC formation.

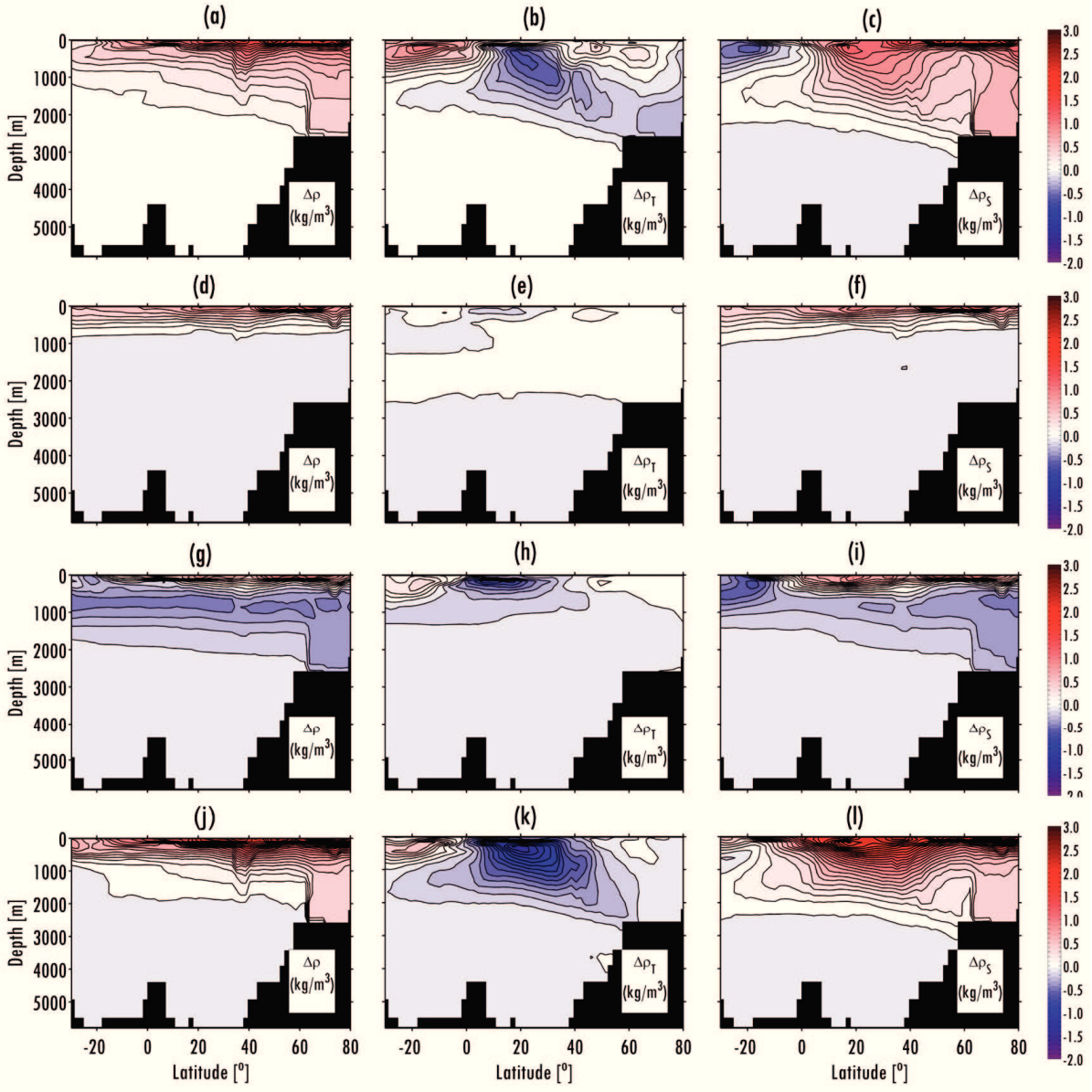

Figure 4.3 Annual-mean anomaly density plots showing differences between time T1, after 500 years of adding freshwater in region B, and time T0, at the end of the freshwater perturbation at region A, for sequences PI (a-c), GL (d-f), H1 (g-i), and H1_EXT (j-l); for each sequence the plots are decomposed into contributions from temperature changes $\Delta\rho_T$ (b, e, h, k) and salinity changes $\Delta\rho_S$ (c, f, i, l). The isoline differences for each plot are 0.1 kg m^{-3}.

The steric height gradient between the latitudes of 35ºS and 60ºN in the PI sequence at T1 decreased with respect to the simulation at T0 (Fig. 4.4a) due to the intensified AMOC after the freshwater perturbation in region B (Fig. 4.1a). This was consistent with the dominance of the salinity component within the decreased steric height anomaly (Fig. 4.4a). A small change of the difference in density in the GL sequence between T1 and T0 (Fig. 4.3d) was consistent with small changes in the steric height gradient between 35ºS and 60ºN and the AMOC in these simulations (Fig. 4.4b). The

temperature and salinity contributions to the change in the steric height gradient were also small. The difference in the steric height gradient in the H1 sequence between times T1 and T0 was also small, except that in this case the salinity and temperature contributions showed appreciable but opposite changes between 35ºS and 35ºN (Fig. 4.4c). The anomaly pattern in the steric height gradient between times T1 and T0 in the H1_EXT sequence (Fig. 4.4d) was similar to that of the PI sequence (Fig. 4.4a), except that the differences in the temperature and salinity contributions were larger in the H1_EXT than in the PI sequence. Both anomalies resulted in a recovery of the AMOC, although in different ways.

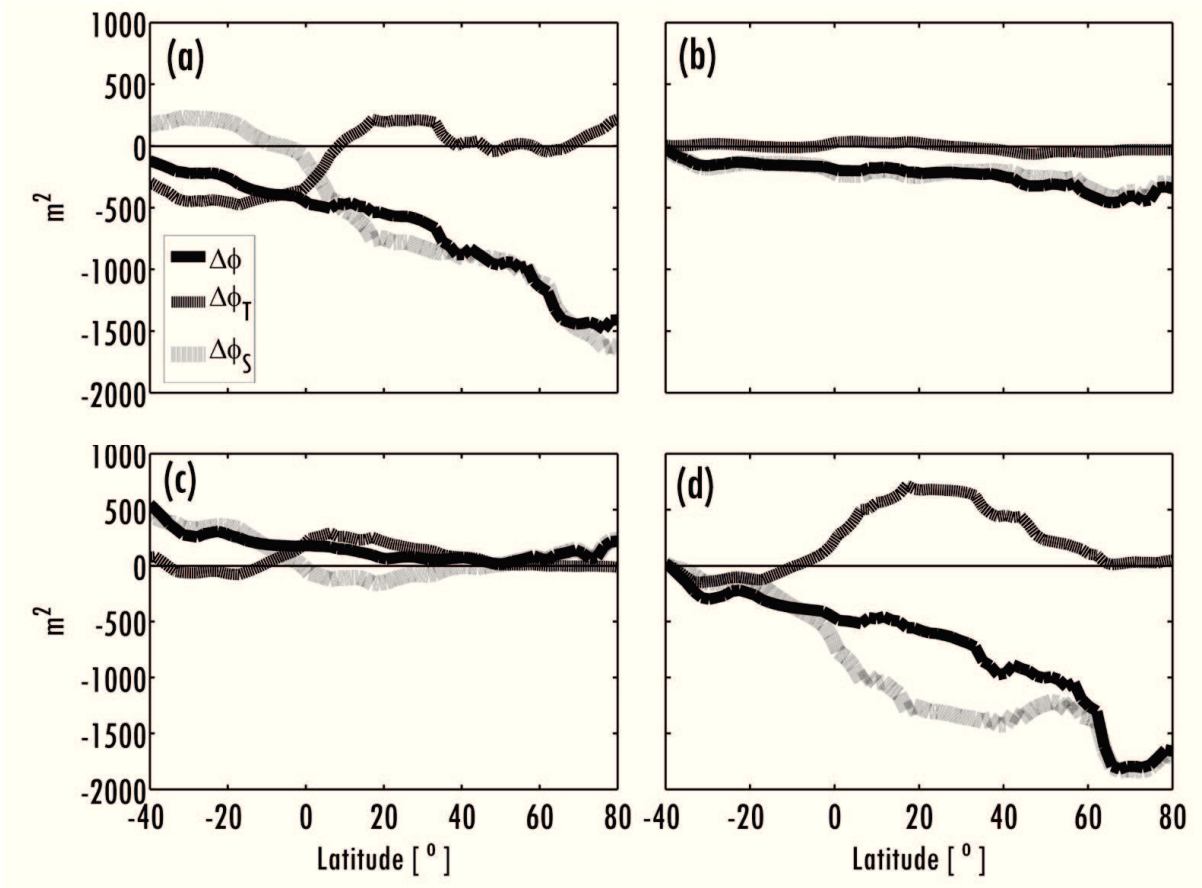

Figure 4.4 Same as Fig. 4.3 but for annual zonally averaged depth-integrated steric height for sequences (a) PI, (b) GL, (c) H1, and (d) H1_EXT. The total differences in steric height ($\Delta\phi$) is a combination of temperature ($\Delta\phi_T$) and salinity changes ($\Delta\phi_S$).

Differences in sea-surface temperature (SST) between the collapsed state (T0, after adding freshwater to region A) and the partial recovery of the AMOC (T1, after 500 years of adding freshwater to region B or extracting freshwater from region C) for the PI, GL, H1 and H1_EXT sequences are given in Figs. 4.5a-4.5d. For the PI sequence, the temperature decreased both in the North and South Atlantic Ocean. For the GL

sequence, it hardly changed or showed only a slight warming in the southern North Atlantic Ocean. In the case of the H1 and H1_EXT sequences, the SST increased in the North Atlantic Ocean and decreased in the South Atlantic Ocean, whereby the anomalies were bigger in the North Atlantic Ocean after extracting freshwater from region C in the North Atlantic Ocean (H1_EXT) than after adding freshwater to region B near Antarctica (H1). The mean anomalies in SST in the North Atlantic Ocean (0º-100ºW and 25º-70ºN) were -0.85ºC for the PI and 0.26ºC for the H1 sequence, respectively. For comparison, in the South Atlantic Ocean (20ºE-73ºW and 25º-70ºS), the mean anomalies were -1.52ºC for the PI and -0.78ºC for the H1 sequence. The mean SST anomalies in the GL sequence were slightly smaller, -0.17ºC in the North Atlantic Ocean and -0.11ºC in the South Atlantic Ocean. The SST anomalies show that adding freshwater to region B led to a warming in the North Atlantic Ocean, although the AMOC did not necessarily recover (Fig. 4.2).

4.4.2 Precipitation and vegetation response

Precipitation was generally higher over the North Atlantic Ocean than over the South Atlantic Ocean for all simulation sequences (Figs. 4.5e-4.5h). This was due to a northward shift of the region of high tropical precipitation, associated with the ITCZ. A warmer SST in the North Atlantic Ocean was accompanied by significantly increased precipitation from 0º to 30ºN and reduced precipitation from 0º to 30ºS. Over land, the anomaly pattern was similar in all simulations. The western Sahara showed the largest anomaly of the Northern Hemisphere. Northeast Brazil and southwestern Africa became drier compared with other parts of the Southern Hemisphere. An interesting feature occurred in the simulation initialized from the PI sequence (Fig. 4.5e), in which precipitation increased between 15º and 30ºN and decreased between 15ºN to 30ºS. This precipitation pattern was stronger compared to that of the other sequences.

Generally, the vegetation response at time T1 compared to time T0 was relatively minor in all sequences (Fig. 4.6). Relatively strong responses occurred in western South America, southern Europe, northwest Eurasia, and in Africa (Sahara and Sahel). This was connected with the substantial precipitation changes in those areas. For example, in the PI sequence, precipitation strongly increased in the western Sahara, corresponding to an increase in grasses (Fig. 4.6e). Like the precipitation pattern (Figs. 4.5a-4.5h), the vegetation response in the PI sequence (Figs. 4.6a and 4.6e) differed considerably from the other simulated sequences (Figs. 4.6b-4.6d and 4.6f-4.6h). Significant changes occurred in tropical Africa and northern South America, as well as in the mid- to high

latitudes. Trees and grasses sharply decreased in the eastern Sahel region, while only trees decreased in western South America (Figs. 4.6a and 4.6e). In contrast, a sharp increase in grasses occurred in northwest Africa. This feature was also found in the H1_EXT simulation (Fig. 4.6h), which developed a strength of the AMOC similar to that of the PI simulation 500 years after extracting freshwater from region C or adding freshwater to region B (~13 Sv), respectively. Furthermore, in the GL and H1 sequences, vegetation cover remained relatively unchanged, whereas tree and grass cover after 500 years of the freshwater perturbation in region B remained similar to those at the end of the freshwater perturbation in region A (Figs. 4.6b-4.6c and 4.6f-4.6g). However, an exception occurred in the H1 sequence (Fig.s 4.6c and 4.6g), where trees decreased sharply (~60%) and grasses increased in the center of the Sahel.

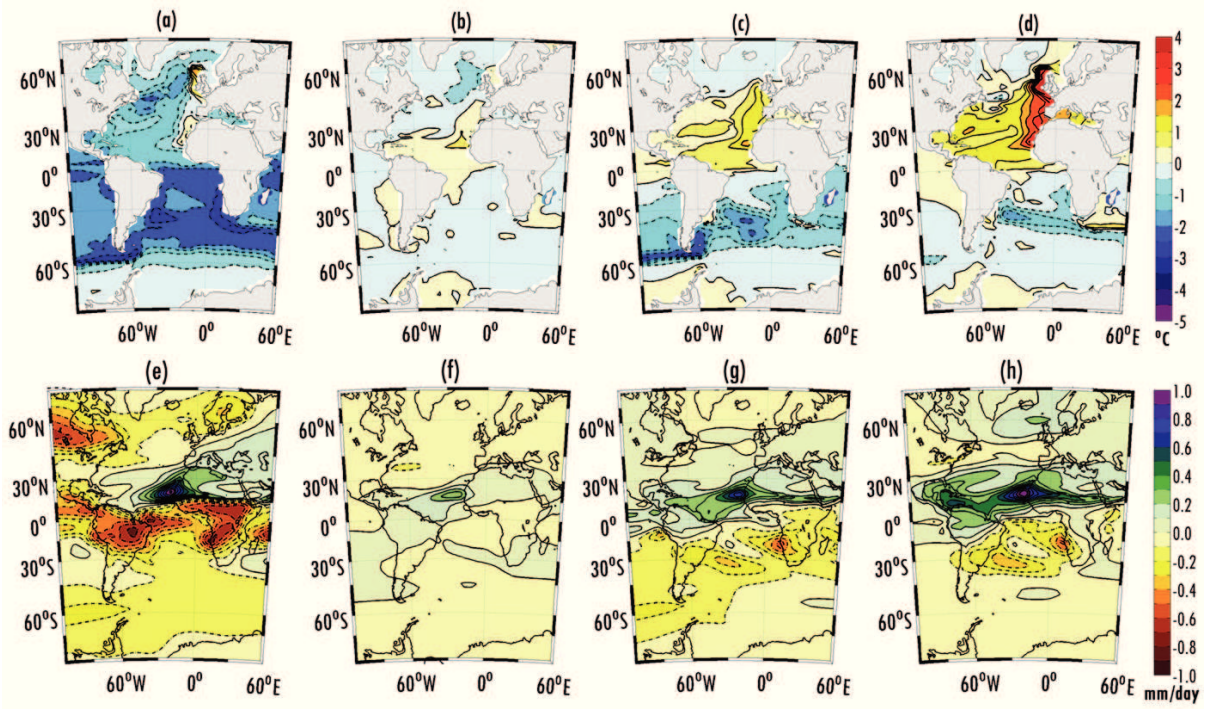

Figure 4.5 Same as Fig. 4.3 but for annual mean anomaly of sea surface temperature (SST, top panel) and precipitation (bottom panel) for sequences PI (a,d), GL (b,f), H1 (c,g), and H1_EXT (d,h).

Distinct changes of vegetation occurred in the mid- to high latitudes around the North Atlantic Ocean (e.g., in North America, Europe, and western Russia) in the PI and H1_EXT sequences. In the PI sequence, trees strongly decreased in eastern North America while grasses increased. In western Europe, grasses decreased by ~60%, while trees increased by 20% (Figs. 4.6a-4.6b). A unique feature occurred in eastern North America where grasses increased by 80% in the PI sequence and decreased in all other sequences. The magnitude by which grasses decreased varied, however. The largest

decrease (of ~40%) was in the GL sequence (Fig. 4.6f). In Eastern Europe (around present-day Ukraine), grasses increased substantially in all sequences. The biggest increase was in the PI sequence by ~70% (Fig. 4.6e), while in the other sequences it increased by ~ 20%–60 % (Fig. 4.6a, Figs. 4.6g–4.6h).

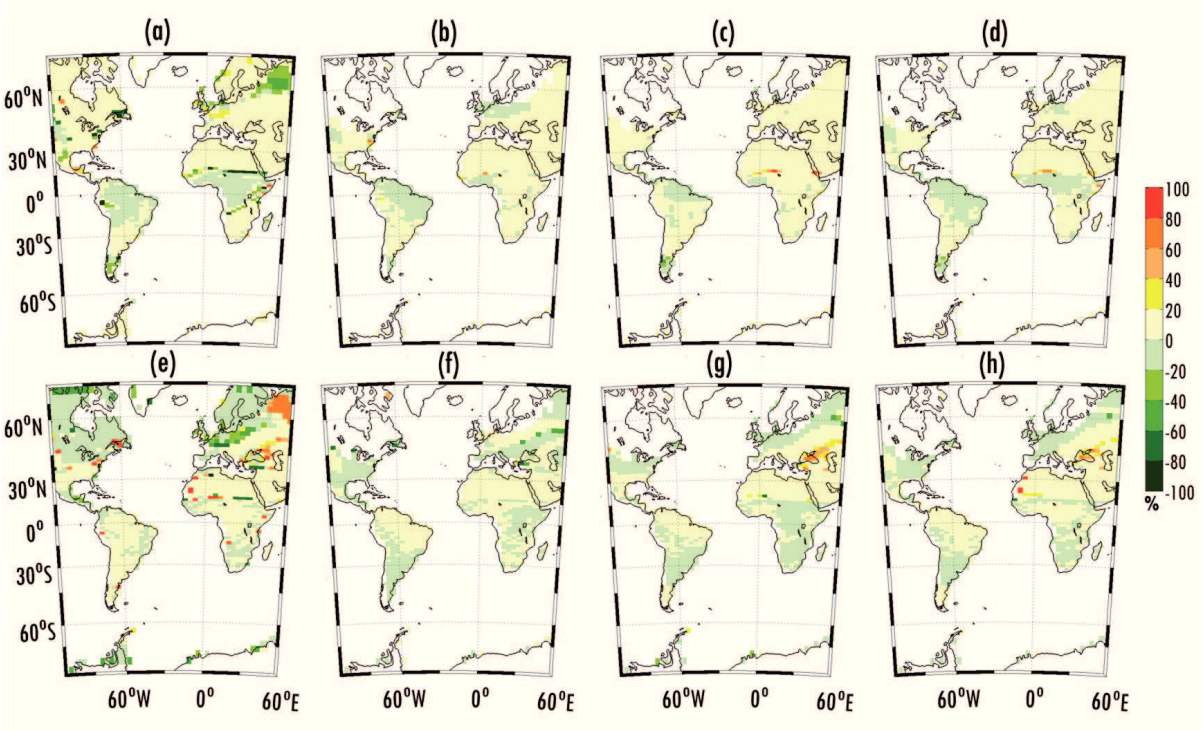

Figure 4.6 Same as Fig. 4.3 but for annual mean anomaly of tree cover (a-d) and grass cover (e-h) for sequences PI (a, e), GL (b, f), H1 (c,g), and H1_EXT (d, h).

To understand the vegetation differences between the climate conditions before and after the AMOC recovery, we compared the tree and grass cover at times T2 and T-1 between 110°W and 60°E longitude and between 50°S and 70°N latitude (Fig. 4.7). There was relatively little vegetation change between these two climate conditions in the PI and HE1_EXT sequences, except for some slight changes in the Northern Hemisphere (from the equator to 60°N) and in southern South America (around 20°S). The total changes in trees or grasses were less than 10% (Figs. 4.7a and 4.7d). The tree and grass cover changes of the GL and H1 sequences were substantial and followed similar trends, although the magnitude of the changes were slightly smaller in the H1 sequence (Fig. 4.7c). At the end of both sequences, grass cover decreased between 20°N and 50°N, the maximum increase of grasses (with differences up to 40%) occurred at 60°N, and tree cover declined near 20°N (Figs. 4.7b and 4.7c).

Distinct changes of vegetation occurred in the mid- to high latitudes around the North Atlantic Ocean (e.g., in North America, Europe, and western Russia) in the PI and

H1_EXT sequences. In the PI sequence, trees strongly decreased in eastern North America while grasses increased. In western Europe, grasses decreased by ~60%, while trees increased by 20% (Figs. 4.6a-4.6b). A unique feature occurred in eastern North America where grasses increased by 80% in the PI sequence and decreased in all other sequences. The magnitude by which grasses decreased varied, however. The largest decrease (of ~40%) was in the GL sequence (Fig. 4.6f). In Eastern Europe (around present-day Ukraine), grasses increased substantially in all sequences. The biggest increase was in the PI sequence by ~70% (Fig. 4.6e), while in the other sequences it increased by ~ 20%–60 % (Fig. 4.6a, Figs. 4.6g–4.6h).

To understand the vegetation differences between the climate conditions before and after the AMOC recovery, we compared the tree and grass cover at times T2 and T-1 between 110ºW and 60ºE longitude and between 50ºS and 70ºN latitude (Fig. 4.7). There was relatively little vegetation change between these two climate conditions in the PI and HE1_EXT sequences, except for some slight changes in the Northern Hemisphere (from the equator to 60ºN) and in southern South America (around 20ºS). The total changes in trees or grasses were less than 10% (Figs. 4.7a and 4.7d). The tree and grass cover changes of the GL and H1 sequences were substantial and followed similar trends, although the magnitude of the changes were slightly smaller in the H1 sequence (Fig. 4.7c). At the end of both sequences, grass cover decreased between 20ºN and 50ºN, the maximum increase of grasses (with differences up to 40%) occurred at 60ºN, and tree cover declined near 20ºN (Figs. 4.7b and 4.7c).

4.4.3 Comparison between model and paleovegetation data

Pollen studies for the BA period show mostly grassland and temperate forest in western and southeast North America, as well as in southern Europe, although warm temperate and boreal forest also occurred in western North America. Tropical Africa and South America were covered by savannah and warm temperate forest (Figs. 1b, Table 2).

The reconstructed biomes of our model simulations showed a pattern at time T1 similar to that of the proxy reconstructions for the beginning of the BA period, albeit a few differences exist (Fig. 4.8). In the PI sequence, grass cover dominated in eastern Europe and North America, while boreal forest was found in Europe and central America. In this sequence, the tropics were mainly covered by tropical forest except for small regions of savannah found in western South America and Africa (Fig. 4.8a). The biome patterns in southeastern North America, Europe, and South America were similar in all sequences,

except in the extent of the area covered. The GL sequence was the most different. For example, temperate forest in eastern Europe (Ukraine) covered the smallest area in the GL sequence (Fig. 4.8b). Warm temperate forest in southeast North America occupied the same small area in all sequences, except for the GL sequence, where forest cover was simulated along the North and South Carolina coastline (compare Figs. 4.8b with 4.8a, 4.8c, 4.8d).

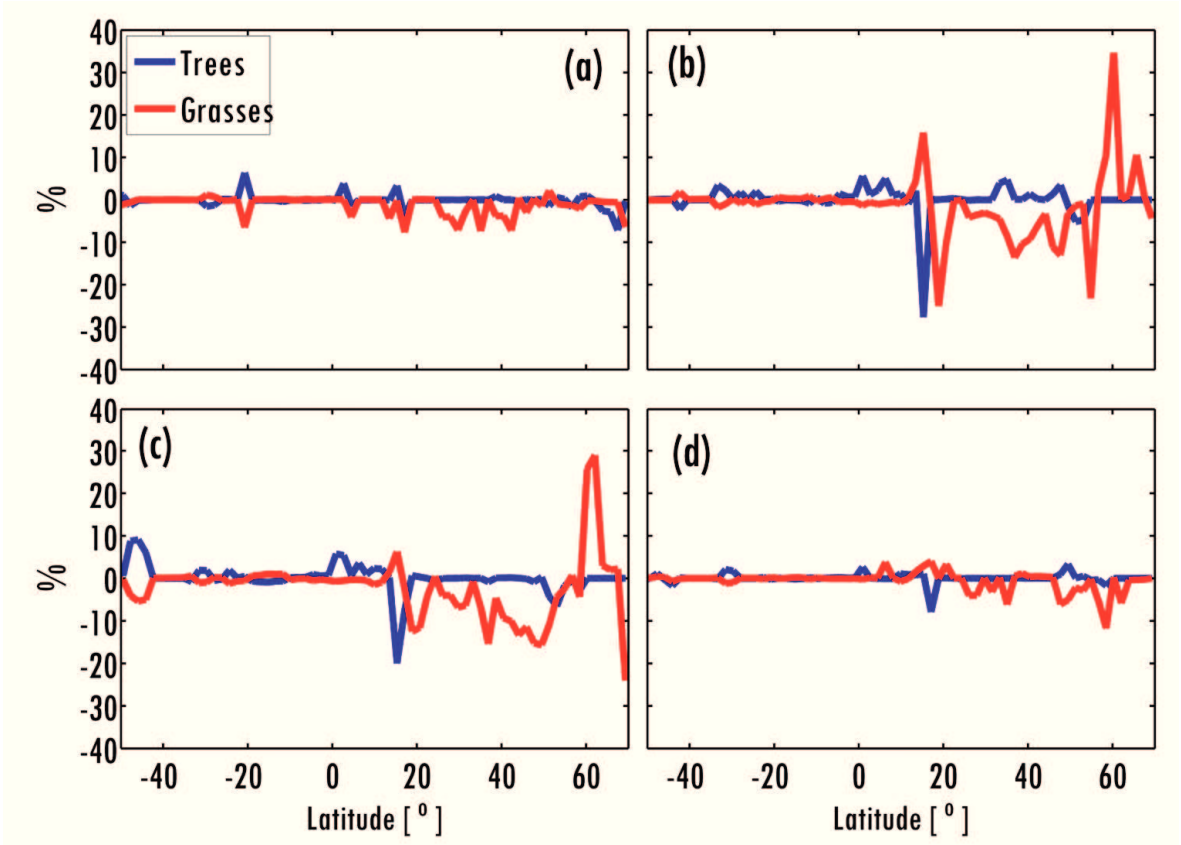

Figure 4.7 Annual anomaly of zonally averaged tree and grass cover showing differences between time T2, at the end of sequence (see Fig. 4.2), and time T-1, before adding freshwater to region A, for sequences PI (a), GL (b), H1 (c), and H1_EXT (d) in the area between 110°W to 60°E and 50°S to 70°N.

The model results and paleovegetation data of grass covered regions in western North America, southern Europe, and the Mediterranean are in good agreement (compare Figs. 4.8 and 4.1). The savannah and warm temperate forest in southeast Africa in the model output is supported by paleo-records. Temperate forest in southeast North America was not simulated by the model, in which grassland and warm temperate forest dominated (Fig. 4.8d). Model and paleovegetation data disagree in northeast and southeast Brazil as well as in western tropical South America. The model output indicates tropical forest in these regions, while pollen records suggest a warm temperate forest in tropical

western South America and northeast Brazil, and savannah grassland in southeast Brazil.

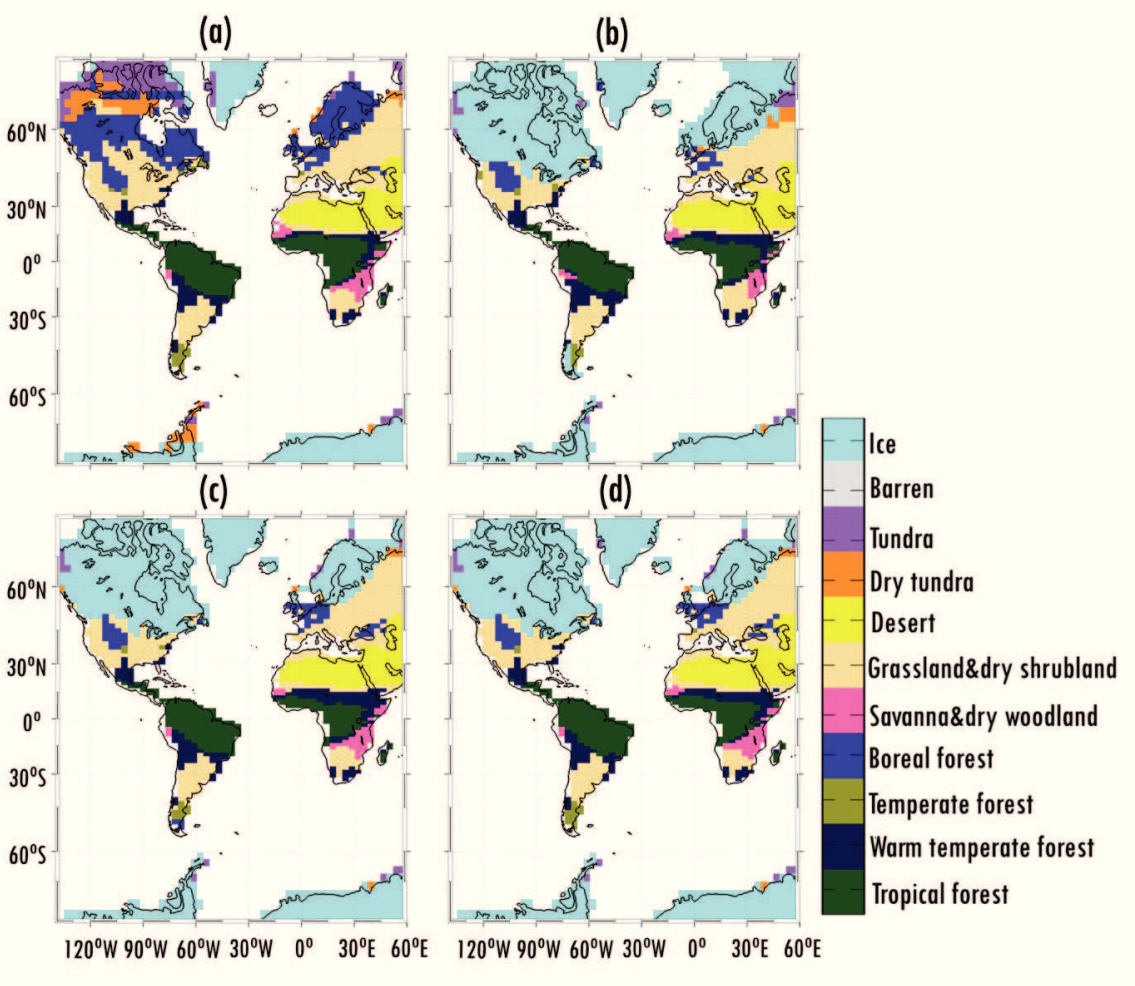

Figure 4.8 Biome distribution at time T1, after 500 years of adding freshwater in region B, calculated after a simply algorithm (Handiani et al., 2012) combining the potential PFTs and the environmental limitations from the model output for sequences (a) PI, (b) GL, (c) H1, and (d) H1_EXT. The simulated biomes were compilated into mega-biomes as defined by Harrison and Prentice (2003).

4.5 Discussion

Whether, or to what degree, deepwater formation in the North Atlantic Ocean during the last deglaciation is controlled by perturbing the freshwater balance of the Southern Ocean is still under debate (Trevena et al., 2008; Swingedouw et al., 2009). We note that in all simulation sequences the North Atlantic Ocean warmed relative to the South Atlantic Ocean after freshwater was added in the Southern Hemisphere, although the AMOC strength did only recover in one out of three simulations. The AMOC strength recovered only in the PI sequence that used present-day orbital parameters and CO_2 concentration. This result was similar to that of Weaver et al. (2003) who point out that

there is a strong interhemispheric link between global-scale water masses distribution and the thermohaline circulation. By applying a freshwater perturbation in the area of AAIW formation, the density of AAIW decreases and, in turn, the density of NADW relatively increases, inducing a gradual intensification of the AMOC.

In contrast, adding freshwater in the Southern Hemisphere did not lead to a recovery of the AMOC strength under GL and H1 sequences. Either the AMOC remained in a collapsed state, or it temporally intensified, albeit only slightly. The surface of the North Atlantic Ocean slightly warmed, became slightly more saline and overall became less dense. At greater depths, density did not change in the GL sequence and slightly decreased in the H1 sequence. Slightly reduced density of deep waters in the H1 sequence was mainly due to the freshwater perturbation applied to region B in the Southern Hemisphere. This suggests that perturbing the freshwater balance in the Southern Hemisphere to form denser AAIW is not guaranteed to drive the deep overturning circulation from a collapsed state back to an active state at its initial strength. This is probably because the density contrast between the North and South Atlantic Oceans has less impact on the strength of the AMOC strength when the NADW is already fresher and shallower (as it was in the case of the GL and H1 sequences). Furthermore, when the freshwater balance in the Northern Hemisphere was perturbed, the collapse of the AMOC was faster under LGM and HE1 than under present day background climate conditions. Our simulations thus support that the glacial AMOC is more vulnerable to a perturbation of the freshwater balance of the North Atlantic Ocean and less susceptible to a recovery of the AMOC by a perturbation of the freshwater balance in the Southern Ocean (e.g. Ganopolski and Rahmstorf, 2001; Schmittner et al., 2002a; Trevena et al., 2008; Kageyama et al., 2009).

Salinity played an important role in the AMOC recovery mechanism. This is indicated by the salinity contribution to the density anomalies in the PI and H1_EXT sequences, which showed a similar pattern after the AMOC recovered. The pattern was different from the one seen in the GL and H1 sequences, although the temperature component of the density anomalies contributed to warming at time T1 in all sequences. The salinity component of the density anomalies in the PI and H1_EXT sequences contributed to saltier waters, foremost in the North Atlantic Ocean. On the other hand, in the GL and particularly the H1 sequences, the deep water became less saline.

Stouffer et al. (2006) use an atmosphere-ocean general circulation (AOGCM) to investigate the response to freshwater perturbations in the North Atlantic Ocean (50º-

70ºS) and the Southern Ocean (south of 60ºS). They suggest that the AMOC is mainly unchanged in the case of the freshwater perturbation near Antarctica, although a slight weakening of the AMOC is seen at the end of their simulation, for which they propose two mechanisms: firstly, the reduced contrast of sea surface salinity (SSS) between the North Atlantic and the North Pacific Oceans and, secondly, freshwater from the Southern Hemisphere reaching far into the North Atlantic Ocean hindering the sinking of surface waters at high latitudes, which leads to a reduced AMOC. These mechanisms are also found in our simulations. When the effect of the freshwater perturbation west of West Antarctica reaches the North Atlantic Ocean, it is responsible for SSS changes and hinders the sinking of surface waters, thus influencing the AMOC.

Weber et al. (2007) compare the response of the AMOC to LGM boundary conditions in nine Paleoclimate Modeling Intercomparison Project (PMIP) models with respect to three mechanism: changes in net evaporation over the Atlantic basin, local processes within the Atlantic basin as expressed by the density difference between its northern and southern ends, and the deep overturning cell associated with the formation of AABW in the Southern Ocean. For two EMICs, the UVic ESCM and the ECBilt-CLIO (de Vries and Weber, 2005), they cannot identify the process that dominates the AMOC response. In a subsequent study, however, Weber and Drijfhout (2007) determine for the ECBilt-CLIO that under LGM climate conditions the AMOC remains in a collapsed state after a freshwater perturbation as long as the initial AMOC transports freshwater out of the Atlantic basin. Furthermore, they find that the AMOC recovers when the AMOC transports freshwater into the Atlantic basin. Similarly, in our glacial simulations (GL and H1), the freshwater transport by the initial AMOC at the southern boundary was into the Atlantic basin (northward), and both our simulations remained in a collapsed state after a freshwater perturbation was applied to the North Atllantic Ocean. The AMOC intensified under preindustrial boundary conditions with a northward overturning freshwater transport at the southern boundary of the Atlantic basin.

The H1_EXT sequence - which applied extraction of freshwater from the North Atlantic Ocean (e.g. Manabe and Stouffer, 1997; Schmittner et al., 2002b) - succeeded in recovering the AMOC. The density profile in the North Atlantic Ocean after the extraction of freshwater indicated warmer and saltier surface waters and denser and cooler waters at the depth of the NADW. This density profile was similar to that of the PI sequence, except that the salinity and temperature components were stronger than in the PI sequence. The negative freshwater flux applied in the H1_EXT sequence may

correspond to reduced precipitation, enhanced evaporation or reduced runoff and melting. The effect of freshwater extraction has been investigated in detail in an earlier version of the UVic model by Schmittner et al. (2002b), who reviewed the feedbacks between the Atlantic overturning and the ice sheet mass balance. They proposed the mechanism of growing ice sheet volume in response to the transition from a stadial to an interstadial during the LGM climate. Schmittner et al. (2002b) started their simulation with a linear decrease of freshwater in the North Atlantic Ocean and continued forcing with a constant negative freshwater perturbation until the end of the simulation. In one of their cases, the interstadial was stable and led to a constant increase of the North Atlantic salinities, which allowed recovery of the AMOC. Using a transient simulation with the coupled atmosphere-ocean general circulation model (AOGCM) of the National Center for Atmospheric Research (NCAR) Community Climate System Model version 3 (CCSM3), Liu et al. (2009) suggest that the abrupt warming at the onset of the BA may not be caused by freshwater forcing alone, but by overlapping climatic responses to increasing atmospheric CO_2 concentrations, the recovery of the AMOC after the HE1 period, and an AMOC overshoot.

In order to examine the effects of changing CO_2 concentrations in the UVic ESCM, preliminary investigations with transient CO_2 for different initial climate conditions have been performed by Weaver et al. (2007). They find that the AMOC declines in all their experiments and that the largest decline is in the experiment with the strongest initial value of the AMOC. However, they also find that all experiments in which the initial atmospheric CO_2 concentration is 240 ppm or below and the initial AMOC strength less than 17.4 Sv, the freshwater fluxes act to strengthen the AMOC. In contrast, the freshwater flux acts to weaken the AMOC in an experiment with a CO_2 concentration exceeding 240 ppm. Thus the dominance of heat flux over freshwater flux changes as a cause of the AMOC weakening appears to depend on the initial climate state. This result argues in favor of performing similar simulations using glacial boundary conditions to examine climate and AMOC changes at the onset of the BA period.

The warm climate in the North Atlantic Ocean, which possibly results from the recovery of the AMOC after its collapse (e.g. Boyle and Keigwin, 1987; McManus et al., 2004), may also be linked to changes in tropical precipitation and vegetation. During the abrupt warming in the H1_EXT sequence, vegetation showed no response in tropical South America, while in the PI sequence, tree cover decreased in the region of present-day

Peru. Furthermore, in the H1_EXT sequence, trees increased in the central Sahel, grasses increased markedly in a small region of northwest Africa (Mauritania), while tree cover decreased regionally in the western tip of Senegal. A compilation of vegetation records from western equatorial Africa (Hessler et al., 2010) shows a reduction of forest biomes between 18.5 and 14.7 ka BP as well as at the end of the deglacial period (~12 ka BP) in agreement with our model results. Paleovegetation records from northeast Brazil indicate a decline in forest between 15-13.5 ka BP, while southeast Brazil is dominated by open vegetation, mostly grasses, from 23-12 ka BP (Hessler et al., 2010). Although our model simulated large changes in precipitation, which would have been expected from the paleovegetation data, the resulting vegetation changes were small. Records from eastern tropical Africa show the development of montane and tropical forest during the warming climate after the HE1 (Hessler et al., 2010), which we did not find in our simulated vegetation.

The model-data comparison in North America and Europe gave mixed results. We compared the pollen records with the simulated H1_EXT sequence, which is our best simulation of B/A period. The warm climate in the North Atlantic Ocean in response to AMOC recovery corresponded to a warmer vegetation pattern indicated by grassland, boreal and warm temperate forest over Europe and North America. Grassland at the west coast of North America agreed with the terrestrial record of Walker Lake (Jiménez-Moreno et al., 2010) showing mostly xerophytic shrublands implying a cold and dry climate in that area. The simulated grassland also agreed with the reconstruction using southwest European and Mediterranean sites (Fletcher et al., 2010), which recorded mostly steppe forest. This type of forest includes more than 40% xerophytic steppe elements indicating warm and dry conditions. However, the model failed to simulate temperate forest in southeast North America and southern Europe (Jiménez-Moreno et al., 2010; Fletcher et al., 2010). For southeast North America our model suggested a warm temperate forest. Temperate and warm temperate forest biomes are distinguished by different temperature ranges, whereby the minimum temperature limitation for warm temperate forest is greater than for temperate forest (Handiani et al., 2012). The reason for the mismatch between model and proxy data is not fully understood. The climatic thresholds used in the biome reconstruction may require further study. Other discrepancies occurred in southern Europe and the Mediterranean, where grassland was simulated instead of temperate forest. This discrepancy corresponds to a lack of tree cover and a dominance of grasses simulated in the model.

In our simulations with the UVic ESCM, the changes in northern tropical Africa were induced by a northward shift of the region of high precipitation (corresponding to the ITCZ) during abrupt warming resulting from the recovery of the AMOC. This complements studies (e.g. Kageyama et al., 2010; Swingedouw et al., 2009; Handiani et al., 2012) that have investigated the sensitivity of the tropical African vegetation to a southward shift of the ITCZ during abrupt cooling, e.g., at the onset of a Heinrich event.

We compared the vegetation patterns of two warmer climate phases: the pattern before the collapse of the AMOC (Heinrich event 1-like conditions, time T-1) with that at the end of sequence (after AMOC recovery, time T2). The comparison is intended to show similarities and differences of the vegetation cover during these two warmer climates. We found the vegetation patterns of the two climates state (PI and H1_EXT) to be very similar. Differences in tree and grass cover were less than 10% and only occurred in a few areas, mostly around the North Atlantic Ocean. This finding may be compared to the hypothesis by Aitken et al. (2008) who propose that plant species respond to rapid climate change in three different ways: they either become extinct, persist in situ, or migrate to more suitable habitats. Our model results would be consistent with the second and third way, that is, persistence in situ or migration to more suitable habitats. Moreover, the total terrestrial carbon storage was nearly conserved in each sequence. The values before the abrupt cooling and at the end of the PI and H1_EXT simulation sequences differed by about 10 gigatons of carbon (GtC) and 11 GtC, respectively. The corresponding relative changes were 0.5% and 0.8%, respectively.

4.6 Conclusion

Our simulations confirmed that under present-day climate conditions the addition of freshwater (in amounts comparable to meltwater pulse 1A) to the Southern Ocean may lead to a recovery of the AMOC after collapse (Weaver et al. 2003). However, under glacial climate conditions the AMOC behaved differently. With LGM-type initial conditions the AMOC remained in a collapsed state, while with HE1-type initial conditions, the AMOC first slightly increased only to collapse again after freshwater hosing stopped. The North Atlantic Ocean warmed in response to adding freshwater to the Southern Ocean. It appears that in our model the AMOC is less sensitive to freshwater input to the Southern Ocean under glacial climate conditions than under present-day climate conditions. The AMOC did recover under glacial conditions when we

extracted freshwater from the North Atlantic, mimicking a reduction of iceberg calving into the North Atlantic Ocean.

The impact of an intensifying AMOC and warming climate in the North Atlantic Ocean on vegetation patterns depended on background climatic conditions, although tropical northern Africa was clearly the most sensitive area in terms of precipitation. With respect to vegetation changes during the BA period, in our model the zone of intense tropical precipitation shifted northward, followed by immediate and considerable vegetation changes, mostly in northern tropical and subtropical Africa. Comparison with pollen compilation records from North America and Europe showed reasonable agreement.

The vegetation patterns before the AMOC collapsed and after it recovered were very similar. Changes in tree and grass cover were smaller than 10% and limited to a few areas around the North Atlantic Ocean, and the total terrestrial carbon storage was largely conserved. This transient nature of the simulated vegetation change is consistent with the hypothesis that vegetation cover persisted in situ or migrated to more appropriate habitats in response to abrupt climate change.

4.7 Acknowledgements

This work was funded by the Deutsche Forschungsgemeinschaft (DFG) as part of the German contribution to the Integrated Ocean Drilling Program (SPP 527) “Abrupt Climate Change in the African Tropics (ACCAT)” and the DFG Research Center/Excellence Cluster “The Ocean in the Earth System”. A part of financial support during the final production in this study was also given by “The Excellent Scholarship Program by Bureau of Planning and International Cooperation”, Secretary-General of Ministry of Education and Culture, Indonesia. The authors are grateful to the Climate Modelling Group at the University of Victoria for providing the UVic ESCM.

Chapter 5

Tropical vegetation response to Heinrich event 1 as simulated with the UVic ESCM and CCSM3

D. Handiani, A. Paul, X. Zhang, M. Prange, U. Merkel and L. Dupont
(Under discussion for publication in *Climate of the Past*, *Special Issue: Progress in paleoclimate modelling*, doi:10.5194/cpd-8-5359-2012)

5.1 Abstract

We investigated changes in tropical climate and vegetation cover associated with abrupt climate change during Heinrich event 1 (HE1) using two different global climate models: the University of Victoria Earth System-Climate Model (UVic ESCM) and the Community Climate System Model version 3 (CCSM3). Tropical South American and African pollen records suggest that the cooling of the North Atlantic Ocean during HE1 influenced the tropics through a southward shift of the rainbelt. In this study, we simulated the HE1 by applying a freshwater perturbation to the North Atlantic Ocean. The resulting slowdown of the Atlantic Meridional Overturning Circulation was followed by a temperature seesaw between the Northern and Southern Hemispheres, as well as a southward shift of the tropical rainbelt. The shift was more pronounced in the CCSM3 than in the UVic ESCM simulation. Nevertheless, both models suggested a similar response of the vegetation patterns in the tropics around the Atlantic Ocean, where the grass cover increased and the tree cover decreased, specifically in tropical North Africa around 15ºN in the UVic ESCM simulation and around 10ºN in CCSM3. In the CCSM3 model, the tree and grass cover in tropical Southeast Asia responded to the abrupt climate change during the HE1, which could not be found in the UVic ESCM. The biome distributions derived from both models corroborate findings from pollen records in southwestern and equatorial western Africa as well as northeastern Brazil.

5.2 Introduction

Heinrich events in general are associated with layers of ice-rafted debris (IRD) in the sediments of the North Atlantic Ocean dated between 70 ka BP (ka BP = thousand years before present) and 14 ka BP (Heinrich, 1988; Broecker, 1994). The Heinrich event 1 (HE1, ca. 17.5 ka BP) is the most recent of these distinctive cold periods in the North Atlantic region. Paleoceanographic evidence suggests a connection between the abrupt climate changes during these events and the variability of the North Atlantic Deep

Water (NADW) formation and Atlantic Meridional Overturning Circulation (AMOC, Sarnthein et al., 1994; McManus et al., 2004).

Frequently, a change in the AMOC during the HE1 is invoked to explain an unusual hydrological cycle in the tropics and a southward shift of the Intertropical Convergence Zone (ITCZ) and its associated rainbelt (e.g., Behling et al., 2000). Since vegetation and climate are tightly coupled, tropical climate changes influence the tropical vegetation patterns. This is demonstrated by pollen proxy records, which exhibit changes in the tropics simultaneous with the North Atlantic temperature changes during this event (e.g. Hessler et al., 2010). Some examples are found in eastern tropical Africa (Kashiru swamp, Burundi), where grassland and dry shrubland occurred due to a fairly cold and dry climate (Bonnefille and Riollet, 1988; Hessler et al., 2010) and at Lake Masoko, Tanzania, where warm temperate and mixed forests were formed due to a moderately wet climate (Vincens et el., 2007; Hessler et al., 2010). In tropical South America, pollen records indicate contrasting vegetation changes between the northern and southern limits of the ITCZ (Hessler et al., 2010), e.g., at the Cariaco Basin site (equatorial northern South America), which had a more open vegetation due to dry climate conditions (González et al., 2008; González and Dupont, 2009), while the Lake Caçó region (equatorial southern South America) was occupied by a denser forest during the HE1 than in the Last Glacial Maximum (LGM) period due to moist climate conditions (Ledru et al., 2001; Dupont et al., 2009). In Indonesia an open grass-rich vegetation during the LGM was inferred from a marine pollen record (van der Kaars, 1991), although the Borneo rainforest was probably preserved and might have extended to the continental shelf of the South China Sea (Morley, 2000). At the terrestrial Rawa Danau site (West Java, Indonesia), the lowland forest and C3 plant cover increased and the grass cover decreased between 17 ka BP to 15.4 ka BP indicating enhanced precipitation (van der Kaars, 2001; Turney et al., 2006).

Previous model studies suggested that the southward shift of the ITCZ occurred as a response to a slowdown of the AMOC during the HE1 (e.g., Stouffer et al., 2006; Kageyama et al., 2009). In these studies, the AMOC weakening has been induced by perturbing the freshwater balance of the North Atlantic Ocean (e.g., Köhler et al., 2005; Menviel et al., 2008; Kageyama et al., 2010). Using an Earth System Model of Intermediate Complexity (EMIC, Claussen et al., 2002) which includes a dynamic vegetation component, it has been demonstrated that model results and pollen records in tropical Africa and northern South America are generally consistent (Kageyama et al.,

2005; Handiani et al., 2012). However, in many EMICs the atmospheric component is simplified, in particular with respect to the representation of the hydrological cycle. This demands a modeling study using a more complex atmospheric component.

The purpose of our study was to compare the tropical vegetation response to climate changes during the HE1 as simulated by two global climate models that differ in the complexity of their atmospheric components. We employed the University of Victoria Earth System-Climate Model (UVic ESCM, cf. Weaver et al., 2001) and the Community Climate System Model version 3 (CCSM3, Collins et al., 2006; Yeager et al., 2006). Both models contained a dynamic global vegetation component (Meissner et al., 2003; Levis et al., 2004). In addition, the model results were compared to the available pollen records from tropical vegetation. However, the comparison between model results and pollen records is not a straightforward approach. Mostly, a dynamic global vegetation component represents the type of vegetation cover as Plant Functional Types (PFTs), while compilations of pollen records are available in terms of biome distributions (Prentice et al., 1996; Hessler et al., 2010). To allow comparison between models and pollen records directly, either the pollen records are assigned to PFTs or the model results are converted into biome distributions. In our study, the simulated vegetation covers were mapped onto biome distributions (Schurgers et al., 2006; Handiani et al., 2012) allowing for both a model intercomparison and a comparison of the simulated biogeographies to pollen-based reconstructions.

5.3 Models and experimental design

In the present study, we used the UVic ESCM version 2.8 (Weaver et al., 2001). The atmospheric component of this model contains a parameterization of anomalous near-surface winds to take into account the dynamical wind feedback (Fanning and Weaver, 1997). Furthermore, the dynamic vegetation model TRIFFID (Cox, 2001) is included in this version of the UVic ESCM to simulate the terrestrial biosphere in terms of soil carbon storage and five PFTs (Table 5.1). All components of the UVic ESCM share the same resolution of 3.6º by 1.8º (longitude×latitude) with one vertically-averaged layer in the atmospheric model and nineteen vertical levels in the ocean model.

In addition, we made use of the state-of-the-art coupled general circulation model CCSM3 (Collins et al., 2006). Here, we employed the low-resolution version of CCSM3 which is described in detail by Yeager et al. (2006). In this version, the resolution of the atmosphere is given by T31 (3.75° transform grid) spectral truncation with 26 layers,

while the ocean model has a nominal horizontal resolution of 3° (like the sea-ice component) with 25 levels in the vertical. The latitudinal resolution of the ocean grid is variable, with finer resolution around the equator (0.9°).

Table 5.1 The original PFTs as simulated by the UVic ESCM and CCSM3 are combined into four main types of PFTs to simplify the model intercomparison (Bonan et al., 2006). The UVic ESCM classification also makes use of the lowest temperature criteria (e.g. Kaplan et al., 2003; Sitch et al., 2003).

PFT description		Broadleaf Evergreen trees	Needleleaf Evergreen trees	Deciduous trees	Grasses
UVic ESCM	Broadleaf tree (BL)	X IF Tc_{min} >=15.5ºC		X IF Tc_{min} <15.5ºC	
	Needleleaf tree (NL)		X IF Tc_{min} >=-2 ºC	X IF Tc_{min} <-2ºC	
	C_3 grass (C3)				X
	C_4 grass (C4)				X
	Shrubs (SH)				X
CCSM3	Tropical broadleaf evergreen tree	X			
	Tropical broadleaf deciduous tree			X	
	Temperate broadleaf evergreen tree	X			
	Temperate needleleaf evergreen tree		X		
	Temperate broadleaf deciduous tree			X	
	Boreal needleleaf evergreen tree		X		
	Boreal deciduous			X	
	C4 grass				X
	C3 grass				X
	C3 Arctic grass				X

The dynamic global vegetation model (DGVM; Levis et al., 2004) is based on the Lund-Potsdam-Jena (LPJ) model (Sitch et al., 2003; Bonan and Levis, 2006). It is coupled to the Community Land Model version 3 (CLM3; Oleson et al., 2004), and thus we refer to it as the CLM-DGVM. CLM-DGVM has the same horizontal resolution as the atmosphere. In order to improve the simulation of land surface hydrology, which affects the biogeography of vegetation, we implemented new parameterizations for canopy interception and soil evaporation into the CLM-DGVM following Oleson et al. (2008). The model simulates ten PFTs, which differ in their physiological, morphological, phenological, bioclimatic and fire-response attributes. Seven PFTs refer to trees and three PFTs to non-tree vegetation cover (Table 5.1).

We performed two sets of experiments with each model. Each set of experiments was meant to simulate the vegetation distribution characteristic of the background climate of the LGM and HE1. The experimental design is summarized below:

(i) The LGM simulations were forced by the boundary conditions of 21 ka BP. The LGM simulation with the UVic ESCM (LGM_UVic) was similar to the LGM simulation by Handiani et al. (2012). The LGM simulation with the CCSM3 (LGM_CCSM) was similar to the CCSM3 LGM simulation by Merkel et al. (2010), except that the DGVM was activated and the land surface hydrology was improved (see above). Both LGM simulations were integrated until equilibrium was reached, which was taken to be after 2000 years for the LGM_UVic and 1500 years for the LGM_CCSM simulation.

(ii) The HE1 simulations were identical to the LGM simulations as described in (i), except that a freshwater flux anomaly was imposed on the North Atlantic Ocean, which was added in both models at the same constant rate of 0.2 Sv (1 Sv = 10^6 m^3 s^{-1}) for the whole duration of the experiment (500 model years). The location of the freshwater flux anomaly is described in Handiani et al. (2012) for the HE1_UVic and in Merkel et al. (2010) for the HE1_CCSM simulation.

In contrast to the UVic simulations by Handiani et al. (2012), the UVic ESCM simulations used here included a parameterization of the dynamic wind feedback. In the parameterization, wind field and wind stress anomalies are calculated from surface air temperature anomalies (Weaver et al., 2001). These wind field and wind stress anomalies are then added to the prescribed mean wind field in order to account for the dynamic response of the atmosphere to sea surface temperature anomalies, which has a stabilizing effect on the AMOC (Fanning and Weaver, 1997).

The model analysis and discussion refer to model output time-averaged over the last 100 years of each simulation. As specified above, the two models simulate a different number of PFTs. Therefore, to facilitate model comparison, the PFT output of each model was classified into four generic types of PFTs, namely broadleaf evergreen trees, needleleaf evergreen trees, deciduous trees and grasses (see Table 5.1). The PFT cover and the surface temperature of each model were used to generate the biome distribution. Given the different number of simulated PFTs, a different scheme to estimate the biome distribution had to be used for each model. The scheme for the UVic ESCM (Table 5.2) is described by Handiani et al. (2012) and uses the fractional coverage of the five PFTs and

the atmospheric temperature from the model output. The percentage of PFT coverage allowed to evaluate the dominant PFT in each grid cell of the model (Table 5.2a). The simulated atmospheric temperatures served to calculate the environmental constrains for the biomes, such as temperature of the coldest month (Tc), temperature of the warmest month (Tw), and the number of growing degree-days above 0ºC and 5ºC (GDD0 and GDD5, respectively, Table 5.2b). The scheme for the CCSM3 was adopted from a study by Schurgers et al. (2006), who applied it to the LPJ model output for the Eemian and the Holocene (Table 5.3). It was used applied to the fractional coverage of the ten PFTs (Table 5.1) from the output of the CLM-DGVM model, together with the air surface temperature from the atmospheric model. These biomes (1) can be derived from the UVic ESCM and the CCSM3 output without degenerating into arbitrariness and still show shifts of vegetation cover in simulations of long time scales and (2) allow for a direct comparison to the vegetation cover reconstructed from the pollen records.

5.4 Results

5.4.1 Climate changes

The AMOC gradually decreased in both models in response to the freshwater perturbation, but in each model the degree of reduction was different (not shown). In the LGM_UVic simulation, the maximum of the AMOC streamfunction started from a maximum strength of ~12 Sv, and eventually collapsed after 100 years simulation time, while in the LGM_CCSM simulation, it decreased from 14 Sv to 4 Sv. This weakened or even collapsed AMOC was in both models accompanied by a strong cooling in the Northern Hemisphere and a slight warming in the Southern Hemisphere (Figs. 5.1a and 5.1c). The cooling is most pronounced in the surface air temperature decrease over the North Atlantic Ocean. However, the regional pattern and amplitude of the surface air temperature anomaly is very different between the two models. The negative surface temperature anomalies for HE1 were around -2ºC for the UVic ESCM and around -4ºC for the CCSM3 off Northwest Africa. The positive temperature anomalies in the Southern Hemisphere were also larger in the CCSM3 than in the UVic ESCM. In the tropics, the climate simulated by the UVic ESCM was only slightly (between 0ºC to 1ºC) colder in the HE1 experiment compared to the LGM experiment, whereas in the CCSM3, the northern equatorial Atlantic Ocean was colder by up to 2ºC (Fig. 5.1c).

Table 5.2. (a) Distribution of dominant PFTs which is based on the percentage of PFT coverage for the UVic ESCM results simulation. (b) The combination of environmental constraints and potential PFTs are used to compute the biome distribution from UVic ESCM results, Handiani et al. (2012).

(a)

Dominant PFTs or PFTs mixture	PFT coverage
	BL, NL, SH, C_3, C_4 over 50%
Broadleaf tree (BL)	BL ≥ 50%
Needleleaf tree (NL)	NL ≥ 50%
Shrubs (SH)	SH ≥ 50%
C_3 grass (C_3)	C_3 ≥ 50%
C_4 grass (C_4)	C_4 ≥ 50%
	BL, NL, SH, C_3, C_4 less than 50%
Mixed trees	BL+NL ≥ 50%
Mixed vegetation (without trees)	SH+C_3+C_4 ≥ 50%
Open vegetation	20% ≤ BL+NL+SH+C_3+C_4 ≥ 50%
Barren soil	BL+NL+SH+C_3+C_4 < 20%

If the percentage is over 50%, the PFT potential is set equal to the dominant PFT (broadleaf tree, needleleaf tree, shrubs, C3 grass, or C4 grass). If it is less than 50%, the grid cell is designated as mixed trees if it is dominated by tree PFTs, as mixed vegetation if non-trees PFTs are dominant, as open vegetation if all PFTs are between 20% and 50% and as desert if all PFTs together are less than 20% (Crucifix et al., 2005).

(b)

Dominant PFTs or PFTs mixture	Environmental Constraints					Mega biomes
	Tc min (ºC)	GDD5 min	GDD0 min	Tw (ºC) min	Tw (ºC) max	
BL tree	15.5					Tropical forest
BL tree or mixed trees	5					Warm temperate forest
BL tree or NL tree or mixed trees	-2					Temperate forest
BL tree or NL tree or mixed trees	-32.5					Boreal forest
Grass (C3, C4) or mixed vegetation or open vegetation	17					Savannah and dry woodland
Grass (C3, C4) or mixed vegetation or open vegetation		500		10		Grassland and dry shrubland
Barren soil				22		Desert
SH or mixed vegetation					15	Dry tundra
SH or mixed vegetation			800		15	Tundra

The environmental constraints were chosen based on the definition of biomes in the BIOME 4 model (Kaplan et al., 2003).

Table 5.3. The biome distribution estimation scheme adopted from a study by Schurgers et al. (2006) applied to the CCSM3 output. The temperature limitation is based on bioclimatic parameters for survival and establishment of PFTs in the CCSM3 (Bonan et al., 2003). The high latitude biome distribution is only classified by Tundra.

PFT fraction (%)			Temperature limitation (ºC)	Mega biomes and non-biomes description
$C_v > 20$	$C_f > 80$	$C_{f,trop} > C_{f,temp}$ $C_{f,trop} > C_{f,bor}$		Tropical forest
		$C_{f,temp} > C_{f,trop}$	$3.0 < T_c < 18.8$	Warm temperate forest
		$C_{f,temp} \geq C_{f,bor}$		Temperate forest
		$C_{f,bor} > C_{f,trop}$ $C_{f,bor} \geq C_{f,temp}$		Boreal forest
	$C_f <= 80$	$C_{v,C4} \geq C_{v,C3}$		Savannah and dry woodland
		$C_{v,C3} \geq C_{v,C4}$	$T_c > -17.0$	Grassland and shrubland
			$T_c \leq -17.0$	Tundra/Dry tundra
$C_v <= 20$			$T_c > 0.0$	Desert
			$T_c < 0.0$	Ice
				Barren

C_f forest fraction (sum of cover of all tree PFTs);
$C_{f,trop}$ tropical forest fraction (sum of cover of all tropical tree PFTs) ;
$C_{f,temp}$ temperate forest fraction; $c_{f,bor}$ boreal forest fraction;
C_v vegetation fraction (sum of cover of all PFTs);
T_c air surface temperature; $C_{v,C3}$ C_3 grasses fraction; $C_{v,C4}$ C_4 grasses fraction.

The weakening of the AMOC and an asymmetric surface temperature response between the two hemispheres were responsible for a southward shift of the tropical rainbelt as suggested by the simulated precipitation patterns (Figs. 5.1b and 5.1d). The pattern in the UVic ESCM was of rather large scale and extended beyond the ITCZ region. In the tropical Atlantic region, the precipitation differences between the HE1_UVic and the LGM_UVic simulation were around -0.25 mm day^{-1} north of the equator and 0.5 mm day^{-1} south of the equator (Fig. 5.1b). In the CCSM3, the precipitation differences between the HE1 and the LGM simulation were around -2.5 mm day^{-1} north of the equator and 2.0 mm day^{-1} south of the equator (Fig. 5.1c). The precipitation differences for CCSM3 were much larger between 10ºS and 10ºN in the tropics than in the other regions. The anomalies of the zonally averaged precipitation in CCSM3 showed a drying north of the equator by up to 0.8 mm day^{-1} and a wetting south of the equator by a similar amount, thus sharply reflecting the southward shift of the rainbelt (Fig. 5.1e). A comparison of the magnitude of precipitation anomalies in the HE1_UVic and the HE1_CCSM simulations revealed that the minimum and maximum anomalies in the HE1_UVic simulation were clearly weaker (min. -0.86 mm day^{-1} and max. of 0.48 mm day^{-1})

compared to the HE1_CCSM simulation (min. of -4.19 mm day^{-1} and max. of 2.80 mm day^{-1}).

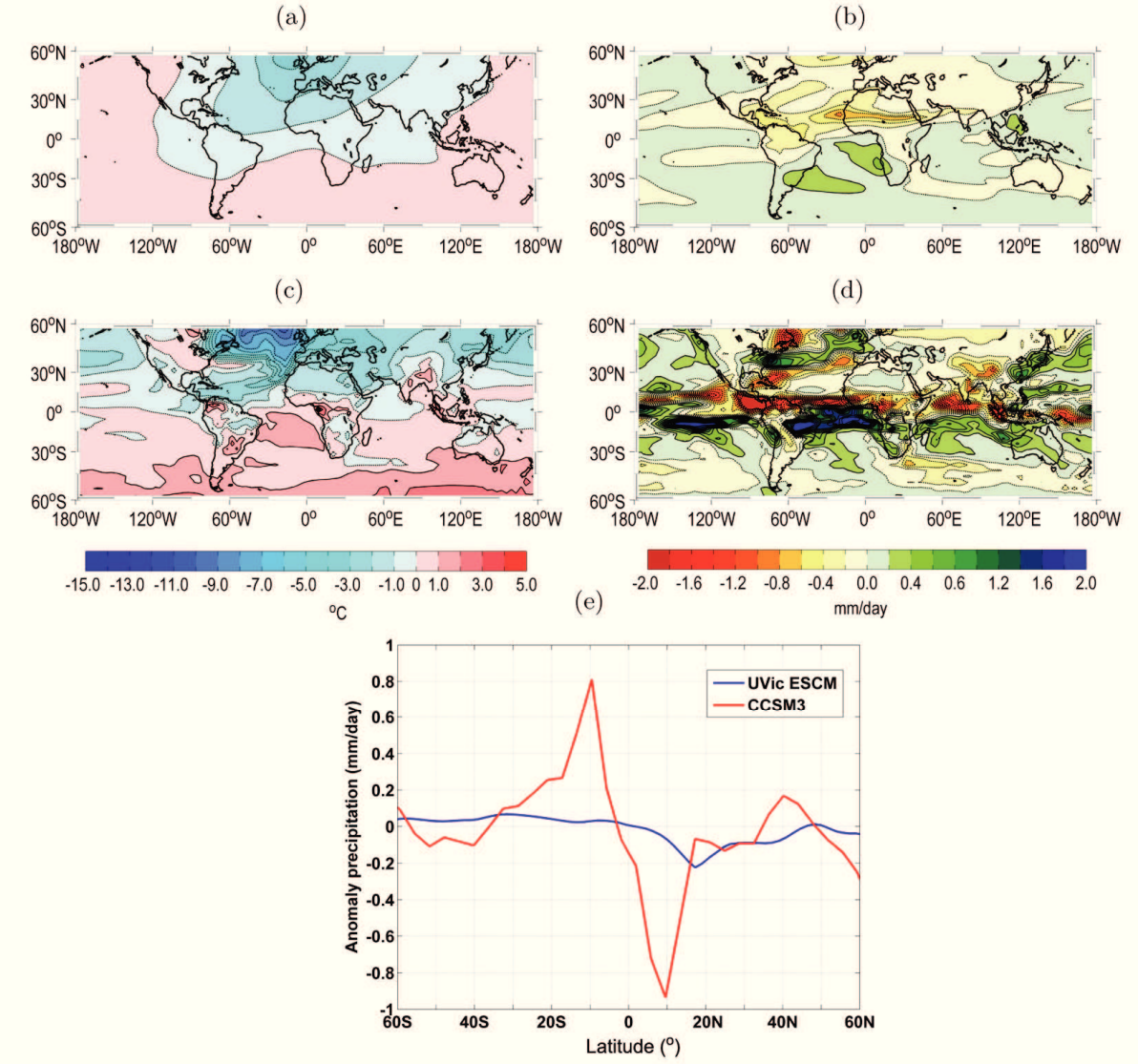

Figure 5.1 Annual mean anomalies of surface temperature (a, c) and precipitation (b, d) between HE1_UVic and LGM_UVic (top) and between HE1_CCSM and LGM_CCSM (middle) simulations. The contour intervals are fixed at 1°C for surface temperature and 0.5 mm day-1 for precipitation. (e) The global zonally averaged precipitation differences between HE1 and LGM simulations for the UVic ESCM (blue) and the CCSM3 (red) model.

5.4.2 The vegetation cover response

In this section, we will discuss changes in vegetation cover in terms of the simplified PFTs as defined in Table 5.1 (see also Section 2), which allows for a direct comparison between the output from the UVic ESCM and the CCSM3. Our results showed that the southward shift of the tropical rainbelt triggered vegetation changes in the tropics, with spatially varying degree and dominance. In both HE1 experiments, broadleaf evergreen trees cover decreased in equatorial northern Africa (Figs. 5.2a and 5.2b). In the UVic

ESCM, it was reduced by 60% in the Sahel region and southeastern Brazil and between 20% to 40% in equatorial western South America (Fig. 2a). The pattern was similar in CCSM3, specifically in equatorial Africa region, except that the change amounted to 40% (Fig. 5.2b). Moreover, in CCSM3 the broadleaf evergreen tree cover also decreased in southeast Brazil and by 40% in a small region on the west coast of Africa, and it increased with similar percentages in equatorial western South America. Furthermore, the decrease in broadleaf tree cover in Southeast Asia was less than 10% in the UVic ESCM but around 20% in the CCSM3 (Figs. 5.2a and 5.2b).

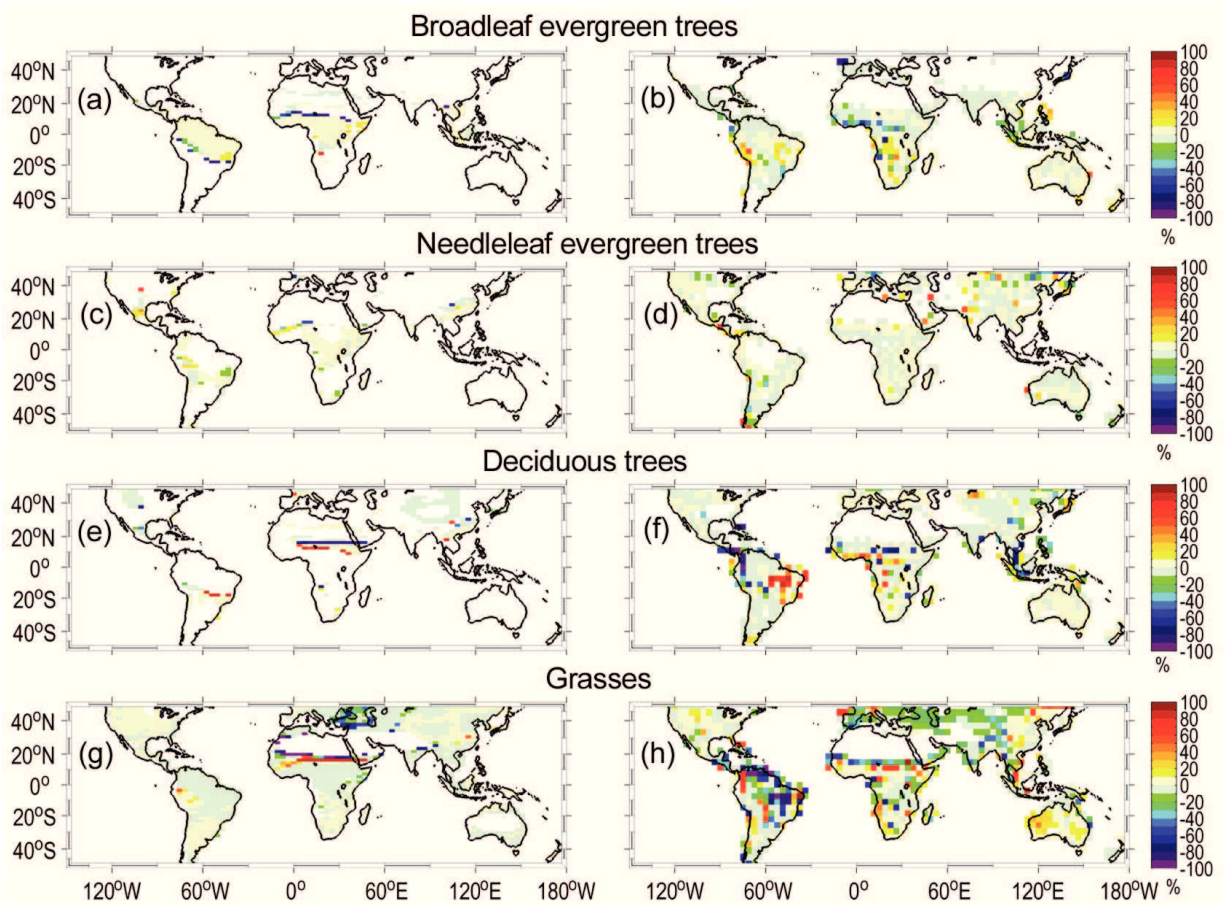

Figure 5.2 Annual mean differences of PFT cover between HE1 and LGM simulations for the UVic ESCM (left panels) and the CCSM3 (right panels). The classification into the four PFTs is defined in Table 5.1.

In the tropics, the needleleaf evergreen tree cover was relatively unaffected in both HE1 experiments, except for a small decrease in eastern Brazil and the central Sahel region in the UVic ESCM and in southwest South America in the CCSM3 simulation (Figs. 5.2c and 5.2d). However, the deciduous tree cover was reduced by more than 60% in the eastern Sahel region in the UVic ESCM and by a similar percentage in equatorial western South America, the central Sahel region and southeast Asia in the CCSM3

(Figs. 5.2e and 5.2f). In contrast, the deciduous tree cover in central Brazil increased by around 60% in both models. Meanwhile, in tropical northern Africa (i.e., the Sahel region), the grass cover increased by around 60% in both models. However, with the UVic ESCM result located the grass cover further north and has over a wider longitude ranges than compare to the CCSM3. In tropical South America, the grass cover was relatively unchanged in the UVic ESCM simulation, while it mostly decreased in the CCSM3 simulation (Figs. 5.2g and 5.2h). The grass cover change was more pronounced in the CCSM3 simulation than in the UVic ESCM simulation, e.g., it was reduced in tropical North America and South America, while it increased by 20% to 40% in northwest South America and tropical Africa and by about 60% in Southeast Asia (Fig. 5.2h). It was reduced by 20% to 80% in tropical western Africa, while it increased by up to 80% in tropical central and eastern Africa (Fig. 5.2g).

The annual-mean anomalies of the zonally averaged tree and grass cover between the HE1 and the LGM experiments reflected the PFT differences in tropical locations of South America (Figs. 5.3a and 5.3b), Africa (Figs. 5.3c and 5.3d) and Southeast Asia (Figs. 5.3e and 3f). In some locations equal but opposite vegetation changes occurred, e.g., the tree cover in the UVic ESCM was reduced by 60% in tropical Africa around 15ºN, while the grass cover increased by a similar percentage at the same latitude (Fig. 5.3c). A similar pattern also emerged from the CCSM3 simulation, where at around 10ºN the tree cover decreased by 20% while the grass cover increased by a similar percentage (Fig. 5.3d). Moreover, in tropical South America, the tree and the grass cover in the CCSM3 simulation were reduced by about 30% – 50% between 5ºN – 10ºN, while an opposite change of tree and grass cover by about 10% – 30% occurred around 10ºS (Fig. 5.3b). The tree and grass cover in the UVic ESCM south of the equator (~15ºS) discussed so far (Figs. 5.3a, 5.3c and 5.3e) showed differences of less than 5%, whereas the differences in CCSM3 (Figs. 5.3b, 5.3d and 5.3f) are at least larger than 10%. While the UVic ESCM did not show any pronounced changes in tropical Southeast Asia (Fig. 5.3e), the CCSM3 tree cover generally decreased and the grass cover increased in that region (Fig. 5.3f).

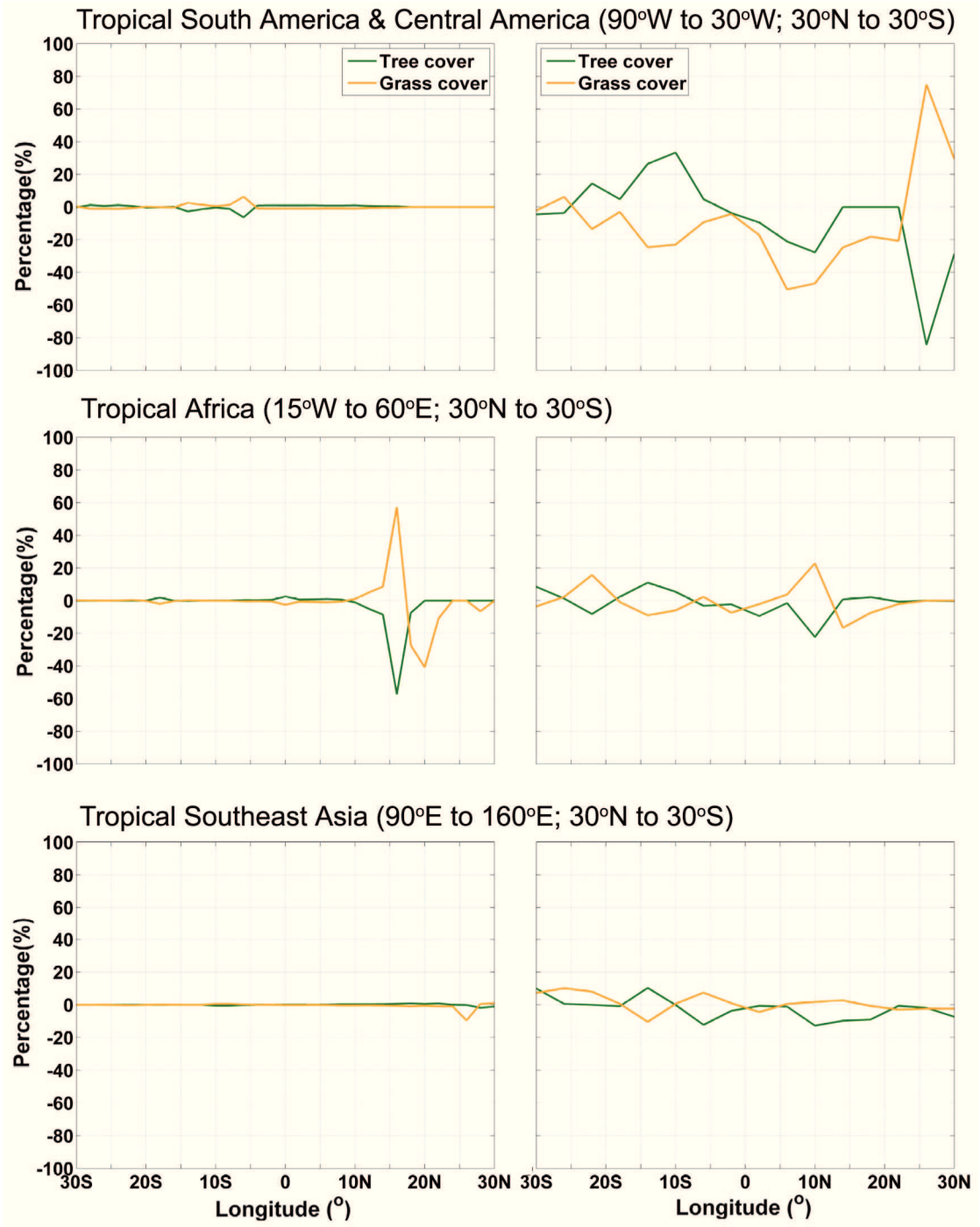

Figure 5.3 Annual mean anomalies of regional zonally averaged tree and grass cover between HE1 and LGM for the UVic ESCM (left panels) and the CCSM3 (right panels). The regional areas are tropical South America and Central America (top), tropical Africa (middle) and tropical Southeast Asia (bottom).

5.4.3 Biomes distribution comparison

In this section, we compare our model results to data. For this comparison, we used pollen records for HE1 from tropical South America and tropical Africa (Fig. 5.4a) compiled by Hessler et al. (2010). In Fig. 5.4, a comparison is presented to show where

model results are consistent with proxy information. The changes in tropical African forest as found in the HE1_UVic and the HE1_CCSM simulations mostly agreed with the pollen reconstruction (Figs. 5.4b and 5.4c).

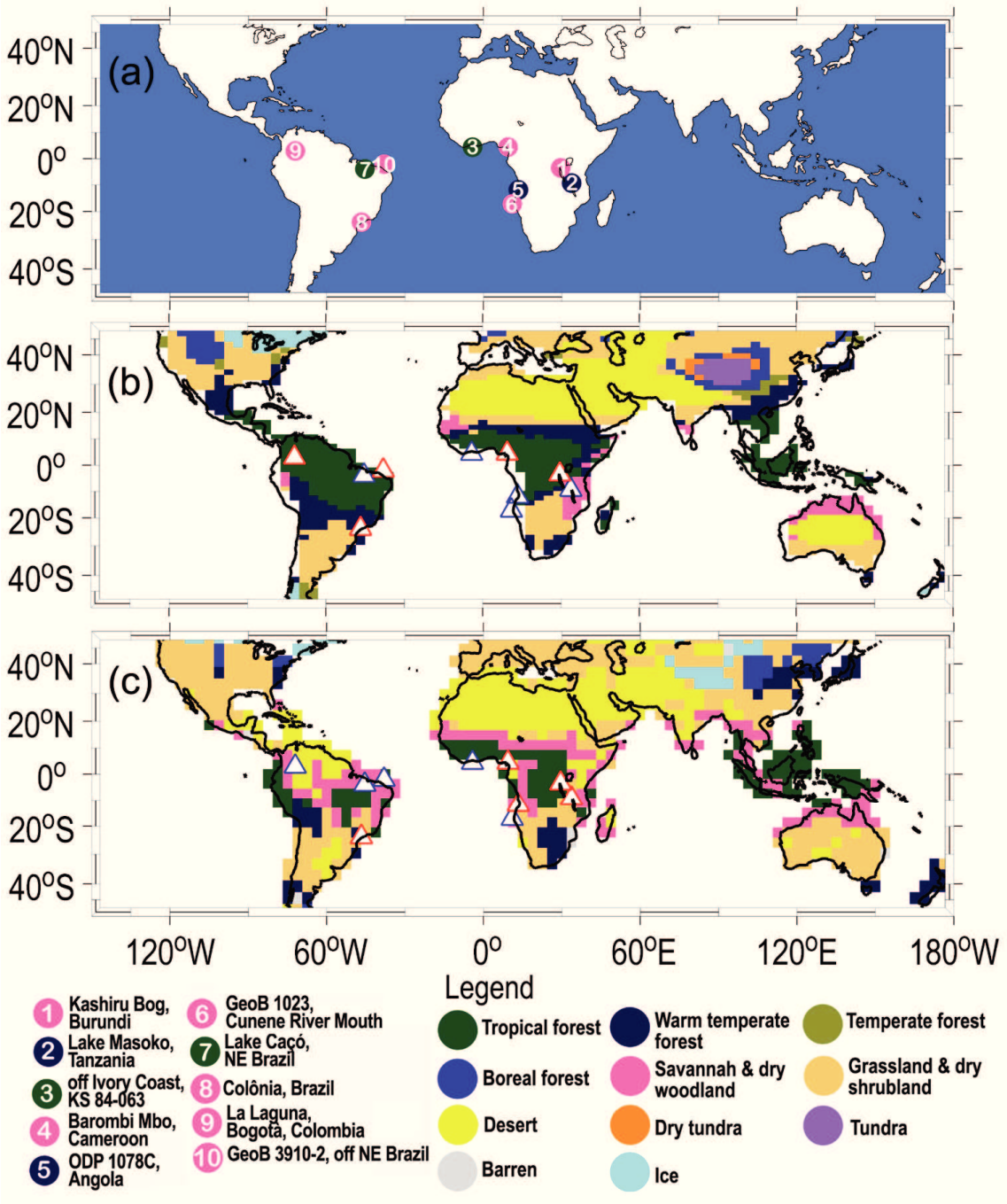

Figure 5.4 Sites of HE1 pollen records compiled by Hessler et al. (2010) and the biome reconstruction of each site as represented by the colour of the circle (a, see legend biome distribution). The biome distribution computed from the HE1_UVic simulation (b) and the HE1_CCSM simulation (c) are shown. A comparison between model output and biome reconstruction of each location is indicated by white-blue triangles where biomes are similar in both the model and the reconstruction; white-red triangles denote where modelled and reconstructed biomes differ.

According to both models and the pollen records, equatorial western Africa was covered by tropical forest corresponding to a wet climate. In southwest Africa, the pollen records indicated a warm temperate forest and farther south savannah (Fig. 5.4a). The HE1_UVic simulation agreed with both records in southwest Africa, while the HE1_CCSM simulation only agreed with one record (Figs. 5.4a and 5.4b) because the HE1_CCSM predicted savannah due to a relatively warm climate in these locations (Fig. 5.4c). Another discrepancy between the HE1_CCSM simulation and the pollen records is found in eastern Africa, where the model predicted tropical forest and grassland, while the records suggest warm-temperate forest and savannah (Fig. 5.4c).

The biome distributions derived from the model and pollen results were in disagreement at the Colônia site (Brazil). According to the pollen record, savannah covered this region indicating a warm and dry climate (Fig. 5.4). The tropical forest in the HE1_UVic and the HE1_CCSM simulations was broadly consistent with the pollen records of Lake Caçó (northeast Brazil). The HE1_CCSM simulations was also in agreement with the pollen record of core GeoB 3910-2 off the coast of northeast Brazil (site number 10 in Fig. 5.4a); both model and data indicated savannah (Fig. 5.4c). In contrast, for the same region, the HE1_UVic simulation predicted tropical forest (Fig. 5.4b).

A tropical Asian biome reconstruction for HE1 is not available yet; hence it is difficult to perform a thorough model-data comparison. However, the simulation of a savannah corridor in Sundaland in CCSM3 is worth noting as the existence of such a feature during the last glaciation is highly debated (e.g. Bird et al., 2005). From a modeling perspective, the changes in the biome distributions between the HE1 and LGM simulations were insignificant (not shown, but see the PFT cover anomalies), although some changes did occur in the CCSM3 model. For example, grass cover increased in southeast China and replaced savannah in the HE1_CCSM simulation (Fig. 5.4c).

5.5 Discussion

The simulations in the UVic ESCM presented here are different from Handiani et al. (2012). Both studies used the UVic ESCM and an identical experimental design, however, Handiani et al. (2012) did not include the dynamical wind feedback parameterization. Regarding the precipitation patterns in the tropics, there are a few differences between the earlier study by Handiani et al. (2012) and our present study. Our preindustrial simulation (not shown) resulted in a climate that was warmer and drier than in the study by Handiani et al. (2012), most notably in equatorial southern

South America and Africa as well as the Sahel region. Nevertheless, the HE1 simulations of both studies suggested similar tropical precipitation anomalies. Thus including the dynamical wind feedback parameterization in the UVic ESCM improved the representation of the precipitation pattern in the ITCZ region in the preindustrial simulation (not shown), but it only had a slight impact on the tropical precipitation response in the HE1 simulation. Moreover, despite the additional moisture transport by advection in this version of the UVic ESCM, the precipitation in the terrestrial tropics and the ITCZ region was still weaker as compared to the CCSM3. Weaver et al. (2001), who introduce the moisture transport by advection in the UVic ESCM, identify additional regions such as the mid-latitude North Atlantic Ocean and Pacific Ocean regions that need further improvement. The inclusion of dynamical wind feedback parameterization in the atmospheric model in this version of the UVic ESCM barely influences the tropical vegetation cover distribution in the preindustrial simulation (not shown). The comparison between Handiani et al. (2012) and this study (not shown) shows a great similarity of preindustrial tropical vegetation cover. The smooth precipitation distribution from both preindustrial simulations led to a similar smooth vegetation distribution in the tropics. For example, tree cover penetrated into the subtropics of northern and southern Africa (not shown, see Handiani et al., 2012).

The slowdown of the AMOC during the HE1 simulation caused an adjustment of the surface temperature called the “bipolar seesaw”, which is characterized by a cooling in the Northern Hemisphere and a slight warming in the Southern Hemisphere (Broecker et al., 1985). In the tropics, the bipolar seesaw in turn influenced the precipitation patterns. Positive anomalies developed over the equatorial South Atlantic Ocean and surrounding regions, while negative anomalies appeared over the tropical North Atlantic Ocean. In the CCSM3, the positive anomaly spanned an entire band south of the equator from central Brazil to central Africa with the maximum of this band over eastern Brazil. The negative anomalies ranged from the Sahel to Central America. These anomalies also occurred in the UVic ESCM, although much less pronounced as compared to the CCSM3. In the UVic ESCM, the highest positive anomalies extended farther into southeast South America and western Angola, while maximum negative anomalies were found in the Sahel region.

Pronounced changes in broadleaf tree cover in the tropics were confined to the Sahel region, equatorial southern South America and western Africa. This suggests that these regions were most sensitive to a shift of the tropical rainbelt in response to a slowdown

of the AMOC. Changes in tree cover were related to changes in grass cover. We indeed expected a shift from tropical trees to grass cover due to a drier climate in the Sahel region and a shift from grass cover to tree cover due to a wetter climate in equatorial southern South America. This was confirmed by the HE1_CCSM results around 10ºS in tropical South America and around 10ºN in tropical Africa, where tree cover and grass cover changed by comparable magnitudes. Similarly, according to the HE1_UVic results around 15ºN in tropical Africa, tree cover decreased significantly while grass cover increased. Such a pattern is also found in the HE1 experiments by Scholze et al. (2003), Köhler et al. (2005) and Menviel et al. (2008), where the vegetation shifts occur in the latitudinal band between 5ºS and 15ºN.

According to Bonan and Levis (2006), the tropical forest in South America under present climate conditions is less extensive in CCSM3 than in the observations. The complex interaction within the hydrological cycle (between soil moisture, vegetation, evaporation, transpiration and precipitation) in that region leads to a considerable decrease in precipitation and tree cover. As a consequence, the broadleaf tree cover in tropical South America under preindustrial climate conditions was smaller in the CCSM3 than in the UVic ESCM. Similarly, in the HE1_CCSM simulation, tropical South America was covered by more open vegetation (e.g., savannah and grassland) than in the HE1_UVic simulation. However, the biome distribution in the HE1_CCSM simulation proved to be in agreement with pollen sites in tropical South America, and in spite of the deficiency of the simulated hydrological cycle in tropical South America, the CCSM3 captured the climate change in western tropical Africa during HE1 quite well.

The tropical forest simulated by both models in Southeast Asia is supported by Morley (2000), who suggests that the Borneo tropical forest persisted and even extended onto the continental shelf of the South China Sea during the last glacial period. Nevertheless, CCSM3 also suggested the appearance of a savannah corridor in Sundaland as it has first been proposed by Heaney (1991). Moreover, in the HE1_CCSM simulation, the vegetation cover in tropical Southeast Asia responded to abrupt climate change in the northern Atlantic Ocean with changes in tree and grass cover of around 20%. These changes were significantly larger than in the HE1_UVic simulation, which were less than 10%. The CCSM3 results can be considered as an indication of a teleconnection between North Atlantic Ocean climate and vegetation cover in tropical Southeast Asia (e.g., Zhou et al., 2007; Lee et al., 2011). However, a more extensive compilation of

paleovegetation data from this region is needed to ease the comparison between model and data and to corroborate this finding.

Comparing model output and pollen records is not an easy task; one example from our study is that the definitions of the PFTs are not exactly the same. This problem becomes apparent when comparing pollen reconstructions from specific geographic locations (e.g., a mountain or lake) with model results, which often cannot represent those locations in the required detail. Since models are mostly formulated in terms of PFTs, but are checked for consistency against pollen records or the present-day vegetation distribution, either the PFTs from the model output have to be converted into a biome distribution, or the biome distribution from the pollen records has to be converted into PFTs. Several model studies have tackled this situation by developing a scheme to compute biomes based on the PFTs from the model output (e.g., Crucifix et al., 2005; Roche et al., 2007; Schurgers et al., 2006; Handiani et al., 2012). The weakness of this approach is that the calculation depends on specific model output; hence a scheme for one model can not be used directly for another model. This was suggested in our two schemes for the UVic ESCM and the CCSM3. In contrast, a number of techniques have been developed to convert the biome distribution derived from satellite or observational data into PFTs (e.g., Meissner et al., 2003; Poulter et al., 2011). Unfortunately, these approaches can only be used for present-day model results, since biome distributions derived from satellite data is only available for the present-day vegetation.

5.6 Conclusion

This study compared two simulations of HE1 by two different earth system models. Both models simulated a slowdown of the AMOC in response to a freshwater perturbation in the North Atlantic Ocean. The associated bipolar seesaw in surface temperature influenced the tropical climate through a southward shift of the rainbelt. However, the effect on precipitation was smaller in the UVic ESCM than in the CCSM3.

The shift of the tropical rainbelt caused drier climate conditions in the northern equatorial region and wetter climate conditions in the southern equatorial region, which also influenced the tropical vegetation patterns, specifically in tropical Africa around 15ºN in the UVic ESCM and 10ºN in the CCSM3. In southern equatorial Africa, there was no visible response to the freshwater hosing in the UVic ESCM, while in the CCSM3 opposite tree and grass cover changes occurred around 15ºS. The tree and grass cover in the CCSM3 in tropical South America also suggested opposite changes south of the

equator (10ºS), while north of the equator (between 5ºN and 10ºN) both decreased due to a drier climate. In addition, tree cover decreased and grass cover increased between 15ºN and 10ºS in Southeast Asia during the HE1 experiment in CCSM3.

The direct comparison of the simulated biome distribution and pollen records provides for an assessment of the model-data agreement without relying on indirect reconstructions of precipitation and temperature distributions from pollen records. Nevertheless, comparing model and pollen records has its own uncertainties; one of it is to have a coherent classification of biome distribution for both model and pollen records. For our study, we applied two such biomisation schemes, specific to each model, which allowed for a comparison between the model results and the available pollen records.

Finally, the agreement with the reconstructed biome distribution during HE1 varied in each model. The best correspondence was found in southwestern and equatorial western Africa as well as in northeastern Brazil. The vegetation cover simulated by CCSM3 in tropical Southeast Asia opens up the possibility that abrupt climate change in the North Atlantic Ocean may have a large-scale, even global impact on the terrestrial biosphere.

5.7 Acknowledgements

This work was funded by the Deutsche Forschungsgemeinschaft (DFG) as part of the German contribution to the Integrated Ocean Drilling Program (SPP 527) “Abrupt Climate Change in the African Tropics (ACCAT)” and the DFG Research Center/Excellence Cluster “The Ocean in the Earth System”. The CCSM3 climate model experiments were run on the SGI Altix Supercomputer of the “Norddeutscher Verbund für Hoch- und Höchstleistungsrechnen” (HLRN). The authors are grateful to the Climate Modelling Group at the University of Victoria for providing the UVic ESCM.

Chapter 6

Summary of the results

Unlike the relatively stable climate that earth has experienced over the last 10,000 years, more than a decade ago, ice core records from Greenland revealed that abrupt climate change has recurred on a millennial time scale. One of the main questions regarding this change has to do with the impacts of these events on the tropics. The focus of this study was to understand how abrupt climate change signals during the last glacial period could be transmitted from the North Atlantic Ocean to the tropics and influence the tropical climate and vegetation cover. The study emphasized the HE1 and the BA events during the last glacial period. The AMOC variability and changes in the tropical rainbelt were considered as the possible mechanisms associated with these events.

To this end, numerical simulations were carried out using the UVic ESCM. The freshwater perturbation experiments triggered a slowdown of the AMOC, followed by high-latitude climate changes. These changes influenced the climate and vegetation cover in the tropics and also in the region around the Atlantic Ocean through the shift of the tropical rainbelt. Along with the UVic ESCM, the CCSM3 was used for a model inter-comparison, and a comparison between the model and pollen records was also provided to understand and to test the hypothesis of climate and vegetation responses caused by typical abrupt climate variability during the last glaciation.

6.1 The HE1 climate and vegetation in the tropics

To replicate the abrupt climate change of the HE1 period, the freshwater hosing experiments were carried out. In the UVic ESCM, the additional freshwater forcing was applied at the mouth of the St. Lawrence River, and this freshwater experiment resulted in a collapse of the AMOC, followed by a cooler climate in the Northern Hemisphere as well as a warmer climate in the Southern Hemisphere (as described by the bipolar seesaw hypothesis). The inter-hemispheric temperature differences generated the

rainbelt changes, which drove a southward shift of tropical and subtropical biomes. The response of the tropical climate and vegetation cover in the freshwater experiment depended on which background climate was used; the pre-industrial and the last glacial maximum periods, which represent warm-interglacial and cold-glacial conditions, were used respectively. Both simulations suggested that temperature and precipitation were the key influential climate parameters in the tropics. Although these two simulations resulted in different AMOCs, the tropical vegetation cover response did not show distinct differences, and most changes encompassed rather small areas. We suspected that the initial vegetation conditions for the vegetation model or the relative simplicity of the land-atmosphere model caused this similarity. However, a number of locations suggested different responses, such as in northern tropical Africa (the Sahel region), western South America, and central North America. In Africa, where warmer and wetter climate conditions were predicted for the interglacial background climate, tropical forest and savannah were found. However, when we used a different background climate (the glacial), the same climate conditions were predicted, but with an extension of temperate forest and grassland.

In addition, we compared the UVic ESCM to the CCSM3 for simulations of the HE1 with similar experimental design. The CCSM3 has a more complex atmospheric component than the UVic ESCM. In both models, the AMOC either collapsed or slowed down, followed by a seesawing of surface temperatures in the Northern and Southern Hemispheres, as well as a southward shift of the tropical rainbelt. This shift was more distinct in the CCSM3 than in the UVic ESCM simulation, which also influenced the tropical vegetation patterns. In tropical Africa the vegetation changes occured around 15ºN in the UVic ESCM and 10ºN in the CCSM3. In southern equatorial Africa no visible vegetation response was found in the UVic ESCM, while in the CCSM3 the response occurred around 15ºS. The vegetation patterns in tropical South America in the CCSM3 suggested changes south of the equator (10ºS) and north of the equator (between 5ºN and 10ºN). Meanwhile, the UVic ESCM showed only small vegetation changes around 5ºS. In addition, based on the vegetation cover simulated by CCSM3 between 10ºN and 15ºN and between 0 and 10ºS in Southeast Asia, the results suggested that there is a possibility for an abrupt climate change in the North Atlantic Ocean to have a large-scale, even global impact on the terrestrial biosphere. The agreement with the reconstructed biome distribution during HE1 varied in each model. The best agreement was found in southwestern and equatorial western Africa and in northeastern Brazil. A

discrepancy between the biome distribution of the CCSM3 and vegetation data is found for tropical South America. The simulated tropical forest in the CCSM3 is much smaller than even in present-day observations.

6.2 The BA climate and vegetation in the region around the Atlantic Ocean

The BA climate was studied concerning the abrupt warming that would be associated with an onset or a recovery of the AMOC after the HE1 period and its influence on heat transport in the Atlantic Ocean (e.g Boyle and Keigwin, 1987; McManus et al., 2004). Two types of freshwaters suggested that an intensification of the AMOC would be followed by a warming of the climate in the North Atlantic Ocean. In the first type of experiment freshwater was added in the Southern Ocean under a present-day background climate. The response of the AMOC could be explained by a strong inter-hemispheric connection between the water mass of the global ocean and by the thermohaline circulation. By applying a freshwater perturbation in the area of AAIW formation, the density of AAIW decreased and, in turn, the relative density of NADW increased proportionally, inducing a gradual intensification of the AMOC. The proposed mechanism is supported by a study by Weaver et al. (2003). An intensification of the AMOC was also found in the second type of experiment, when the freshwater was extracted from the North Atlantic Ocean (e.g. Manabe and Stouffer, 1997; Schmittner et al., 2002b) under a glacial background climate. The mechanism possibly corresponded with an increase in evaporation or a decrease in precipitation in this region.

A bipolar seesaw of the surface temperature occurred in the BA experiment, with an increase in the SST in the North Atlantic Ocean and a decrease in the South Atlantic Ocean. This was also associated with a northward shift of high tropical precipitation and linked to changes of vegetation pattern in the tropics. The most sensitive region with respect to an intensifying AMOC and a warming climate in the North Atlantic Ocean was northern tropical Africa, where dry climate conditions caused an increase of grass cover and a decrease of tree cover. This result was in agreement with paleovegetation records from western tropical Africa, where forest cover was reduced during the BA period (e.g., Hessler et al., 2010). The model-data comparison for the BA period in North America and Europe gave mixed results. In the uplands of North America and southern Europe the model result corresponded well with the pollen records, where grassland in warm and dry climates was found (Jiménez-Moreno et al., 2010, Fletcher et al., 2010). A discrepancy between model and data was found along the west and east coasts of North

America, where drier vegetation was found in the model, but not in the pollen records. Further discrepancies were found in South America, southeast North America and southern Europe. In southern Europe, our model predicted grassland instead of temperate forest.

6.3 A method for estimating a biome distribution from model outputs

The development of a method to generate a biome distribution based on model output provides a way to compare model results directly with paleovegetation data. This technique can solve problems occurring when comparing pollen records with reconstructed precipitation or temperature, where it is likely that data-model comparison is strongly biased by seasonality. However, each vegetation model represents the vegetation cover differently (e.g., with respect to the number of PFTs or the temperature or precipitation limitation for each PFT), which makes the technique of generating a biome distribution model-dependent.

The output from the UVic ESCM and the CCSM3 that was used to generate a biome distribution are the PFT fraction and the air surface temperature. The PFT fraction was used to calculate the potential PFT coverage (Tables 3.3, 5.2b, and 5.3) and the surface temperature was used to calculate the parameters limiting the biomes (e.g., the temperature of the coldest month (Tc) or the temperature of the warmest month (Tw); Tables 3.2 and 5.2a). For each model, the potential PFTs and the environmental limitation were calculated differently, depending on the number of PFTs and the temperature limitation for each PFT in each model. Nevertheless, in both cases the biomes were classified according to the mega-biomes in the BIOME6000 project (Harrison and Prentice, 2003), which are also used in the biome distributions derived from the pollen records (Hessler et al., 2010; Jiménez-Moreno et al., 2010; Fletcher et al., 2010).

Methods for generating a biome distribution from model output were successfully implemented in this study for the UVic ESCM and the CCSM3, although a few ambiguities were encountered regarding temperature thresholds or the dominance of certain potential PFTs (Chapter 5). Nevertheless, the comparisons between model and data for the HE1 and BA experiments served as examples that show that the method was indeed useful.

Chapter 7

Conclusion and Outlook

7.1. Conclusion

This study presents the results of simulations of the climate and vegetation cover responses to abrupt climate change during the HE1 and the BA in the tropics and the region around the Atlantic Ocean. It is mostly based on an Earth System Model of Intermediate Complexity (i.e., the UVic ESCM), and available pollen records, but includes results from a comprehensive coupled atmosphere-ocean general circulation model (i.e., the CCSM3) for comparison. The following conclusions have been reached:

1. The variability of the AMOC is an important mechanism for the abrupt climate change during the HE1 and the BA event. The abrupt climate change influences the climate and vegetation cover in the tropics through changes of the tropical rainbelt.

2. In the HE1 experiments, the AMOC is slowed down, which is followed by a cooling of the Northern Hemisphere and a warming of the Southern Hemisphere. The tropical rainbelt is shifted southward, which drives an increase of desertification and a retreat of broadleaf forests in West Africa and northern South America.

3. In the BA experiments, the AMOC intensifies, which resulted in a warmer climate in the Northern Hemisphere and a cooler climate in the Southern Hemisphere. The tropical rainbelt is shifted northward, which reduces the tropical forests in western tropical Africa and also increases the more open vegetation in the uplands of North America and southern Europe.

4. The results of the CCSM3 for the the HE1 experiment exhibits a possibility that the abrupt climate change signal generated in the North Atlantic region can have a global impact on the terresterial biosphere.

5. A simple technique which was used to generate a biome distribution from model output is a useful method for comparing model results with paleorecords.

7.2. Outlook

From this study, it can be concluded that a perturbation of the freshwater balance of the Atlantic Ocean can trigger variability of the AMOC, which in turn is followed by abrupt climate change in high latitudes, as well as changes to the climate and vegetation cover in the tropics and the region around the Atlantic Ocean caused by the rainbelt mechanism.

There are, however, some future studies that could improve the understanding of tropical climate and vegetation responses during abrupt climate changes. First of all, it is highly recommended that the glacial background climate is investigated further, specifically with respect to the state of the AMOC, since it is a crucial parameter in the freshwater perturbation mechanism. Secondly, it would be important to conduct experiments investigating the effect of a transient CO_2 concentration during the freshwater perturbation, and to analyze which parameters in the UVic ESCM model influence the AMOC variability the most. Thirdly, it would be useful to develop a generic algorithm for computing a biome distribution that could be applied to the output of different dynamic vegetation models. It would also be beneficial if in this algorithm, the climate thresholds to generate each biome from the model output were consistent with the thresholds used for interpreting the pollen records. This could help to avoid a mismatch in the comparison between model and paleovegetation data.

With the help of experiments similar to those that were conducted and described in this study, especially focusing on the response of the climate and vegetation cover in the tropics and the region around the Atlantic Ocean to variations of the AMOC, further difficulties can be clarified. Furthermore, the proposed algorithm to generate a biome distribution from model output can be used as a method to directly compare the modeled vegetation with pollen records.

Appendix

Biome estimation flow chart

Systematically, the biome distribution estimation is divided into three steps: collecting input from the model output, calculating the dominant PFTs and the environmental constraints, and generating the biome distribution (Figs. A1 and A2).

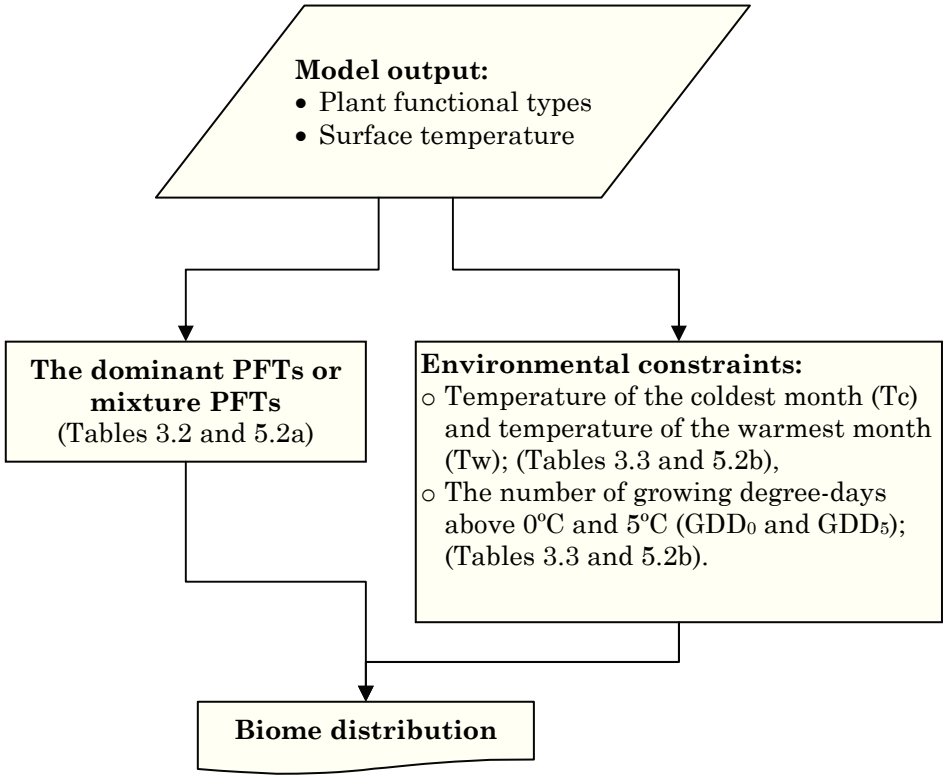

Figure A1 The flow chart of the biome distribution estimation from the UVic ESCM output

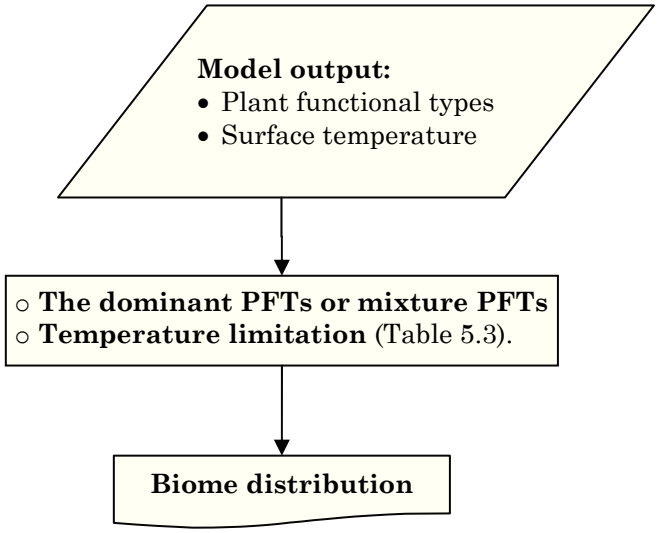

Figure A2 The flow chart of the biome distribution estimation from the CCSM3 output

MATLAB scripts and FORTRAN programs are used for post-processing the model ouput to calculate the dominant PFTs and environmental constraints and to estimate the biome distribution. The scripts and programs can run on UNIX and WINDOWS systems and are found on the CD-ROM attached to this thesis.

All model results of this study will be made available in the PANGAEA database (http://www.pangaea.de/).

Bibliography

Adkins, J.F., Cheng, H., Boyle, E.A., Druffel, E.R.M., and Edwards, R.L.: Deep sea coral evidence for rapid change in ventilation of the deep North Atlantic 15,400 years ago, Science, 280, 725-728, 1998.

Aitken, S.N., Yeaman, S.H., Holliday, J. A., Wang, T., and Curtis-McLane, S.: Adaptation, migration or extirpation: climate change outcomes for tree populations, Evolutionary Applications, 1, 95–111, 2008.

Alley, R.B. and MacAyeal, D.R.: Ice-rafted debris associated with binge/purge oscillations of the Laurentide Ice Sheet, Paleoceanography, 9 (4), doi: 10.1029/94PA01008, 1994.

Alley, R.B., Marotzke, J., Nordhaus, W.D., Overpeck, J.T., Peteet, D.M., Pielke, R.A. Jr., Pierrehumbert, R.T., Rhines, P.B., Stocker, T.F., Talley, L.D., and Wallace, J.M.: Abrupt climate change, Science, 299, 2005-2010, doi:10.1126/science.1081056, 2003.

Alley, R.B.: Wally was right: Predictive ability of the North Atlantic "conveyor belt" hypothesis for abrupt climate change, Annual Reviews of Earth and Planetary Sciences, 35, 241-272, 2007.

Altabet, M. A., Higginson, M. J., and Murray, D. W.: The effect of millennial-scale changes in Arabian Sea denitrification on atmospheric CO_2, Nature, 415, 159–162, 2002.

Ansari, M. H. and Vink, A.: Vegetation history and palaeoclimate of the past 30 kyr in Pakistan as inferred from the palynology of continental margin sediments off the Indus Delta. Review of Palaeobotany and Palynology 145, 201-216, 2007.

Arz, H. W., P¨ atzold, J., and Wefer, G.: Correlated millenial-scale changes in surface hydrography and terrigenous sediment yield inferred from last-glacial marine deposits off Northeastern Brazil, Quaternary Res., 197, 323–333, 1998.

Bard, E., Hamelin, B., and Delanghe-Sabatier, D.: Deglacial meltwater pulse 1B and Younger Dryas sea levels revisited with boreholes at Tahiti, Science, 327, 1235-1237, 2010.

Bard, E., Hamelin, B., and Fairbanks, R.G.: U/Th ages obtained by mass spectrometry in corals from Barbados: sea level during the past 130,000 years, Nature, 346, 456-458, 1990.

Bard, E., Rostek, F., Turon, J.-L., and Gendreau, S.: Hydrological impact of Heinrich events in the subtropical northeast Atlantic, Science, 289, 1321–1324, 2000.

Barker, S., Diz, P., Vautravers, M. J., Pike, J., Knorr, G., Hall., I. R., and Broecker, W. S.: Interhemispheric Atlantic seesaw response during the last deglaciation, Nature, 457, 1097–1101, 2009.

BIBLIOGRAPHY

Behling, H., Arz, H. W., Pätzold, J., and Wefer, G.: Late Quaternary vegetational and climate dynamics in Northeastern Brazil, inferences from marine core GeoB 3104-1, Quaternary Sci. Rev., 19, 981–994, 2000.

Berger, A. L.: Long-term variations of daily insolation and quaternary climate change, J. Atmos. Sci., 35, 2362–2367, 1978.

Bigelow, N. H., Brubaker, L. B., Edwards, M. E., Harrison, S. P., Prentice, I. C., Anderson, P. M., Andreev, A. A., Bartlein, P. J., Christensen, T. R., Cramer, W., Kaplan, J. O., Lozhkin, A. V., Matveyeva, N. V., Murray, D. V., McGuire, A. D., Razzhivin, V. Y., Ritchie, J. C., Smith, B., Walker, D. A., Gajewski, K.,Wolf, V., Holmqvist, B. H., Igarashi, Y., Kremenetskii, K., Paus, A., Pisaric, M. F. J., and Vokova, V. S.: Climate change and Arctic ecosystems. I. Vegetation changes north of 55º N between the Last Glacial Maximum, mid-Holocene and present, J. 10 Geophys. Res., 108(D19), 8170, doi:10.1029/2002JD002558, 2003.

Bird, M.I., Taylor, D., and Hunt, C.: Paleoenvironment of insular Southeast Asia during the last glacial period: a savanna corridor in Sundaland?, Quaternary Sci. Rev., 24, 2228-2242, 2005.

Bitz, C.M., Holland, M., Weaver, A.J., and Eby, M.: Simulating the ice-thickness distribution in a coupled climate model, J. Geophys. Res. ,106, 2441-2464, 2001.

Blunier, T. and Brook, E.J.: Timing of millennial-scale climate change in Antarctica and Greenland during the last glacial period, Science, 291, 109-112, 2001.

Blunier, T., Chappellaz, J., Schwander, J., Dällenbach, A., Stauffer, B., Stocker, T.F., Raynaud, D., Jouzel, J., Clausen, H.B., Hammer, C.U., and Johnsen, S.J.: Asynchrony of Antarctic and Greenland climate change during the last glacial period, Nature, 394, 739-743, 1998.

Bonan, G. B., Levis, S., Sitch, S., Vertenstein, M., and Oleson, K. W.: A dynamic global vegetation model for use with climate models: Concepts and description of simulated vegetation dynamics, Glob. Change Biol., 9, 1543-1566, 2003.

Bonan, G.B. and Levis, S.: Evaluating Aspects of the Community Land and Atmosphere Models (CLM3 and CAM3) Using a Dynamic Global Vegetation Model, J. Climate, 19, 2290-2301, 2006.

Bond, G. C., Broecker, W. S., Johnsen, S., McManus, J., Labeyrie, L., Jouzel, J., and Bonani, G.: Correlation between climate records from the North Atlantic sediment and Greenland ice, Nature, 365, 143–147, 1993.

Bond, G., Heinrich, H., Broecker, W., Labeyrie, L., McManus, J., Andrews, J., Huon, S., Jantschik, R., Clasen, S., Simet, C., Tedesco, K., Klas, M., Bonani, G., and Ivy, S.: Evidence for massive discharges of icebergs into the North Atlantic ocean during the last glacial period, Nature, 360, 245–499, 1992.

Bonnefille, R. and Riollet, G.: The Kashiru pollen sequence (Burundi), Palaeoclimatic implications for the last 40,000 yr. B.P. in tropical Africa, Quat. Research, 30, 19-35, 1988.

Boyle, E.A. and Keigwin, L.D.: North Atlantic thermohaline circulation during the last 20,000 years: link to high latitude surface temperature, Nature, 330, 35-40, 1987.

Broecker, W. S., Bond, G. C., Klas, M., Clark, E., and McManus, J.: Origin of the northern Atlantic's Heinrich events, Clim. Dynam., 6, 265–273, 1992.

BIBLIOGRAPHY

Broecker, W. S., Peteet, D. M., and Rind, D.: Does the ocean-atmosphere system have more 25 than one stable mode of operation?, Nature, 315, 21–26, 1985.

Broecker, W. S.: Massive iceberg discharges as triggers for global climate change, Nature, 372, 421–424, 1994.

Broecker, W. S.: Paleocean circulation during the last deglaciation: A bipolar seesaw?, Paleoceanography, 13, 119-121, 1998.

Broecker, W.S., Bond., G., Klas, M., Bonani, G., and Wolfli, W.: A salt oscillator in the glacial Atlantic?, Paleoceanography, 5 (4), 469-477, 1990.

Broecker, W.S.: The biggest chill', Natural history, 96, 74-82, 1987.

Broecker, W.S.: Thermohaline circulation, the Achilles heel of our climate system: Will man-made CO_2 upset the current balance?, Science, 278, 1582-1588, 1997.

Campbell, N.A.: Biology, 4th Edition. The Benjamin/Cummings Publishing Company, Inc., Menlo Park, California, 1996.

Chappell, J.: Sea-level changes forced ice breakouts in the Last Glacial cycle: new results from coral terraces, Quaternary Sci. Rev., 21, 1229–1240, 2002.

Chiang, J.C.H. and Koutavas, A.: Climate change-Tropical flip-flop connections. Nature 432:684–85, 2004.

Chiang, J.C.H.: The Tropics in Paleoclimate, Ann. Rev. Earth Planet. Sci., 37, 263-297, doi:10.1146/annurev.earth.031208.100217, 2009.

Christensen, T.R. and Cox, P.: Response of methane emissions from arctic tundra to climatic change: results from a model simulation, Tellus-B 47 : 301Ð309, 1995.

Clark, P. U., Hostetler, S. W., Pisias, N. G., Schmittner, A., and Meissner, K. J.: Mechanisms for a ~7-kyr climate and sea-level oscillation during Marine Isotope Stage 3, in: Ocean Circulation: Mechanisms and Impacts, Geophysical Monograph 173, 209–246, AGU, Washington, DC, 2007.

Clark, P.U., Alley, R.B., Keigwin, L.D., Licciardi, J.M., Johnsen, S.J., and Wang, H.: Origin of the first global meltwater pulse following the last glacial maximum, Paleoceanography, 11, 563–577, 1996.

Clark, P.U., Mitrovica, J. X., Milne, G. A., and Tamisiea, M. E.: Sea-Level Fingerprinting as a Direct Test for the Source of Global Meltwater Pulse IA, Science, 295, 2438-2441, doi: 10.1126/science.106879, 2002a.

Clark, P.U., N.G. Pisias, T.F. Stocker and A.J. Weaver.: The role of the thermohaline circulation in abrupt climate change. Nature, 415, 863-869, 2002b.

Claussen, M., Brovkin, V., Ganopolski, A., Kubatzki, C., and Petoukhov, V.: Climate change in northern Africa: the past is not the future, Climatic Change, 57(1), 99–118, 2003.

Claussen, M., Mysak, L.A., Weaver, A.J., Crucifix, M., Fichefet, T., Loutre, M.F., Weber, S.L., Alcamo, J., Alexeev, V.A., Berger, A., Calov, R., Ganopolski, A., Goosse, H., Lohmann, G., Lunkeit, F., Mokhov II, Petoukhov, V., Stone, P., and Wang, Z.: Earth system models of intermediate complexity: closing the gap in the spectrum of climate system models, Clim. Dyn., 18, 579-586, 2002.

Clement, A.C. and Cane, M.: A role for the tropical Pacific coupled ocean-atmosphere system on Milankovitch and millennial timescales. Part I: A Modeling study of tropical Pacific variability, Geophysical monograph series, 112, 363-371, 1999.

BIBLIOGRAPHY

Collatz, G. J., Ball, J. T., Grivet, C., and Berry, J. A.: Physiological and environmental regulation of stomatal conductance, photosynthesis and transpiration: a model that includes a laminar boundary layer, Agric. Forest Meteorol., 54, 107–136, 1991.

Collins, J. A., Schefuß, E., Heslop, D., Mulitza, S., Prange, M., Zabel, M., Tjallingi, R., Dokken, T. M., Huang, E., Mackensen, A., Schulz, M., Tian, J., Zarriess, M., and Wefer, G.: Interhemispheric symmetry of the tropical African rainbelt over the past 23 000 years, Nat. 10 Geosci., 4, 42–45, doi:10.1038/ngeo1039, 2011.

Collins, W. D., Bitz, C. M., Blackmon, M. L., Bonan, G. B., Bretherton, C. S., Carton, J.A., Chang, P., Doney, S. C., Hack, J. J., Henderson, T. B., Kiehl, J. T., Large, W. G., McKenna, D. S., Santer, B. D., Smith, R. D., 2006. The Community Climate System Model Version 3 (CCSM3). Journal of Climate 19, 2122-2143, 2006.

Conkright, M. E., Levitus, S., O'Brien, T., Boyer, T. P., Stephens, C., Johnson, D., Stathoplos, L., Baranova, O., Antonov, J., Gelfeld, R., Burney, J., Rochester, J., and Forgy, C.: World Ocean Database 1998 Documentation and Quality Control, available at: http://iridl.ldeo.columbia.edu/SOURCES/.NOAA/.NODC/.WOA98/.ANNUAL/., National Oceanographic Data Center, 15 Silver Spring, MD, 1998.

Cortijo, E., Labeyrie, L., Vidal, L., Vautravers, M., Chapman, M., Duplessy, J. C. Elliot, M., Arnold, M., Turon, J. L., and Auffret, G.: Changes in sea surface hydrology associated with Heinrich event 4 in the North Atlantic Ocean between 40º N and 60º N, Earth Planet. Sci. Lett., 146, 29–45, 1997.

Cox, P. M., Betts, R. A., Bunton, C. B., Essery, R. L. H., Rowntree, P. R., and Smith, J.: The impact of new land surface physics on the GCM simulation of climate and climate sensitivity, Clim. Dynam., 15, 183–203, 1999.

Cox, P. M., Huntingford, C., and Harding, R. J.: A canopy conductance and photosynthesis model for use in a GCM land surface scheme, Journal of Hydrology, 212-213, 79-94., 1998.

Cox, P. M.: Description of the "TRIFFID" dynamic global vegetation model, Hadley Centre Technical Note 24, Met Office, Bracknell, 2001.

Cramer, W.: Biome models, in Mooney H & Canadell J (eds.) The Earth System: Biological and Ecological Dimensions of Global Environmental Change, Encyclopaedia of Global Environmental Change, Wiley International, Chichester, 2002.

Crucifix, M., Betts, R. A., and Hewitt, C. D.: Pre-industrial potential and Last Glacial Maximum global vegetation simulated with a coupled climate-biosphere model: diagnosis of bioclimatic relationships, Global Planet. Change, 45, 295–312, 2005.

Cuffey, K.M., and Clow, G.D.: Temperature, accumulation, and ice sheet elevation in central Greenland through the last deglacial transition. Jour. Geophys. Res., 102, 26,383-26,396, 1997

Dansgaard, W., Johnsen, S. J., Clausen, H. B., Dahl-Jensen, D., Gundestrup, N. S., Hammer, C. U., Hvidberg, C. S., Steffensen, J. P., Sveinbj¨ornsdottir, A. E., Jouzel, J., and Bond, G.: Evidence for general instability of past climate from a 250-kyr ice-core record, Nature, 364, 218-220, 1993.

De Vries, P. and Weber, S. L.: The Atlantic freshwater budget as a diagnostic for the existence of a stable shut down of the meridional overturning circulation, Geophys. Res. Lett., 32, L09606, doi:10.1029/2004GL021450, 2005.

BIBLIOGRAPHY

Delworth, T.L., Clark, P.U., Holland, M., Johns, W.E., Kuhlbrodt, T., Lynch-Stieglitz, J., Morril, C., Seager, R., Weaver, A.J., and Zhang, R.: The Potential for Abrupt Change in the Atlantic Meridional Overturning Circulation, Abrupt climate change: Final report, Synthesis and Assessment Product 3.4, CSSP, Reston, VA, U.S. Geological Survey, 258-359, 2008

Dixon, K., Delworth, T., Spelman, M., and Stouffer, R.: The influence of transient surface fluxes on North Atlantic overturning in a coupled GCM climate change experiment, Geophysical Research Letters, 26, 2749–2752, 1999.

Driesschaert, E., Fichefet, T. , Goosse, H., Huybrechts, P., Janssens, I., Mouchet, A., Munhoven, G., Brovkin, V., and Weber, S. L.: Modeling the influence of Greenland ice sheet melting on the Atlantic meridional overturning circulation during the next millennia, Geophys. Res. Lett., 34, L10707, doi:10.1029/2007GL029516, 2007.

Duffy, P. B. and Caldeira, K.: Sensitivity of simulated salinity in a three dimensional ocean model to upper-ocean transport of salt from sea-ice formation. Geophys. Res. Lett., 24, 1323–1326, 1997.

Duffy, P. B., Eby, M., and Weaver, A.J.: Climate model simulations of effects of increased atmospheric CO_2 and loss of sea ice on ocean tracer uptake. J. Clim. 14: 520–532, 2001.

Duffy, P. B., Eby, M., and Weaver, A.J.: Effects of sinking of salt rejected during formation of sea ice on results of a global ocean-atmosphere-sea ice climate model. Geophys. Res. Lett. 26: 1739–1742, 1999

Dupont, L. M., Jahns, S., Marret, F., and Ning, S.: Vegetation change in equatorial West Africa: time-slices for the last 150 ka, Palaeogeogr. Palaeocl. 155, 95–122, 2000.

Dupont, L., Behling, H.: Land-sea linkages during deglaciation: High-resolution records from the eastern Atlantic off the coast of Namibia and Angola. Quaternary International 148, 19-28, 2006.

Dupont, L.M., Behling, H., Kim, J.-H.: Thirty thousand years of vegetation development and climate change in Angola (Ocean Drilling Program Site 1078). Climate of the Past 4, 111-147, 2008.

Dupont, L.M., Schlütz, F., Teboh Ewah, C., Jennerjahn, T.C., Paul, A., and Behling, H., Two-step vegetation response to enhanced precipitation in Northeast Brazil during Heinrich event 1, Glob. Change Biol., 16, 1647-1660, 2009.

Elliot, M., Labeyrie, L., and Duplessy, J.C.: Changes in North Atlantic deep-water formation associated with Dansgaard-Oeschger temperature osciallation (60-10 ka), Quat. Sci. Rev., 21, 1153-1165, 2002.

EPICA Community Members: One-to-one coupling of glacial climate variability in Greenland and Antarctica, Nature, 444, 195-198, doi:10.1038/nature05301, 2006.

Essery, R.L.H., Best, M.J., and Cox, P.M.: MOSES 2.2 technical documentation. Hadley Centre Technical Note 30. Met Office, Bracknell. www.met-office.gov.uk/research/ hadleycentre/pubs/HCTN/HCTN_30.pdf, 2001.

Ewen, T. L., Weaver A. J., and Schmittner, A.: Modelling carbon cycle feedbacks during abrupt climate change, Quaternary Sci. Rev., 23(3 – 4), 431 – 448, 2004.

Fairbanks, R.G.: A 17,000 year glacio-eustatic sea level record: influence of glacial melting rates on the Younger Dryas event and deep ocean circulation, Nature, 342, 637-642, 1989.

BIBLIOGRAPHY

Fanning, A. G. and Weaver, A. J.: An atmospheric energy-moisture model: climatology, interpentadal climate change and coupling to an ocean general circulation model, J. Geophys. Res., 101, 15111–15128, 1996.

Fanning, A. G. and Weaver, A. J.: On the role of flux adjustments in an idealized coupled climate model, Clim. Dynam., 13, 691-701, 1997.

Fletcher, W.J., Sanchez Goñi, M.F., Allen, J.R.M., Cheddadi, R., Combourieu Nebout, N., Huntley, B., Lawson, I., Londeix, L., Magri, D., Margari, V. , Müller, U., Naughton, F., Novenko, E., Roucoux, K. Tzedakis, P.C.: Millennial-scale variability during the last glacial in vegetation records from Europe, Quaternary Sci. Rev., 29: 2839-2864, 2010.

Flückiger, J., Knutti, R., and White, J. W. C.: Oceanic processes as potential trigger and amplifying mechanisms for Heinrich events, Paleoceanography, 21, 1–11, 2006.

Ganopolski, A. and Rahmstorf, S.: Rapid changes of glacial climate simulated in a coupled climate model, Nature, 409 (6817), 153–158, doi:10.1038/35051500, 2001.

Gent, P. R. and McWilliams, J. C.: Isopycnal mixing in ocean circulation models. J. Phys. Ocean., 20, 150-155, 1990.

Gherardi, J.-M., Labeyrie, L., McManus, J., Francois, R., Skinner, L. C., and Cortijo, E.: Evidence from the Northeastern Atlantic basin for variability in the rate of the meridional overturning circulation through the last deglaciation, Earth Planet. Sci. Lett., 240, 710–723, 2005.

González, C. and Dupont, L.M.: Tropical salt marsh succession as sea-level indicator during Heinrich events, Quat. Sci. Rev., 28, 939-946, 2009.

González, C., Dupont, L. M., Behling, H., and Wefer, G.: Neotropical vegetation response to rapid climate changes during the last glacial period: Palynological evidence from the Cariaco Basin, Quaternary Res., 69, 217-230, 2008.

Gordon, A.L.: Inter-ocean exchange of thermocline water. Journal of Geophysical Research-Oceans, 91, 5037-5046, 1986.

Gregory, J.M., Dixon, K.W., Stouffer R.J., Weaver, A.J., Driesschaert, E., Eby, M., Fichefet, T., Hasumi, H., Hu, A., Jungclaus, J.H., Kamenkovich, I.V., Levermann, A., Montoya, M., Murakami, S., Nawarth, S., Oka, A., Sokolov, A.P., and Thorphe, R.B.: A model intercomparison of changes in the Atlantic thermohaline circulation in response to increasing atmospheric CO_2 concentration. Geophys. Res. Lett., 32, L12703, doi: 10.1029/2005GL023209, 2005.

Grimm, E.C., Jacobson Jr., G.L., Watts, W.A., Hansen, B.C.S., and Maasch, K.A.: A 50,000-year record of climate oscillations from Florida and its temporal correlation with the Heinrich events, Science, 261, 198-200, 1993.

Grootes, P.M., Stuiver, M., White, J.W.C., Johnsen, S., and Jouzel, J.: Comparison of oxygen isotope records from the GISP2 and GRIP Greenland ice cores, Nature, 366, 552-554, 1993.

Grousset, F.E., Pujol, C., Labeyrie, L., Auffret, G., Boelaert, A.: Were the North Atlantic Heinrich events triggered by the behaviour of the European ice sheets?, Geology 28, 123-126, 2000.

Hammer, C.U., Clausen, H.B. and Langway, Jr, C.C.: Electrical conductivity method (ECM) stratigraphic dating of the Byrd Station ice core, Antarctica. Ann. Glaciol., 20, 115–120, 1994.

BIBLIOGRAPHY

Handiani, D., Paul, A., and Dupont, L., Tropical climate and vegetation changes during Heinrich Event 1: a model-data comparison, Clim. Past 8 (1), 37-57, doi: 10.5194/cp-8-37-2012, 2012.

Harrison, S. P. and Prentice, I. C.: Climate and CO_2 controls on global vegetation distribution at the last glacial maximum: analysis based on palaeovegetation data, biome modelling and palaeoclimate simulations, Glob. Change Biol., 9, 983–1004, 2003.

Harrison, S. P., Yu, G., Takahara, H., and Prentice, I. C.: Palaeovegetation - diversity of temperate plants in East Asia, Nature, 413, 129-130, 2001.

Heaney, L.R.: A synopsis of climatic and vegetational change in Southeast Asia, Climatic Change, 19, 53-61, doi:10.1007/BF00142213, 1991.

Heinrich, H.: Origin and consequences of cyclic ice rafting in the northeast Atlantic Ocean during the past 130,000 years, Quaternary Res., 29, 142-152, 1988.

Helmens, K.F., Kuhry, P., Rutter, N.W., van der Borg, K., De Jong, A.F.M.: Warming at 18,000 yr B.P. in the tropical Andes, Quaternary Res., 45, 289–299, 1996.

Hemming, S. R.: Heinrich events: massive late pleistocene detritus layers of the North Atlantic and their global climate imprint, Rev. Geophys., 42, 1-43, RG1005, doi:10.1029/2003RG000128, 2004.

Henrot, A.-J., François, L., Brewer, S., and Munhoven, G.: Impacts of land surface properties and atmospheric CO_2 on the Last Glacial Maximum climate: a factor separation analysis, Clim. Past, 5, 183–202, doi:10.5194/cp-5-183-2009, 2009.

Hessler I., Dupont, L.M., Bonnefille, R., Behling, H., González, C., Helmens, K.F., Hooghiemstra, H., Lebamba, J., Ledru, M-P., Lézine, A-M, Maley, J., Marret, F., and Vincens, A.: Millennial-scale changes in vegetation records from tropical Africa and South America during the last glacial, Quaternary Sci. Rev., 29, 2882–2899, doi:10.1016/j.quascirev. 2009.11.029, 2010.

Hibler,W. D.: A dynamic thermodynamic sea ice model, J. Phys. Oceanogr., 9, 815–846, 1979.

Hughen, K. A., Eglinton, T. I., Xu, L., and Makou, M.: Abrupt tropical vegetation response to rapid climate changes, Science, 304, 955–1959, 2004.

Hughes, J. K., Valdes, P. J., and Betts, R. A.: Dynamical properties of the TRIFFID dynamic global vegetation model, Technical Note 56, Hadley Centre, Met Office, UK, 2004.

Hughes, T.M.C. and Weaver, A.J.: Multiple equilibria of an asymmetric two-basin ocean model, J. Phys. Oceanogr., 24, 619-637, 1994.

Hunke, E. C. and Dukowicz, J. K.: An elastic-viscous-plastic model for sea ice dynamics, J. Phys. Oceanogr., 27, 1849–1867, 1997.

IPCC: Contribution of Working Groups 1, 2, and 3 to the Fourth Assessment Report of the Intergovernmental Panel on Climate Change. Core Writing Team, Pachauri, R.K. and Reisinger, A. (Eds.), Geneva, Switzerland, pp 104, 2007.

Jennerjahn, T. C., Ittekkot, V., Arz, H. W., and Behling, H.: Asynchronous terrestrial and marine signals of climate change during Heinrich Events, Science, 306, 2236–2239, 2004.

Jiménez-Moreno, G., Anderson, R.S., Desprat, S., Grigg, L., Grimm, E., Heusser, L.E., Jacobs, B.F., López-Martínez, C., Whitlock, C., and Willard, D.A.: Millenial-scale variability during the last glacial in vegetation records from North America, Quaternary Sci. Rev., 29, 2865-2881, 2010.

Johnsen, S.J., Dansgaard, W., and Clausen, H.B., and Langway, Jr. C.C.: Oxygen isotope profiles through the Antarctic and Greenland ice sheets. Nature, 235, 429-434, 1972.

Kageyama M., Mignot, J., Swingedouw, D., Marzin, C., Alkama, R., and Marti, O.: Glacial climate sensitivity to different states of the Atlantic Meridional overturning circulation: results from the IPSL model, Clim. Past, 5, 551-570, 2009.

Kageyama, M., Combourieu Nebout, N., Sepulchre, P., Peyron, O., Krinner, G., Ramstein, G., and Cazet, J.-P.: The Last Glacial Maximum and Heinrich Event 1 in terms of climate and vegetation around the Alboran Sea: a preliminary model-data comparison, Comp. Rend. Geosci., 337, 983–992, 2005.

Kageyama, M., Laîné, A., Abe-Ouchi, A., Braconnot, P., Cortijo, E., Crucifix, M., de Vernal, A., Guiot, J., Hewitt, C.D., Kitoh, A., Marti, O., Ohgaito, R., Otto-Bliesner, B., Peltier, W.R., Rosell-Melé, A., Vettoretti, G., Weber, S.L., and MARGO Project Members.: Last Glacial Maximum temperature over the North Atlantic, Europe and western Siberia: a comparison between PMIP models, MARGO sea-surface temperatures and pollen-based reconstructions, Quaternary Sci. Rev., 25, 2082–2102, 2006.

Kageyama, M., Paul, A., Roche, D. M., and Van Meerbeeck, C. J.: Modelling glacial climatic millennial-scale variability related to changes in the Atlantic meridional overturning circulation: a review, Quaternary Sci. Rev., 29, 2931–2956, 2010.

Kalnay, E., Kanamitsu, M., Kistler, R., Collins,W., Deaven, D., Gandin, L., Iredella, M., Saha, S., White, G., Woollen, J., Zhu, Y., Chelliah, M., Ebisuzaki, W., Higgins, W., Janowiak, J., Mo, K. C., Ropelewski, C., Wang, J., Leetmaa, A., Reynolds, R., Jenne, R., and Dennis Joseph.: The NCEP/NCAR 40-Year Reanalysis Project, B. Am. Meteorol. Soc., 77 (3), 437–471, 1996.

Kanfoush, S. L., Hodell, D.A., Charles, C.D., Guilderson, T.P., Mortyn, P.G., and Ninnemann, U.S.: Millennial-scale instability of the Antarctic ice sheet during the last glaciation, Science, 288, 1815 – 1818, 2000.

Kaplan, J. O., Bigelow, N. H., Bartlein, P. J., Christensen, T. R., Cramer, W., Harrison, S. P., Matveyeva, N. V., McGuire, A. D., Murray, D. F., Prentice, I. C., Razzhivin, V. Y., Smith, B., Walker, D. A., Anderson, P. M., Andreev, A. A., Brubaker, L. B., Edwards, M. E., Lozhkin, A. V., and Ritchie, J.: Climate change and Arctic ecosystems II: Modeling, palaeodata-model comparisons, and future projections, J. Geophys. Res., 108, 8171, doi:10.1029/2002JD002559, 2003.

Knorr, G. and Lohmann, G.: Rapid transitions in the Atlantic thermohaline circulation triggered by global warming and meltwater during the last deglaciation, Geochem. Geophys. Geosyst., 8, Q12006, doi:10.1029/2007GC001604, 2007.

Köhler, P., Joos, F., Gerber, S., and Knutti, R.: Simulated changes in vegetation distribution, land carbon storage, and atmospheric CO_2 in response to a collapse of the North Atlantic thermohaline circulation, Clim. Dynam., 25, 689–708, 2005.

Kuhlbrodt, T., Griesel, A., Montoya, M., Levermann, A., Hofmann, M., and Rahmstorf, S.: On the driving processes of the Atlantic meridional overturning circulation, Rev. Geophys., 45, RG2001, doi:10.1029/2004RG000166, 2007.

Lamy, F., Kaiser, J., Arz, H. W., Hebbeln, D., Ninnemann, U. S., Timm, O., Timmermann, A., and Toggweiler, J. R.: Modulation of the bipolar seesaw in the Southeast Pacific during Termination 1, Earth Planet. Sci. Lett., 259, 400–413, 2007.

Ledru, M.-P., Campello, R.C, Landim-Dominguez, J.M., Martin, L, Mourguirat, P., Sifeddine, A., and Turcq, B.: Late-Glacial cooling in Amazonia inferred from pollen at Lagoa do Caçó, Northern Brazil, Quaternary Res., 55, 47-56, 2001.

Ledru, M.-P., Ceccantini, G., Gouveia, S. E. M., Lopez-Saez, J. A., Pessenda, L. C. R., and Ribeiro, A. S.: Millenial-scale climatic and vegetation changes in a northern Cerrado (Northeast, Brazil) since the Last Glacial Maximum, Quaternary Sci. Rev., 25, 1110–1126, 2006.

Lee, S.-Y., Chiang, J. C. H., Matsumoto, K., and Tokos, K. S.: Southern Ocean wind response to North Atlantic cooling and the rise in atmospheric CO_2: Modeling perspective and paleoceanographic implications, Paleoceanography, 26, PA1214, doi:10.1029/ 2010PA002004, 2011.

Liu, Z., Otto-Bliesner, B. L., He, F., Brady, E. C., Tomas, R., Clark, P. U., Carlson, A. E., Lynch-Stieglitz, J., Curry, W., Brook, E., Erickson, D., Jacob, R., Kutzbach, J., and Cheng, J.: Transient Simulation of Last Deglaciation with a New Mechanism for Bølling-Allerød Warming, Science, 325, 310-314, 2009.

Loveland, T. R., Reed, B. C., Brown, J. F., Ohlen, D. O., Zhu, S., Yang, L., and Merchant, J. W.: Developments of a global land cover characteristics database and IGBP DISCover from 1 km AVHRR data, Int. J. Remote Sens., 21, 1303–1330, 2000.

Lumpkin, R. and Speer, K.: Global ocean meridional overturning, J. Phys. Oceanogr., 37, 2250– 2262, 2007.

Manabe, S. and Stouffer, R.J.: Coupled ocean-atmosphere model response to freshwater input: comparison to Younger Dryas event, Paleoceanography, 12, 321-336, 1997.

Manighetti, B., and McCave, I.N.: Late glacial and Holocene palaeocurrents through South Rockall Gap, NE Atlantic Ocean. Paleocean., 10, 611–626, 1995.

Marchal, O., François, R., Stocker, T. F., and Joos, F.: Ocean thermohaline circulation and sedimentary 231Pa/230Th ratio, Paleoceanography, 15, 625–641, 2000.

MARGO Project Members: Constraints on the magnitude and patterns of ocean cooling at the Last Glacial Maximum, Nat. Geosci., 2, 127–132, 2009.

Matthews, H. D., Weaver, A. J., and Meissner, K. J.: Terrestrial carbon cycle dynamics under recent and future climate change, J. Clim., 18, 1609 – 1628, 2005.

McManus, J. F., François, R., Gherardi, J.-M., Keigwin, L. D., and Brown-Leger, S.: Collapse and rapid resumption of Atlantic meridional circulation linked to deglacial climate changes, Nature, 428, 834-837, 2004.

Meissner, K. J., Weaver, A. J., Matthews, H. D., and Cox, P. M.: The role of land surface dynamics in glacial inception: a study with the UVic Earth System model, Clim. Dynam., 21, 515-537, 2003.

Menviel, L., Timmermann, A., Mouchet, A., and Timm, O.: Meridional reorganizations of marine and terrestrial productivity during Heinrich events, Paleoceanography, 23, 2008.

Merkel, U., Prange, M., and Schulz, M.: ENSO variability and teleconnections during glacial climates, Quat. Sci. Rev., 29, 86-100, 2010.

Morley, R.J.: Origin and Evolution of Tropical Forests, Wiley, Chichester, 2000.

BIBLIOGRAPHY

Mulitza, S, Prange, M., Stuut, J.-B., Zabel, M., Dobeneck, T. V., Itambi, A. C., Nizou, J., Schulz, M., and Wefer, G.: Sahel megadroughts triggered by glacial slowdowns of Atlantic meridional overturning, Paleoceanography, 23, 1–11, PA4206, doi:10.1029/2008PA001637, 2008.

Muller, J., Kylander, M., Wüst, R. A. J., Weiss, D., Martinez-Cortizas, A., LeGrande, A. N., Jennerjahn, T., Behling, H., Anderson, W. T. and Jacobson, G.: Possible evidence for wet Heinrich phases in tropical NE Australia: the Lynch's Crater deposit, Quaternary Science Reviews 27, 468-475, 2008.

National Research Council: Understanding Climate Change Feedbacks, National Academy Press, Washington, DC, 152 pp, 2003.

Oleson, K. W., Lawrence, D.M., Bonan, G.B., Flanner, M.G., Kluzek, E., Lawrence, P.J., Levis, S., Swenson, S.C., Thornton, P.E., Dai, A., Decker, M., Dickinson, R., Feddema, J., Heald, C.L., Hoffman, F., Lamarque, J-F., Mahowald, N., Niu, G-Y., Qian, T., Randerson, J., Running, S., Sakaguchi, K., Slater, A., Stöckli, R., Wang, A., Yang, Z-L., Zeng, X., and Zeng, X.: Technical description of the Community Land Model (CLM), NCAR Tech. Note TN-461+STR, 173, 2004.

Oleson, K.W., Niu, G.-Y., Yang, Z.-L., Lawrence, D.M., Thornton, P.E., Lawrence, P.J., Stockli, R., Dickinson, R.E., Bonan, G.B., Levis, S., Dai, A., and Qian, T.: Improvements to the Community Land Model and their impact on the hydrological cycle, J. Geophys. Res., 113, G01021, DOI:10.1029/2007JG000563, 2008.

Otto-Bliesner, B. L., Brady, E. C., Clauzet, G., Tomas, R., Levis, S., and Kothavala, Z.: Last Glacial Maximum and Holocene Climate in CCSM3, J. Climate, 19, 2526–2544, 2006.

Otto-Bliesner, B. L., Hewitt, C. D., Marchitto, T. M., Brady, E., Abe-Ouchi, A., Crucifix, M., Murakami, S., and Weber, S. L.: Last Glacial Maximum ocean thermohaline circulation: PMIP2 model intercomparisons and data constraints, Geophys. Res. Lett., 34, 1–6, L12706, doi:10.1029/2007GL029475, 2007.

Pacanowski, R. C.: MOM 2 Documentation: Users Guide and Reference Manual, Version 1.0. GFDL Ocean Group Technical Report No. 3, Geophysical Fluid Dynamics Laboratory, Princeton, New Jersey, 1995.

Peltier, W.R., Vettoretti, G., and Stastna, M.: Atlantic Meridional Overturning and Climate Response to Arctic Ocean Freshening, Geophys. Res. Lett., 33, L06713, 2006.

Peltier, W.R: Global Glacial Isostasy and the Surface of the Ice-Age Earth: The ICE-5G (VM2) Model and GRACE, Annu. Rev. Earth Planet. Sci., 32, 111-149, 2004.

Peterson, L. C., Haug, G. H., Hughen, K. A., and Röhl, U.: Rapid changes in the hydrologic cycle of the tropical Atlantic during the last glacial, Science, 290, 1947–1951, 2000.

Pickett, E., Harrison, S. P., Hope, G., Harle, K., Dodson, J. R., Kershaw, A. P., Prentice, I. C., Backhouse, J., Colhoun, E. A., D'Costa, D., Flenley, J., Grindrod, J., Haberle, S., Hassell, C., Kenyon, C., Macphail, M., Martin, H., Martin, A. H., McKenzie, M., Newsome, J. C., Penny, D., Powell, J., Raine, I., Southern, W., Stevenson, J., Sutra, J.-P., Thomas, I., van der Kaars, S., and Ward, J.: Pollen-based reconstructions of biome distributions for Australia, South East Asia and the Pacific (SEAPAC region) at 0, 6000 and 18000 14C yr BP, J. Biogeogr., 31, 1381–1444, 2004.

Piotrowski, A.M., Goldstein, S.L., Hemming, S.R., and Fairbanks, R.G.: Intensification and variability of ocean thermohaline circulation through the last deglaciation. Earth Planet. Sci. Let., 225, 205-220, 2004.

Poulter, B, Ciais, P., Hodson, E., Lischke, H., Maignan, F., Plummer, S. and Zimmermann, N.: Plant functional type mapping for Earth System Models, Geosci. Model Dev., 4:1-18, 2011.

Prentice, I. C. and Webb III, T.: BIOME 6000: reconstructing global mid-Holocene vegetation patterns from paleoecological records, J. Biogeogr., 25, 997–1005, 1998.

Prentice, I. C., Cramer, W., Harrison, S. P., Leemans, R., Monserud, R. A., and Solomon, A. M.: A global biome model based on plant physiology and dominance, soil properties and climate, J. Biogeogr., 19, 117–134, 1992.

Prentice, I. C., Jolly, D., and BIOME 6000 Members.: Mid-Holocene and glacial-maximum vegetation geography of the northern continents and Africa, J. Biogeogr., 27, 507–519, 2000.

Prentice, J.C., Guiot J., Huntley B., Jolly D., and Cheddadi, R.: Reconstructing biomes from palaeoecological data: a general method and its application to European pollen data at 0 and 6 ka, Clim. Dynam., 12, 185-194, 1996.

Rahmstorf, S.: Ocean circulation and climate during the past 120,000 years, Nature 419, 207-214, 2002.

Ray, N. and Adams, J. M.: A GIS-based Vegetation Map of the World at the Last Glacial Maximum (25000–15000 BP), Internet Archaeology, 11, available at: http://intarch.ac.uk/journal/issue11/rayadams toc.html, 2001.

Roche, D. M., Dokken, T. M., Goosse, H., Renssen, H., and Weber, S. L.: Climate of the Last Glacial Maximum: sensitivity studies and model-data comparison with the LOVECLIM 20 coupled model, Clim. Past, 3, 205–224, doi:10.5194/cp-3-205-2007, 2007.

Roche, D.M., Wiersma, A.P., and Renssen, H.: A systematic study of the impact of freshwater pulses with respect to different geographical locations, Climate Dynamics, 34, 997-1013, doi: 10.1007/s00382-009-0578-8, 2010

Sakai, K, and Peltier, W.R.: A simple model of the Atlantic thermohaline circulation: Internal and forced variability with paleoclimatological implications, J. Geophys. Res., 100, 13455-13479, 1995.

Sakai, K, and Peltier, W.R.: Dansgard-Oeschger oscillations in a coupled atmosphere-ocean climate model, J. Clim, 10, 949-970, 1997.

Sarnthein, M., Stattegger, K., Dreger, D., Erlenkeuseur, H., Grootes, P.M., Haupt, B., Jung, S., Kiefer, T., Kuhnt, W., Pflaumann, U., Schäfer-Neth, C., Schulz, M., Sveidov, M., Simstich, J., van Kreveld-Alfane, S., Vogelsang, E., Völker, A., Weinelt, M.: Fundamental modes and abrupt changes in North Atlantic Circulation and climate over the last 60 ky- Concepts, reconstruction, and numerical modelling, The northern North Atlantic: A changing environment (Springer Verl.), 365-410, 2001.

Sarnthein, M., Winn, K., Jung, S.J.A., Duplessy, J.C., Labeyrie, L., Erlenkeuser, H., and Ganssen, G.: Changes in East Atlantic deep water circulation over the last 30,000 years: an eight time-slice record, Paleoceanography, 9, 209-267, 1994.

Schmittner, A., Brook, E., and Ahn, J.: Impact of the ocean's overturning circulation on atmospheric CO_2 in Ocean Circulation: Mechanisms and Impacts, AGU Geophysical Monograph Series, vol. 173, edited by A. Schmittner, J. Chiang, and S. Hemming, 209-246, 2007.

Schmittner, A., Galbraith, E.D., Hostetler, S.W., Pedersen, T.F., and Zhang, R.: Large fluctuations of dissolved oxygen in the Indian and Pacific oceans during Dansgaard-Oeschger oscillations caused by variations of North Atlantic deep water subduction, Paleooceanography, 22, PA3207, doi:10.1029/2006PA001384, 2007.

Schmittner, A., Meissner, K.J., Eby, M., and Weaver, A.J.: Forcing of the deep ocean circulation in simulations of the Last Glacial Maximum, Paleoceanography, 17, doi: 10.1029/2001PA000633, 2002a.

Schmittner, A., Yoshimori, M., and Weaver, A.J.: Instability of glacial climate in a model of the ocean-atmosphere-cryosphere system, Science, 295, 1489-1493, 2002b.

Scholze, M., Knorr, W., and Heimann, M.: Modelling terrestrial vegetation dynamics and carbon cycling for an abrupt climatic change event, Holocene, 13, 327-333, 2003.

Schurgers, G., Mikolajewicz, U. Gröger, M., Maier-Reimer, E., Vizcaino, M., and Winguth, A.: Dynamics of the terrestrial biosphere, climate and atmosphere CO_2 concentration during interglacials: a comparison between Eemian and Holocene, Clim. Past, 2, 205-220, 2006.

Siddall, M., Smeed, D.A., Hemleben, C., Rohling, E.J., Schmelzer, I., and Peltier, W.R.: Understanding the Red Sea response to sea level, Earth Planet. Sci. Lett., 225, (3-4), 421-434, doi:10.1016/j.epsl.2004.06.008, 2004.

Siddall, M., Stocker, T.F., Henderson, G.M., Joos, F., Frank, M., Edwards, N.R., Ritz, S., and Müller, S.A. :Modeling the relationship between 231Pa/230Th distribution in North Atlantic sediment and Atlantic meridional overturning circulation. Paleoceanography, 22, PA2214, doi:10.1029/2006PA001358, 2007.

Sitch, S., Smith, B., Prentice, I. C., Arneth, A., Bondeau, A., Cramer, W., Kaplan, J. O., Levis, S., Lucht, W., Sykes, M. T., Thonicke, K., and Venevsky, S.: Evaluation of ecosystem dynamics, plant geography and terrestrial carbon cycling in the LPJ dynamic global vegetation model, Glob. Change Biol., 9, 161-185, 2003.

Stanford, J. D., Rohling, E. J., Hunter, S. E., Roberts, A. P., Rasmussen, S. O., Bard, E., McManus, J., and Fairbanks, R. G.: Timing of meltwater pulse 1a and climate responses to meltwater injections, Paleoceanography, 21, PA4103, doi:10.1029/2006PA001340, 2006.

Stenni, B., Burion, D., Frezzotti, M., Albani, S., Barbante, C., Bard, E., Barnola, J. M., Baroni, M., Baumgartner, M., Bonazza, M., Capron, E., Castellano, E., Chappellaz, J., Delmonte, B., Falourd, S., Genoni, L., Iacumin, P., Jouzel, J., Kipfstuhl, S., Landais, A., Lemieux-Dudon, B., Maggi, V., Masson-Delmotte, V., Mazzola, C., Minster, B., Montagnat, M., Mulvaney, R., Narcisi, B., Oerter, H., Parrenin, F., Petit, J.R., Ritz, C., Scarchilli, C., Schilt, A., Schüpbach, S., Schwander, J., Selmo, E., Severi, M., Stocker, T. F., and Udisti, R.: Expression of the bipolar see-saw in Antarctic climate records during the last deglaciation, Nature Geoscience, 4, 46-49, 2011.

Stocker, T. F. and Wright, D. G.: The effect of a succession of ocean ventilation changes on radiocarbon, Radiocarbon, 40, 359-366, 1998.

Stocker, T. F., Knutti, R., and Plattner, G.-K.: The future of the thermohaline circulation - a perspective, In: The Ocean and Rapid Climate Changes: Past, Present, and Future, D. Seidov et al. (eds.), Geophysical Monograph, 126, American Geophysical Union, 277-293, 2001.

Stocker, T. F., Wright, D. G., and Broecker, W. S.: Influence of high-latitude surface forcing on the global thermohaline circulation, Paleoceanography, 7, 529 – 541, 1992.

Stocker, T.F. and Johnsen, S.J.: A minimum model for the bipolar seesaw, Paleoceanography, 18, 1087, doi: 10.1029/2003PA000920, 2003.

Stouffer, R.J., Seidov, D., and Haupt, B.J.: Climate response to external sources of freshwater: North Atlantic versus the Southern Ocean, J. Clim, 20, 436-448, 2007.

Stouffer, R.J., Yin, J., Gregory, J.M., Dixon, K.W., Spelman, M.J., Hurlin, W., Weaver, A.J., Eby, M., Flato, G.M., Hasumi, H., Hu, A., Jungclaus, J.H., Kamenkovich, I.V., Levermann, A., Montoya, M., Murakami, S., Nawrath, S., Oka, A., Peltier, W.R., Robitaille, D.Y., Sokolov, A., Vettoretti, G., and Weber, S.L.: Investigating the causes of the response of the thermohaline circulation to past and future climate changes, J. Climate, 19, 1365-1387, 2006.

Stouffer, R.J., Seidov, D., and Haupt, B.J.: Climate response to external sources of freshwater: North Atlantic versus the Southern Ocean, J. Clim, 20, 436-448, 2007.

Stouffer, R.J., Yin, J., Gregory, J.M., Dixon, K.W., Spelman, M.J., Hurlin, W., Weaver, A.J., Eby, M., Flato, G.M., Hasumi, H., Hu, A., Jungclaus, J.H., Kamenkovich, I.V., Levermann, A., Montoya, M., Murakami, S., Nawrath, S., Oka, A., Peltier, W.R., Robitaille, D.Y., Sokolov, A., Vettoretti, G., and Weber, S.L.: Investigating the causes of the response of the thermohaline circulation to past and future climate changes, J. Climate, 19, 1365-1387, 2006.

Stuiver, M. and Grootes, P.M.: GISP2 oxygen isotope ratios. Quat. Res., 53, 277-284, 2000.

Swingedouw, D., Mignot, L.J., Braconnot, P., Mosquet, E., Kageyama, M., and Alkama, R.: Impact of freshwater release in the North Atlantic under different climate conditions in an OAGCM, J. Clim., 22, 6377-6401, 2009.

Tjallingii, R., Claussen, M., Stuut, J_B., Fohlmeister, J., Jahn, A., Bickert, T., Lamy, F., and Röhl, U.: Coherent high- and low-latitude forcing of the Northwest African humidity. Nature Geoscience, Vol. 1, Issue 10, 670 – 675, doi:10.1038/ngeo289, 2008.

Trevena, J., Sijp, W. P., and England, M. H.: North Atlantic Deep Water collapse triggered by a Southern Ocean meltwater pulse in a glacial climate state, Geophys. Res. Lett., 35, L09704, doi:10.1029/ 2008GL033236, 2008.

Turney, C.S.M., Kershaw, A.P., Lowe, J.J., van der Kaars, S., Johnston, R., Rule, S., Moss, P., Radke, L., Tibby, J., McGlone, M.S., Wilmshurst, J., Vandergoes, M., Fitzsimons, S., Bryant, C., James, S., Branch, N.P., Cowley, J., Kalin, R.M., Ogle, N., Jacobsen, G., and Fifield, L.K.: Climate variability in the southwest Pacific during the Last Termination (20 - 10 kyr BP), Quat. Sci. Rev., 25, 886-903, 2006.

Van der Kaars, S., Penny, D., Tibby, J., Fluin, J., Dam, R. A.C., and Suparan, P.: Late Quarternary palaeoecology, palynology and palaeolimnology of tropical lowland swamp: Rawa Danau, West-Java, Indonesia, Palaeogeography, Palaeoclimatology, Palaeoecology, 171, 185-212, 2001.

Van der Kaars, W.A.: Palynology of eastern Indonesian marine piston-cores: A Late Quaternary vegetational and climatic record for Australia, Palaeogeography, Palaeoclimatology, Palaeoecology, 85, 239-302, 1991.

Vidal, L., Labeyrie, L., Cortijo, E., Arnold, M., Duplessy, J., Michel, E., Becque, S., and van-Weering, T.: Evidence for changes in the North Atlantic DeepWater linked to meltwater surges during the Heinrich events, Earth Planet. Sci. Lett., 146, 13–27, 1997.

Vincens, A., Garcin, Y., and Buchet, G.: Influence of rainfall seasonality on African lowland vegetation during the Late Quaternary: pollen evidence from Lake Masoko, Tanzania, J. Biogeogr., 34, 1274-1288, 2007.

Weaver, A. J., Eby, M., Wiebe, E. C., Bitz, C. M., Duffy, P. B., Ewen, T. L., Fanning, A. F., Holland, M.M., MacFadyen, A., Matthews, H.D., Meissner, K.J., Saenko, O., Schmittner, A., Wang, H., and Yoshimori, M.: The UVic Earth System Climate Model: model description, climatology, and applications to past, present and future climates, Atmos.-Ocean, 39, 361-428, 2001.

Weaver, A. J., Saenko, O. A., Clark, P. U., and Mitrovica, J. X.: Meltwater pulse 1A from Antarctica as a trigger of the Bølling-Allerød warm interval, Science, 299, 1709–1713, 2003.

Weaver, A.J., Eby, M., Kienast, M., and Saenko, O.A.: Response of the Atlantic meridional overturning circulation to increasing atmospheric CO_2: Sensitivity to mean climate state, Geophys. Res. Lett., 34, L05708, doi:10.1029/2006GL028756, 2007.

Weber, S. L. and Drijfhout, S. S.: Stability of the Atlantic meridional overturning circulation in the Last Glacial maximum climate, Geophys, Res. Lett., 34, 1-5, L22706, doi:10.1029/2007GL031437, 2007.

Wiebe, E.C. and Weaver, A.J.: On the sensitivity of global warming experiments to the parametrisation of sub-grid scale ocean mixing, Clim. Dynam., 15, 875-893, 1999.

Wunsch, C.: What is the thermohaline circulation?. Science, 298, 1179, 2002.

Yeager, S. G., Shields, C. A., Large, W.G., and Hack, J. J.: The low-resolution CCSM3, J. Climate, 19, 2545-2566, doi: dx.doi.org/10.1175/JCLI3744.1, 2006.

Yokoyama, Y., De Deckker, P., Lambeck, K., Johnston, P., and Fifield, L. K.: Sea-level at the last glacial maximum: evidence from northwestern Australia to constrain ice volumes for oxygen isotope stage 2, Palaeogeogr. Palaeocl., 165, 281–297, 2001.

Yu, E. F., Francois, R., and Bacon, M. P.: Similar rates of modern and last-glacial ocean thermohaline circulation inferred from radiochemical data, Nature, 379, 689–694, 1996.

Zhou, H., Zhao, J., Feng, Y., Gagan, M.K., Zhou, G., and Yan, J.: Distinct climate change synchronous with Heinrich event one, recorded by stable oxygen and carbon isotopic compositions in stalagmites from China, Quaternary Res., 69, 306–315, doi:10.1016/ j.yqres.2007.11.001, 2007.